Alexei Yanchukovich

SCREENING THE CRITICAL LOCATIONS OF A FATIGUE-LOADED WELDED STRUCTURE USING THE ENERGY-BASED APPROACH

ACTA UNIVERSITATIS LAPPEENRANTAENSIS 966

Alexei Yanchukovich

SCREENING THE CRITICAL LOCATIONS OF A FATIGUE-LOADED WELDED STRUCTURE USING THE ENERGY-BASED APPROACH

Dissertation for the degree of Doctor of Science (Technology) to be presented with due permission for public examination and criticism in the Auditorium 1318 at Lappeenranta-Lahti University of Technology LUT, Lappeenranta, Finland on the 4th of June, 2021, at noon.

Acta Universitatis
Lappeenrantaensis 966

Supervisor Professor Dr. Timo Björk
LUT School of Energy Systems
Lappeenranta-Lahti University of Technology LUT
Finland

Reviewers Professor Dr. Cetin Morris Sonsino
Fraunhofer Institute for Structural Durability and System Reliability LBF
Darmstadt
Germany

Docent Dr. Roger Rabb
Department of Mechanical Engineering
Oulu University of Technology
Finland

Opponent Docent Dr. Roger Rabb
Department of Mechanical Engineering
Oulu University of Technology
Finland

ISBN 978-952-335-666-5
ISBN 978-952-335-667-2 (PDF)
ISSN-L 1456-4491
ISSN 1456-4491

Lappeenranta-Lahti University of Technology LUT
LUT University Press 2021

Abstract

Alexei Yanchukovich
Screening the critical locations of a fatigue-loaded welded structure using the energy-based approach
Lappeenranta 2021
140 pages
Acta Universitatis Lappeenrantaensis 966
Diss. Lappeenranta-Lahti University of Technology LUT
ISBN 978-952-335-666-5, ISBN 978-952-335-667-2 (PDF), ISSN-L 1456-4491, ISSN 1456-4491

Fatigue analysis is a very important part of the design process of a welded structure. Several different methods are available, but the principal challenge is the very large number of potential critical points in a complex welded structure. Material development has led to a significant increase in the strength of steel and higher allowed static loading, which requires additional parameters to be considered and complicates the analysis of fatigue-loaded welded components. Reliable fatigue analysis requires an efficient screening procedure to define potential critical locations and limit the number of points for analysis.

A new method for the effective screening of critical locations of complex welded structures under fatigue loading is developed in this thesis. The method's primary area of applicability is high cycle fatigue (HCF) under a combination of a few independent constant amplitude loads. The screening method utilizes energy-based damage criteria in combination with stress-based methods commonly used in the fatigue analysis of welded structures. The method includes the capability to consider multiaxial state, mean and residual stresses, local plasticity, and the yield strengths of materials. Flexible consideration of the different parameters enables the screening procedure to be adapted to ensure compatibility with common fatigue standards and rules for welded structures, and corresponding uniaxial fatigue strengths can be used to determine the required fatigue properties. The implemented fatigue tests demonstrate a good correlation between test results and the estimations of the developed screening method. The location of the site of failure was usually estimated successfully, and the mean fatigue life defined by the screening procedure was close to the results of the implemented fatigue tests. According to the test results obtained, the developed method has good potential as a tool to screen the critical locations of a welded structure.

The developed screening procedure limits the number of potential critical points requiring more detailed fatigue analysis and focuses resources on the accurate analysis of the most critical points. The results of systematic screening using the developed method give preliminary information about fatigue resistance of the structure, which improves efficiency and shortens the design process by avoiding unnecessary detailed analysis of unfinished concepts.

Keywords: Fatigue, welded joint, critical location, screening method

Acknowledgements

This work was carried out in the Department of Energy and Environmental Technology at Lappeenranta-Lahti University of Technology LUT, Finland, between 2017 and 2020. I want to thank Professor Dr. Timo Björk, my supervisor, for the opportunity to work in the Steel Structure Researchers' Group, and for the support and trust he showed me while I carried out this work. I would also like to express my gratitude to the preliminary examiner Professor Dr. Cetin Morris Sonsino as well as to Docent Dr. Roger Rabb who was the preliminary examiner and opponent.

I want to express my great appreciation of my research colleagues and the staff of the Steel Structure and Welding Laboratories for their support, advice, and collaboration: Dr. Antti Ahola, Dr. Tuomas Skriko, Mr. Kalle Lipiäinen, Lic.Sc. Matti Koskimäki, Mr. Olli-Pekka Pynnönen, Mr. Jari Koskinen, Mr. Mika Kärmeniemi, Mr. Jan Muuronen, Mr. Antti Heikkinen, Mr. Antti Kähkönen, and all the others.

I would like to thank Dr. Teuvo Partanen for his support and significant impact on my career choice during the course of my studies and the many years we have worked together. May I also express my gratitude to Mr. Jussi Rinnevalli for the opportunity to gain extensive and varied professional experience in the field of strength calculation over my years of working in the company Stressfield. I would further like to thank Dr. Timo Nykänen, Dr. Tapani Halme, Professor Dr. Matti Suviolahti, Professor Dr. Heikki Handroos, Professor Dr. Heikki Martikka, Professor Dr. Harri Eskelinen, and many others for their support at the beginning of my studies. My gratitude also goes to Professor Emeritus Erkki Niemi, who passed away last fall.

Lastly, my thanks go to my family, my wife Mari, and my children Kristian and Julia for their support, help, and patience, and to my deceased parents, Albert and Inna, for their love and care and the opportunities they gave me.

Alexei Yanchukovich
April 2021
Lappeenranta, Finland

Contents

Nomenclature

In the present work, variables and constants are denoted using *slanted style*, vectors are denoted using **bold regular style**, and abbreviations are denoted using regular style.

Latin alphabet

A_0	material parameter in elastic-plastic correction	–
b	exponent of fatigue strength coefficient σ_f'	–
c	exponent of fatigue ductility coefficient ε_f'	–
C	constant of S-N curve	–
C_u	threshold value of elastic strain energy density (SED)	Nmm/mm^3
D	total damage	–
D_i	partial damage caused by loading block or loading event i	–
e	nominal elastic strain	–
E	Young's modulus of the material	MPa
$f_{x'}$	sectional membrane force	N/mm
f_y	yield stress of the material	MPa
$f_{z'}$	sectional shear force	N/mm
$H(x)$	Heaviside function	–
i	indices of the principal components, index numbers of loading blocks or loading events	–
K, K'	strain-hardening coefficient (monotonic and cyclic correspondingly)	MPa
$K(p)$	combination factor of the individual load p	–
k_{comp}	effectivity factor of the negative stress range	–
$K_{crit}(p)$	combination factor of the individual load p in the critical combination	–
K_e	elastic-plastic correction factor	–
k_{mean}	factor for correcting the effectiveness of the SED related to the positive minimum stress of the range	–
k_{pl}	ratio of plastic SED and the plastic portion of pseudoelastic SED	–
K_t	theoretical elastic stress concentration factor	–
K_w	correction factor for welds around the corner of the detail	–
$K_{t\tau}$	stress concentration factor referring to the shear stress $\tau_{\parallel}$	–
$K_{t\perp}$	stress concentration factor referring to the perpendicular stresses $\sigma_{\perp}$	–
K_f	fatigue notch factor	–
$K_{f\tau}$	fatigue notch factor referring to the shear stress $\tau_{\parallel}$	–
$K_{f\perp}$	fatigue notch factor, referring to the perpendicular stresses $\sigma_{\perp}$	–
K_σ	stress concentration factor	–
K_ε	strain concentration factor	–
m	slope exponent of the S-N curve	–
$m_{y'}$	sectional bending moment	Nmm/mm
n, n'	exponent of strain-hardening coefficient (monotonic and cyclic)	–

N	fatigue life, number of cycles	–
N_f	number of cycles to failure	–
n_i	actual number of cycles in block i	–
N_i	allowable number of cycles for block i	–
p	index number of load case, loading increment	–
p_{max}	maximum number of load cases	–
q	scale factor, multiplication factor (general), or index number of element or location	–
r_f	fictitious notch radius in the ENS method	mm
r_{true}	real notch radius	mm
R	load ratio or applied stress ratio	–
R_{loc}	local stress ratio	–
S	nominal elastic stress	MPa
s_{ij}	deviatoric stress tensor	MPa
t	thickness of the plate	mm
T	time, loading increment, or point of loading history	s
W	strain energy density (SED)	Nmm/mm^3
$W(x)$	SED of the step x (general)	Nmm/mm^3
W_{corr}	corrected value of the fatigue effective SED	Nmm/mm^3
W^D	elastic energy of distortion	Nmm/mm^3
W^e	elastic strain energy density (SED)	Nmm/mm^3
W_{eff}	fatigue effective SED of the cycle	Nmm/mm^3
W^{Ellyin}	fatigue effective SED in Ellyin's model	Nmm/mm^3
$W_{i,over}$	overestimated SED related to the principal component i	Nmm/mm^3
W^p	plastic SED	Nmm/mm^3
W^{pse}	total pseudoelastic SED	Nmm/mm^3
$W^{pse/p}$	portion of pseudoelastic SED related to the plastic behavior	Nmm/mm^3
W^V	elastic energy of volumetric change	Nmm/mm^3

Greek alphabet

α	inverse value of the slope exponent of the W-N curve in Ellyin's model	–
γ	shear strain; material constant in the Walker equation	–
γ_{Mf}, γ_{Ff}	partial factors for fatigue strength and for equivalent constant amplitude stress ranges, respectively	–
Δx	range of value x (general)	[x]
$\Delta\varepsilon$	strain range	–
$\Delta\varepsilon^e$	elastic strain range	–
$\Delta\varepsilon^p$	plastic strain range	–
$\Delta\sigma_{11}$	normal component of the stress ranges (direction 11 or x)	MPa
$\Delta\sigma_{12}$	shear component of the stress ranges (direction 12 or xy)	MPa
$\Delta\sigma_{22}$	normal component of the stress ranges (direction 22 or y)	MPa
$\Delta\sigma_C, \Delta\tau_C$	reference value of the fatigue strength at $2{\cdot}10^6$ cycles	MPa

$\Delta\sigma_{corr}$	plasticity-corrected computational elastic structural stress range	MPa
$\Delta\sigma_{E,2}$, $\Delta\tau_{E,2}$	equivalent constant amplitude stress range related to $2 \cdot 10^6$	MPa
$\Delta\sigma^{pse}$	computational pseudoelastic stress range	MPa
δ	distance between weld toe and considered cross-section	mm
δ_{ij}	Kronecker delta	–
ε	strain	–
ε_a	strain amplitude	–
ε_f'	fatigue ductility coefficient	–
ε_i	principal strain components (i = 1, 2, 3)	–
$\varepsilon^e{}_i$	principal elastic strain components (i = 1, 2, 3)	–
ε_{ij}	strain tensor	–
ε'_{ij}	transformed components of the strain tensor	–
ε'^e_{ij}	elastic part of the transformed strain tensor	–
ε^e	elastic strain	–
ε^p	plastic strain	–
ε^{yield}	value of the strain component at the yielding point	–
κ_u	constant of W-N curve in Ellyin's model	Nmm/mm^3
ν	Poisson's constant	–
ρ	multiaxial constraint factor in Ellyin's model	–
σ	normal stress	MPa
$\sigma_\perp$, $\sigma_\parallel$, $\tau_\parallel$	stress components in the coordinate system, aligned to the weld toe	MPa
σ_{11}	normal component of the stress (direction 11 or x)	MPa
σ_{12}	shear component of the stress (direction 12 or xy)	MPa
σ_{22}	normal component of the stress (direction 22 or y)	MPa
σ_b	bending stress	MPa
σ_f'	fatigue strength coefficient	MPa
σ_H	hydrostatic stress	MPa
σ_i	principal stress components (i = 1, 2, 3)	MPa
σ_{ij}	stress tensor	MPa
$\sigma_{ij}(x)$	stress tensor at the moment or step x (general)	MPa
σ'_{ij}	transformed components of the stress tensor	MPa
σ_{kk}	sum of the normal stress components	MPa
σ_m	membrane stress	MPa
σ_{ref}	reference stress	MPa
σ^{res}	residual stress	MPa
σ_s	structural stress	MPa
σ_{VM}	equivalent von Mises stress	MPa
$\sigma_{w\perp}$	nominal stress in the weld throat	MPa
σ^y, σ^{yield}	value of the stress component at the yielding point	MPa
τ	shear stress	MPa
$\tau_\perp$	transversal shear stress in the weld throat	MPa
φ	angle of principal direction	°

Superscripts

´	transformed component
comb	combined
corr	corrected
D	distortion
e	elastic
e+	elastic positive
e-	elastic negative
Ellyin	fatigue-effective strain energy density in Ellyin's model
ENS	effective notch stress
E-PP	elastic-perfectly plastic
HS	hot spot (or structural)
mean	mean value
new	new (processed) value
offset	offset value
old	old value (before processing)
p	plastic
pse	pseudoelastic (computational elastic value, which exceeds yielding point)
pse/p	portion of pseudoelastic value, related to the plastic area
R	replaced
ref	reference
res	residual
root	root of the weld
y, yield	value, related to the yielding point
V	volumetric

Subscripts

$\parallel$	longitudinal component in coordinate system, aligned to the weld
$\perp$	perpendicular component in coordinate system, aligned to the weld
a	amplitude
b	bending
char	characteristic value
corr	corrected
comp	compression
eff	effective
ij	indices of the components of tensor
loc	local
m	membrane
mean	mean value
s	structural

max	maximum
min	minimum
over	overestimated portion
rel	relative
ref	reference
tot	total
VM	von Mises

Abbreviations

4R	4R-method
CA	constant amplitude
DNV	Det Norske Veritas
DOF	degree of freedom
ENS	effective notch stress
ESED	equivalent strain energy density
E-PP	elastic-perfectly plastic
FAT	fatigue class, allowable stress range at 2 million cycles
FCI	fatigue crack initiation
FE	finite element
FEM	finite element method
FKM	Forschungskuratorium Maschinenbau (Guideline)
HAZ	heat-affected zone
HCF	high cycle fatigue
HS	hot spot (or structural)
IIW	International Institute of Welding
LCF	low cycle fatigue
MCF	multiaxial constraint factor
RHS	rectangular hollow section
S235JRH	type of structural steel
S420MH	type of structural steel
SED	strain energy density
S-N	stress-fatigue life (curve)
SWT	Smith-Watson-Topper
VM	von Mises
W-N	SED-fatigue life (curve) in Ellyin’s model

1 Introduction

1.1 Background

This work relates to the fatigue analysis of welded metal structures. Fatigue is one of the most common causes of structural damage, and fatigue analysis is a very important part of the design process of welded structures. The main task of fatigue analysis is to reliably determine the safe fatigue life of an entire structure, which is based directly on the fatigue life of the most critical location. A large amount of comprehensive research data related to the fatigue analysis of an individual point has been published, and a wide range of methods and approaches exists to perform a fatigue analysis of almost any individual detail or specific location. There are stress-based and strain-based methods, energy-based methods and methods based on fracture mechanics, as well as several versions of critical plane methods for multiaxial conditions and different combinations of these methods. The methods differ significantly in suitability for specific situations, precision, description of the loads, and used assumptions. Some methods are simpler and easier to use, while others are more special and considerably more advanced, which affects the quantity of input information and computational resources required.

However, reliably calculating the fatigue life of an entire structure depends entirely on successfully determining the critical point for the analysis. Incorrectly selecting such a point leads to the analysis of a non-critical location and, correspondingly, to overestimating the fatigue life of the entire structure, regardless of the sophistication of the fatigue analysis method used and the accuracy of the calculation. Analyzing several locations increases the reliability of the analysis but, at the same time, causes extra work and slows the design process. Consequently, successfully determining critical locations, which limits the number of points for detailed analysis and increases the efficiency and reliability of the fatigue analysis, is crucial in the design process of a fatigue-loaded complex welded structure.

Reliably determining the critical locations requires comparable information about fatigue damage at each point of the structure. This is a rather challenging task because different types of structures, uses, and load conditions set their own specific requirements, and a variety of factors must be considered. One possible solution is a special post-processing software which calculates the fatigue damage of selected points according to a given approach, using the required analysis results. Some commercial computer programs of this type are available; however, they are better suited to the detailed analysis of particular points of interest than the overall screening of critical locations within an entire structure. In practical design work, the definition of critical points is often based mostly on the knowledge and experience of an analyst, and a method for more systematic screening of critical locations is urgently required.

The aim of the current work is to develop a screening method to determine the critical locations of a complex welded structure under fatigue loading. A universal screening

method applicable to all cases would be very complicated and difficult to use, even if it were possible. For this practical reason, it is expedient to limit the suitability of the screening method to certain types of structures and situations which are similar enough to be solved by the same approaches. This thesis focuses on the screening of critical locations of a complex welded structure, loaded by combination of several independent constant amplitude loads. The primary area of interest is high cycle fatigue (HCF), extended by capability to consider local plasticity during individual loading cycles. The selected area of applicability covers many typical cases of practical design applications and determines specific requirements related to welded joints and the local influence of the combined loading at the point of interest.

Developing the screening method requires consideration of some seemingly independent sub-areas, such as handling the loading, selecting the appropriate accuracy level of input information, and choosing a suitable fatigue approach and failure criteria. Successful development of the screening method requires the conjugation of these different sub-areas to form a flexible, functioning combination which is applicable for practical design cases and the overall screening of entire structures using finite element (FE) models with a solvable number of degrees of freedom (DOF).

1.2 Goals and methods

1.2.1 Goal and research questions

The aim of this thesis is to develop a method to screen the most critical locations of a complex welded structure for a subsequent, more detailed and accurate, analysis. The appropriate reference fatigue criteria and fatigue model, in combination with the applicable method to process the loading, must be defined to obtain an efficient screening procedure.

The main research question (MRQ) is how to determine the most critical locations of a fatigue-loaded welded structure using the results of conventional analysis, based on the global FE model of the entire structure or a significant part of it. The MRQ can be divided into the following sub-research questions (SRQ):

SRQ1: What level of accuracy of input data is appropriate and suitable for the screening of critical locations in practical design cases? The input data for overall screening of an entire structure must be accessible by global FE models, but the data must include all the necessary information required for the screening method to be implemented.

SRQ2: How can the influence of the most important fatigue factors be considered in the developed screening method while ensuring it remains applicable to practical design cases and compatible with the assumptions of common fatigue standards for welded structures? The influence of local plasticity and the influence of mean and residual stress can be taken into account in the screening procedure using available input data or ignored,

if necessary. Multiaxiality and variation of stress components between different load cases, typical of general practice design cases, must be taken into account.

SRQ3: What approach and failure criteria are most appropriate and best able to take into account multiaxiality and non-proportionality in combination with other important factors, using available input information and utilizing the conventional uniaxial data of fatigue standards to determine the required fatigue properties?

1.2.2 **Research methods**

The research methods used to achieve the aim of this thesis were:

- literature review
- theoretical analysis
- numerical simulations using finite element method (FEM)
- laboratory experiments

A literature review was carried out to enable a preliminary study of the methods and damage parameters potentially applicable for screening the critical locations of entire structures. Fatigue models and criteria suitable for the development of an efficient screening procedure were selected, based on previous publications and other available literature. The selected methods were modified and adopted to efficiently implement the screening procedure using the theoretical analysis and numerical simulations. The developed screening method was verified by FEM simulations and laboratory experiments. The most critical locations of the tested structures under different loading combinations were estimated using the developed screening method and corresponding FEM results. The estimated results were compared to those obtained by fatigue tests implemented using the appropriate test specimens.

1.3 **Scientific contributions**

The aim of this work was to develop a method to reliably determine the critical locations of complicated welded structures for a subsequent detailed fatigue analysis. A critical location is the point at which fatigue failure will begin, and the term “complicated” refers to both geometry and loading conditions. This kind of method for the systematic screening of critical locations is lacking in the available guidelines and rules for the fatigue design of welded structures. A new screening method to determine the critical locations of complicated welded structures in the multiaxial load has been developed.

The developed screening method can be applied to cases loaded by a combination of a few independent constant amplitude fatigue loads, resulting in multiaxial and non-proportional loading. The method is able to take into account assumed or known residual stresses, mean stresses, the yield strength of materials, and local plasticity. The capability to consider these factors is especially important given the increased use of ultra-high

strength steel (UHSS), automatic welding and post-weld treatments, and improvements in welding quality.

Correspondingly, the capability to consider local weld geometry using assumed or known fatigue notch factors confirms that the developed screening procedure is compatible with the effective notch stress (ENS) method, which is now included in several fatigue standards and rules for welded structures. Compatibility with the assumptions of conventional standards is confirmed by the ability to ignore unnecessary parameters and consider the partial efficiency of the compressive stress range, as well as by the capability to use fatigue properties based on standard uniaxial fatigue data. Hence, the developed screening method can take into account the most important factors but can also be used in a form which is compatible with the basic principles of common fatigue standards for welded structures, if necessary.

The method is based on seven-step calculation procedure and includes parts of known theories and previous research, modified to, and combined with, the new complete method. New features of individual elements within the method were developed to ensure it is more applicable to overall screening, for example:

- Capability to consider the portion of negative elastic strain energy density (SED) for compatibility with conventional standards and rules
- Capability to adjust considering the influence of mean stress, according to, for example, the Smith-Watson-Topper (SWT) method within Ellyin's SED-based method
- Utilizing the coordinate system rotation to the principal angles, based on stress ranges for incremental calculation of the SED in non-proportional multiaxial loading

The areas of applicability of the developed screening method and limitations are presented in Section 2 of this thesis.

1.4 Literature review

A variety of factors must be considered to determine the critical points of a structure at which fatigue failure will initiate. Comparable information about damage accumulation at the different points of a construction is required, and a large amount of information related to external factors and internal properties must be taken into account, including information about applied loads and their influence on the different points of a structure, as well as local geometries, stress states, and material properties. A reliable systematic screening requires efficient ways to simplify the calculation and take into account the most important and essential factors while processing the smallest amount of data. The following is a brief overview of previous publications and work relevant to and important for the development of a screening method.

The literature presents different techniques to reduce the loading data which must be processed to determine critical points. Small load omission criteria (SLOC) is a commonly used time editing method utilized to compress long loading histories, especially in tests but also in simulations. Different techniques for elimination are available. Heuler and Seeger (1986) present as allowable the omission of small cycles, below a filter level of about 50% of the constant amplitude endurance limit of the material. Yan et al. (2001) propose that an equivalent stress amplitude lower than or equal to the fatigue crack initiation (FCI) threshold can be omitted in life estimation. However, while filtering and reducing the loading information decreases the amount of data for processing and simplifies the determination of critical locations, it does not essentially define such locations.

A combination of a few independent constant amplitude loads has been chosen as the primary area of applicability for the screening method under development. This combination forms variable amplitude loading with regular nature, which preferably should be processed without constructing an exact loading history and without reducing the loading data. Det Norske Veritas (DNV) rules (2016) propose a solution to combine the fatigue damages of two dynamic processes without having to construct the total loading history. The proposed technique is formulated using the frequencies of the loads but can probably be modified to other formats if necessary.

Ping et al. (2008) propose using the nominal stress method with the assumption of a uniaxial stress state for the preliminary determination of the critical regions of a car body and a subsequent more detailed investigation based on multiaxial fatigue theory. The authors state that, according to experimental studies, multiaxial fatigue analysis gives more reasonable results than the uniaxial nominal stress method.

Veltri (2016) presents the method of identifying fatigue-critical regions by a predicting algorithm, based on the modal reduction method. The aim of this method is to accelerate fatigue simulation by filtering non-critical regions and reducing the finite element (FE) entities for processing. According to the author, the technique is approximative and could be used to save time in the early phases of the design cycle. One of the basic principles underlying the technique is that “a higher stress, strain or strain energy density corresponds to a higher fatigue damage potential.” However, the number of cycles must be considered together with these parameters, because a higher number of cycles with a lower range can be more detrimental than occasional cycles with a higher range. Additionally, the possibility of different fatigue strength at different locations must be taken into account in some cases.

Solutions based on the computer-aided application of conventional fatigue analysis methods to chosen locations of the structure form a separate group. Such applications include the commercial software “DesignLife” (nCode, 2018) and “fe-safe” (fe-safe, 2017). The development of computational capabilities enables the use of these kinds of solutions in a larger number of potential critical locations. In some cases, computer-aided fatigue analysis can be performed at each point of a structure and the critical locations

can be determined directly, without pre-screening. However, the application of computer-aided solutions to the overall fatigue analysis of a complete structure poses certain challenges. Each modelling technique has its own specific requirements, and the suitability of the chosen solution method depends on each point of the structure under consideration. Computer-aided solutions often include different algorithms and tools to screen the local extremum value areas. The software user must understand clearly that the algorithm only searches for nodes or elements of which the value of the selected result is higher than at all adjacent nodes or elements. This tool can be applied successfully to screen critical locations by using the proper data, for example total fatigue damage, which must be already calculated for each point of the construction using an appropriate method and results.

Ince and Glinka (2016) propose a method for the computational multiaxial fatigue analysis of notched components. The method is based on local elastic-plastic strain-stresses and critical plane analysis of the multiaxial state but utilizes theoretical linear-elastic results of linear elastic FE analysis as input information. Using the results of the linear elastic FE analysis with separate external fatigue post-processing simplifies the fatigue analysis of the considered locations and significantly increases the applicability of the method for practical cases. The method requires a high level of accuracy from the element model, limiting its applicability for overall analysis of a complete structure to determine critical locations.

Fermér et al. (1998) present an FE-based method for the fatigue analysis of a thin-walled structure. The method is intended to enable overall fatigue analysis of the entire structure and utilizes the structural stresses at the weld toe, calculated by nodal forces and moments in a mesh-insensitive manner. Another mesh-insensitive method to determine structural stresses is presented by Dong (2001). The commercial fatigue softwares “DesignLife” (nCode, 2018) and a module of the “fe-safe” software, based on the Verity^{TM} method (fe-safe, 2002), determine structural stresses using nodal forces and moments. Mesh-insensitive methods which can be used with relatively coarse element mesh are very useful for the screening analysis.

Only those literature sources which are directly related to the screening of critical points are presented in this section. The theoretical background used in the development of the screening method and related literature sources are presented in Chapter 3. The basic requirements and chosen limitations of the area of applicability for the screening method under development, which determines the required background information, are presented in Chapter 2.

1.5 Structure of the thesis

The thesis has seven chapters. An introduction to the work, background information, the goals, and the scientific contribution as well as a brief literature review are presented in this first chapter. Chapter 2 presents more detailed information about the specific requirements and limitations of the area of applicability of the screening method under

development. The important basic principles and theoretical background relevant to the developed screening method are presented in Chapter 3. Chapter 4 contains a detailed presentation of the developed screening method and describes each step of the screening procedure to determine critical locations. A comparison of the results of the performed tests with estimations given by the developed method, using the results of a corresponding FE analysis, is presented in Chapter 5. Chapter 6 describes the results of the work and discusses the capabilities of the developed method, obtained solutions, and achieved benefits as well as suggesting directions for further research. Finally, Chapter 7 presents conclusions and gives a summary of the thesis. Additional information related to the different chapters of the thesis is presented in the corresponding appendices.

2 General requirements and formulation of the problem

Fermér and Svensson (2001) present three important items of fatigue life calculation: information about load-time histories, calculated stress or other appropriate quantity related to the fatigue failure, and rules for fatigue life estimation by chosen quantity. It is not necessary to calculate exact fatigue life in order to screen critical locations; however, comparable information related to the fatigue damage at each potential point of interest is required. The stresses or strains alone do not determine the magnitude of fatigue damage, and a variety of factors and specific requirements must be considered in the screening analysis. Type of structure, loading conditions, selected limitations, and assumptions all affect which approaches and methods are applicable.

The focus of this work is to develop a method to screen the critical locations of complex welded structures loaded by a combination of a few independent constant amplitude loads. The primary area of interest is high cycle fatigue (HCF) and cases in which the quasi-static approach is valid. The possibility of considering local plasticity is desirable for occasional load combinations and to extend the area of applicability to the transition zone between HCF and low cycle fatigue (LCF). Compatibility of the developed screening method with the basic principles and assumptions of common fatigue standards for welded structures would be desirable for practical design work. The selected area of applicability covers a significant proportion of typical design cases and sets some specific requirements related to the specialty of welded joints.

2.1 Processing of loading

The primary area of interest is limited to a combination of a few independent proportional constant amplitude loads applied to the different points of construction. The combination of these simple loads results in regularly repeated blocks of non-proportional variable amplitude loading. This loading can lead to a multiaxial state in any arbitrary point of interest, which requires that the screening method under development is suitable for multiaxial loading.

The exact interaction between independent loads is not usually defined and several alternative loading combinations may form, which leads to several alternative stress histories at each point of interest. In this case, processing the variable amplitude loading, based on stress histories, requires every possible stress history to be constructed for each potential critical point of the structure. This significantly increases the computational effort required by the screening procedure, which should be avoided if possible.

2.2 Particular features of the welded structure

The fatigue of welded structures differs from the base material and has several significant features that must be taken into account in fatigue analysis. Uneven, variable local geometry and very sharp notches are typical of welded structures. Determining an exact

local geometry at the design stage is impossible, which limits the use of methods which are suitable for the exact local geometry of the notch. Additionally, the element mesh required for this type of method is often too fine for the global screening of the entire structure. Variable local geometry must be considered using safely conservative assumptions, rather than exactly determined. Assumed influence can be included in strength parameters or computationally added into a quantity that is more overall than local stress. However, this type of approach can lead to non-uniform fatigue strengths, depended on the type of location and welded joint, which is undesirable for the screening procedure.

High residual stresses are another feature of welded structures and strongly affect fatigue behavior. Due to high residual stress, the level of local mean stress at the point of interest differs from the mean stress caused by external loading. Additionally, the residual stresses vary greatly between different locations and depend on many factors. The exact determination of the residual stresses for each point of a complex welded structure is very difficult, and conservative assumptions are often used in a fatigue analysis of welded joints.

The influence of the material properties on the fatigue strength of a welded structure differs from that of the parent metal. The dependence between the strength of the material and the fatigue properties is typical for a parent metal, where fatigue crack initiation (FCI) is determinative. The portion of FCI in the total fatigue life of a welded joint is much smaller than in the case of an unwelded parent metal. More significant for a welded structure is the area of stable crack growth, where the strength of the material has less effect. On the other hand, in the initial stage, the residual stresses and occurrence of the local plasticity depend on the material properties. An additional challenge is posed by the variability of the material properties in the weld and heat affected zone (HAZ), as these differ from those of the parent metal.

2.3 Fatigue life duration and local plasticity

Fatigue behavior in the area of HCF differs from LCF, and an appropriate analysis method is required depending on the area of interest. The LCF and associated significant plasticity are limited outside the area of interest in this thesis. The transition area between HCF and LCF for metals is typically 10^3–10^4 cycles (Jussila et al., 2017) and fatigue life over 10^5 cycles corresponds to the HCF region. The nominal stresses are usually elastic on the area of the HCF under constant amplitude loading and even effective notch stress (ENS) remain below the range of the cyclic plasticity, despite relatively high fatigue notch factors.

According to the ENS results presented in Appendix A, the yield stress of 325 MPa is the limit for beginning the cyclic plasticity on an area of HCF at 10^5 loading cycles. The yield stresses of the most common structural steels are higher (SFS-EN 10025-2, 2019), and thus elastic behavior is expected on an area of HCF under constant amplitude loading. However, due to variable amplitude loading, occasional local plasticity can occur in some

combination of independent loads, as explained in Section 2.1, or in the transition area below 10^5 cycles. Therefore, although the ability to consider local elastic-plastic behavior is not the primary purpose, it is beneficial for the screening method under development.

2.4 FE modelling strategy

The screening method under development is intended primarily for utilizing the results of finite element (FE) analysis, which imposes additional requirements. The reference quantity chosen to screen the critical locations sets the requirements for the accuracy of the FE model and the analysis of results. On the other hand, the required applicability of the method to practical design cases limits the size of the FE model and density of the element mesh. A successful screening method requires a compromise between these two restrictions. Welded structures, the primary area of interest, are typically modelled using shell elements, which also affects the choice of method and corresponding reference quantity to screen critical locations. A desirable additional benefit is the possibility of using the same element model without changes, or with minimal modifications, for the preliminary screening of the critical locations and the subsequent detailed analysis of the obtained points.

3 Theoretical background

3.1 Fatigue analysis approaches

Several different approaches to the fatigue life assessment of a specified location have been developed. A wide range of fatigue analysis tools and methods exists in the literature, applicable for the successful analysis of almost any type of individual detail. Some methods are simpler and easier to use, while others are considerably more advanced. The methods differ in suitability for specific situations, used assumptions, and description of loading. Required input information, calculation resources required, and accuracy also differ. There is no intention to offer a detailed review of all methods and approaches, as they are well presented in the literature. This review focuses on the approaches and methods that form the basis of, and set the principal direction for, the development of the screening procedure.

Stress-based approaches are important for screening analysis from the perspective of practical design work, because many existing standards and rules are based on these methods. The local strain approach is presented as background information to the effective notch stress (ENS) method and strain energy method. Ellyin's method, based on the strain energy density (SED), is important for converting the different reference quantities into uniform and directly comparable failure criteria. This energy-based model also offers certain extra benefits without direct conflict with the assumptions used in existing standards.

Critical plane methods have been excluded from this review, although they are well suited to the analysis of individual locations under complex multiaxial loading. Global screening of an entire structure using the critical plane method, based on the analysis of several potential failure planes at each point of interest, requires too great a computational effort. Another option for evaluating the fatigue strength and crack propagation is to use methods based on fracture mechanics. However, fracture mechanics are not used directly in the development of the screening method because of the required computational efforts and limitations related to the cases with a significant crack initiation stage. For this reason, methods based on fracture mechanics are also excluded from the review.

3.1.1 Stress-based approaches

Stress-based approaches usually assume linear-elastic behavior and use the relation between magnitude of stress range or amplitude and fatigue life defined by the appropriate stress-fatigue life curve (S-N curve). The different categories of stresses can be used as reference quantities for the estimation of fatigue life. Depending on the stress category used in a method, some factors are already included in fatigue strength, as defined by fatigue tests. Accordingly, other factors must be taken into account in the results of the stress analysis; hence, in this regard there are differences between the available stress-based methods.

Nominal stress method

This traditional method estimates fatigue life using the nominal stress caused by applied loading, and the appropriate S-N curve defined for a similar classified detail. The method is used in many fatigue standards, rules, and recommendations for welded structures, such as steel structure standard SFS-EN 1993-1-9, crane standard EN 13001-3-1, pressure vessel standard EN 13445-3, DNV rules for offshore steel structure, International Institute of Welding (IIW) recommendations for fatigue design, and so on.

The fatigue strength in this method is defined by nominal stress in the tested detail, which can usually be calculated from applied loading using simple analytical equations and basic cross-sectional properties. One special case is fatigue strength at the root of the fillet or butt weld, usually based on the nominal stress in the weld throat, instead of the overall global stress in the detail. The values of slope constant and fatigue strength related to the specified number of cycles are often used for classification of different S-N curves. For example, standard SFS-EN 1993-1-9 and IIW recommendations for fatigue design (Hobbacher, 2008) classify the S-N curves with a fixed value of the slope constant using an allowable stress range at 2 million cycles, which is called fatigue class (abbreviated as FAT).

The nominal stress method can be easily applied to structural components which are identical to classified details. In this case, the influence of detail geometry and other local factors is considered in the appropriate S-N curve, and only the overall nominal stress must be defined. However, the geometry of a structural component is rarely identical to classified details, which requires some interpretation of similarity. The local stress raising considered in the S-N curve must be excluded from the stress used as nominal, but the macrogeometric effect caused by the difference between the classified detail and the structural component must be taken into account. The modified nominal stress, defined by the stress analysis considering the macrogeometric difference, must be used in the fatigue calculation (Hobbacher, 2008). The applicability of a given S-N curve to cases that differ from classified details is sometimes challenging, and obtained results are unreliable. Additionally, possible differences in the local parameters already included in the fatigue strength and S-N curve must be taken into account in comparing the classified detail and structural component under consideration.

Varying the fatigue strengths, depending on the detail geometry and loading condition, limits the applicability of the nominal stress method to multiaxial cases. Standard SFS-EN 1993-1-9 (2005) considers the interaction between global normal and shear stresses using the following equation:

$$\left(\frac{\gamma_{Ff} \cdot \Delta\sigma_{E,2}}{\Delta\sigma_C/\gamma_{Mf}}\right)^3 + \left(\frac{\gamma_{Ff} \cdot \Delta\tau_{E,2}}{\Delta\tau_C/\gamma_{Mf}}\right)^5 \leq 1.0 \tag{3.1}$$

where

$\Delta\sigma_{E,2}, \Delta\tau_{E,2}$	are equivalent constant amplitude stress ranges related to 2 million cycles (normal and shear correspondingly)
γ_{Mf}, γ_{Ff}	are partial factors for fatigue strength and equivalent constant amplitude stress ranges, respectively
$\Delta\sigma_C, \Delta\tau_C$	are the reference value of the fatigue strength at 2 million cycles

Equation 3.1 is comparable with a direct summation of the partial damages caused by the normal and shear stress components separately, which corresponds to the sequential acting of the normal and shear stress ranges without any effect of simultaneous acting. Sonsino (2009) states that Equation 3.1 leads to non-conservative results in the case of non-proportional loading and recommends using exponent 2 for both terms, which gives better results in combination with the damage parameter, dependent on loading proportionality and material ductility. Bäckström (2003) noted that results calculated using summation of the squares of the normal and shear components related to the strengths correlated better with the experimental data. The repealed standard SFS 2378 (1992) for steel structures, the crane standard SFS-EN 13001-3-1 (2018), and IIW recommendations (Hobbacher, 2008) use the square-based interaction equations for normal and shear stress ranges.

Using the nominal stress method for screening analysis requires the identification of comparable classified details from a global finite element (FE) model of construction and the determination of modified nominal stresses for use with the appropriate S-N curves. Cases which cannot be compared with any classified details present a further challenge. Using the nominal stress method to screen the critical location using a global FE model requires strong interaction with a competent analyst. The consideration of multiaxial cases is also quite challenging in the nominal stress method, which further limits its applicability to the global screening of critical locations.

Structural stress method

The structural stress, or hot spot (HS) stress, method is more flexible and less dependent on the global geometry of the detail under consideration than the nominal stress method. Structural stress, used in this method as a reference quantity for the calculation of fatigue life, includes nominal stress and the effect of structural discontinuities (Niemi, 1995). In the most basic case, the structural stress is the sum of the bending and membrane stresses at the HS location (Niemi et al., 2018). The effect of the local non-linear stress peak caused by the notch at the weld toe is included in the S-N curve and must be excluded from the total surface stress at the HS location for fatigue life approximation using the structural stress method. The structural stress approach is suitable for cases in which fatigue crack initiates at the weld toe, and the direction of the fluctuating principal stress is approximately perpendicular to the weld. The method is not applicable for fatigue cracks growing from the weld root through the weld throat and for continuous welds under longitudinal loading. These cases must be analyzed by the nominal stress method or another suitable approach. (Niemi et al., 2018) The classification of the S-N curves under the structural stress method is similar to that under the nominal stress method. The

allowable stress range at 2 million cycles defines the fatigue class of the appropriate S-N curve with slope $m = 3$.

The structural stress method does not require there to be numerous different S-N curves because the global macrogeometry and effects of the joint (excluding the weld itself) are outsourced to the stress analysis. The fatigue strengths slightly depend on the case under consideration, but the variation is small (FAT90 or FAT100). The structural stress method cannot use a single uniform S-N curve, but the number of different S-N curves required and the variation in fatigue strengths are considerably smaller than in the nominal method. However, different types of HS locations require the use of different rules to determine the structural stresses. The most common classification of HS types divides them into "Type A" and "Type B", as shown in Figure 3.1. Type A HS are located on the plate surfaces at the weld toe, and Type B HS are located on the edges of plates, loaded by in-plane loading.

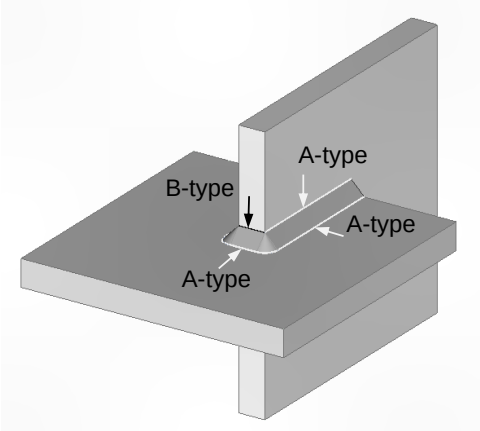

Figure 3.1: Hot spot types A and B. Type A is located on the surface of the plate. Type B is located on the edge of the plate, loaded by in-plane loading.

A wide-ranging and detailed explanation of the different rules used to determine structural stress is presented by Niemi et al. (2018). There are three principal methods:

1) Linearization of the stress distribution through plate thickness
2) Extrapolation of the stress on the plate surface
3) Avoiding the influence of the non-linear stress peak by using a stress at an appropriate single point

Under the first method, the structural stress can be determined by extracting the linear part of the stress distribution through the plate thickness. This method is applicable for use with solid FE models, and its application in different cases is presented in detail by

Dong (2001). Determining structural stresses using the bilinear stress distribution for cases with non-monotonic stress distribution through the plate thickness has also been presented (Dong, 2001).

The second method in the list presents a conventional determination of structural stress, based on the surface extrapolation of the appropriate stress through certain distances to the weld toe. The location of the extrapolation points and extrapolation rule depend on the type of HS location (see Figure 3.1). The structural stress at Type A HS locations can be determined using relatively coarse parabolic element mesh with element size $t \times t$ and linear extrapolation through locations $0.5t$ and $1.5t$ (where t is plate thickness). A fixed element of size 10 × 10 mm and extrapolation through locations 5 mm and 15 mm can be used for Type B HS locations. According to Doerk et al. (2003), there is no significant difference in results between linear extrapolation using a 10-mm parabolic element and parabolic extrapolation using a 4-mm linear element. All these rules are included in IIW recommendations (Niemi, 1995; Hobbacher, 2008; Niemi et al., 2018).

Niemi et al. (2018) present an extensive review of the different methods to approximate structural stress, based on one point at a given location near the weld toe. For example, stress at the distance of $0.5t$ from the weld toe, stress on the plate surface at 2 mm from the weld toe, or stress at the depth of 1 mm below the weld toe have been presented in different publications as representative values of structural stress (Niemi et al., 2018). DNV rules (DNV, 2016) present an approximation of structural stress based on stress at the location of $0.5t$ and a constant multiplication factor 1.12, instead of extrapolation through two points.

Fermér et al. (1998) present a method of determining structural stress using 4-noded plate elements with a fixed size of 10 mm and nodal forces and moments calculated from the nodal results of a FE model. Later, Fermér and Svensson (2001) stated that an "element length of 10 mm is too long for adequately capturing the geometry of real structures" and recommended reducing the element size to approximately 4–5 mm. The test results showed that the critical areas were detected successfully using these methods, despite some variety in fatigue lives. The method was developed for the needs of the automotive industry and introduced element size 4–5 mm is a quite coarse, related to a plate thickness of 1–3 mm, which is typically used in the automotive industry.

Dong (2001) presented mesh-size insensitive formulations to determine structural stresses based on the stress resultants (sectional forces and moments) of the plate elements or on the element nodal forces. According to Dong (2001), structural stress can be approximated using stress resultants in a local coordinate system with the x´-axis perpendicular and y´-axis parallel to the weld toe, respectively (Figure 3.2), using the following equation:

$$\sigma_{\mathrm{s}} = \sigma_{\mathrm{m}} + \sigma_{\mathrm{b}} = \frac{f_{\mathrm{x}'}}{t} + \frac{6 \cdot \left(m_{\mathrm{y}'} + \delta \cdot f_{\mathrm{z}'}\right)}{t^2} \tag{3.2}$$

where

- σ_s is the structural stress
- σ_m is the membrane stress at the weld toe
- σ_b is the bending stress at the weld toe
- $f_{x'}$ is the sectional membrane force perpendicular to the weld toe
- $m_{y'}$ is the sectional bending moment around the axis parallel to the weld toe
- $f_{z'}$ is the sectional shear force transverse to the plane of the plate
- δ is the distance between the weld toe and the considered cross-section (arm of the transversal shear)
- t is the plate thickness

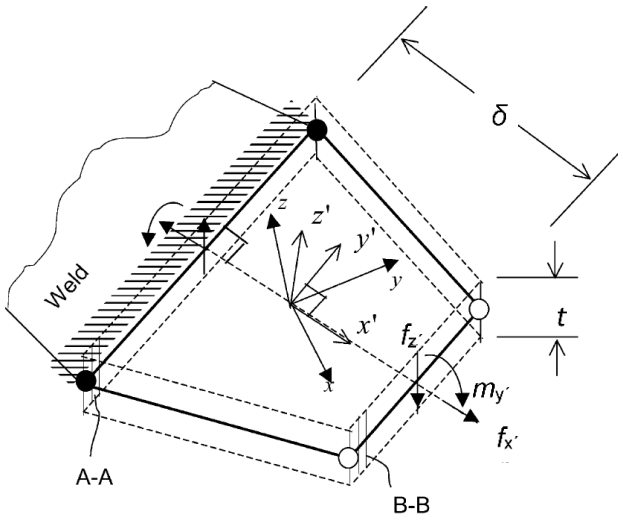

Figure 3.2: Determining structural stress by stress resultants (Dong, 2001, slightly modified).

Determining structural stress based on nodal force and moments is presented in detail by Dong (2001) and Kyuba and Dong (2005). Structural stress can be approximated in a local elemental coordinate system using the element's nodal forces and moments at the weld toe by the following equation:

$$\sigma_s = \sigma_m + \sigma_b = \frac{f_{x'}}{t} + \frac{6 \cdot m_{y'}}{t^2} \tag{3.3}$$

where sectional force $f_{x'}$ and sectional bending moment $m_{y'}$ are calculated by the appropriate element nodal forces and moments at the weld toe using the appropriate averaging rule.

Determining structural stress using the plate element's nodal forces and moments is less mesh-sensitive than using stress extrapolation (Fermér et al., 1998, Dong et al., 2007;

Marin & Nicoletto, 2009), which is very beneficial for the global screening of complex welded structures.

The structural stress method is primarily intended for cases in which the fluctuating principal stress is predominantly perpendicular to weld toe. Limited consideration of multiaxiality is implemented in the structural stress method by using the principal stress range instead of the normal stress component, which is perpendicular to the weld toe. Using the principal stress is usually limited to cases in which the largest fluctuating principal stress acts in a direction within ± 45–60° perpendicular to the weld toe. Outside of these limitations, the structural stress approach can only be applied to a stress component perpendicular to the weld toe. The nominal stress method can be used to consider other directions and stress components (Niemi et al., 2018).

Notch stress and effective notch stress methods

The notch stress, or local elastic notch stress, approach is based on the local stress at the notch, considering all stress concentrations and including nonlinear peak stress. The initiation of the fatigue crack or propagation of the existing or initiated fatigue crack must be avoided to achieve an infinitely long fatigue life under constant amplitude loading. In this case, the notch stress can be approximated as fully elastic and any minor plastic deformation at the notch root may be ignored (Radaj et al., 2006).

The effective notch stress (ENS) method takes into account the micro-support effect in determining fatigue effective stress and uses the local stress at the fictitiously rounded weld notch instead of the maximum local notch stress (Fricke, 2013). Fictitious notch radius, based on a worst-case analysis, are used for welds because the geometry of the weld notch and real radius varies substantially. According to Radaj et al. (2006), the worst case-based fatigue-effective notch stress of the weld can be defined directly using fictitious notch radius r_f = 1 mm, or indirectly using the corresponding fatigue notch factor. This recommendation is applicable for thicknesses over 5 mm. Thinner plates require the use of the fictitious radius r_f = 0.05 mm to avoid an unacceptable decrease to the net section in the local model (Fricke, 2013). The reason for using the smaller fictitious radius is purely related to the modelling technique. The smaller fictitious radius increases the stress concentration, which is compensated by a corresponding increase of the reference fatigue strength.

The same S-N curve or fatigue class (FAT) is applicable to the weld toe and weld root under the ENS method. The use of the ENS method with fictitious radius r_f = 1 mm and characteristic fatigue class FAT225 is included in IIW recommendations (Hobbacher, 2008) and DNV rules (DNV-GL, 2016) with minimum plate thickness restricted to 5 mm. The method is not applicable to loading parallel to the weld toe or for unnotched base metal or welded details with mild notches, where the ratio of ENS and structural stress is below 1.6 (Hobbacher, 2008). For plate thicknesses less than 5 mm, characteristic fatigue class FAT630 must be used with fictitious radius r_f = 0.05 mm (Fricke, 2013). The presented fatigue classes are recommended for use with principal stresses. If von Mises

stress is used instead of the principal stress, the fatigue class should be reduced at least by one (Fricke, 2013).

In general, the stress state at the weld is multiaxial, but on the surface at the weld toe it can be reduced to the plane stress condition with one in-plane shear component and two in-plane normal stress components (Chattopadhyay et al., 2011). Radaj (1984) presented a solution for approximating the local stresses at the weld toe under biaxial condition using the principal structural stresses, represented by the stress components of the coordinate system aligned to the weld toe. The local values of these stress components can be calculated using the following equations (Radaj, 1984):

$$\tau_{\parallel,\mathrm{loc}} = K_{\mathrm{t}\tau} \cdot \tau_{\parallel} = \frac{1}{2}(K_{\mathrm{t}\perp} + 1)\tau_{\parallel} \tag{3.4}$$

$$\sigma_{\parallel,\mathrm{loc}} = \sigma_{\parallel} + \nu\sigma_{\perp}(K_{\mathrm{t}\perp} - 1) \tag{3.5}$$

$$\sigma_{\perp,\mathrm{loc}} = K_{\mathrm{t}\perp}\sigma_{\perp} \tag{3.6}$$

where

$K_{\mathrm{t}\tau}$ is the stress concentration factor, referring to the shear stresses $\tau_{\parallel}$

$K_{\mathrm{t}\perp}$ is the known stress concentration factor, referring to the normal stresses $\sigma_{\perp}$, perpendicular to weld toe

$\sigma_{\perp}$, $\sigma_{\parallel}$, $\tau_{\parallel}$ are the stress components in the coordinate system, aligned to the weld toe

loc is the subscription, referring to the local value at the weld toe

The stress concentration factor of in-plane shear $K_{\mathrm{t}\tau}$ is approximated using the known stress concentration factor of a normal stress component perpendicular to the weld toe (Radaj, 1984):

$$K_{\mathrm{t}\tau} = \frac{1}{2}(K_{\mathrm{t}\perp} + 1) \tag{3.7}$$

A similar relation is also valid for the fatigue notch factor $K_{\mathrm{f}\tau}$ (Radaj et al., 2006) and can be used in Equations 3.4–3.6:

$$K_{\mathrm{f}\tau} = \frac{1}{2}(K_{\mathrm{f}\perp} + 1) \tag{3.8}$$

where

$K_{\mathrm{f}\tau}$ is the fatigue notch factor, referring to the shear stresses $\tau_{\parallel}$

$K_{\mathrm{f}\perp}$ is the known fatigue notch factor, referring to the normal stresses $\sigma_{\perp}$, perpendicular to the weld toe

Equation 3.8, in combination with Equations 3.4–3.6, enables consideration of the multiaxial stress state and approximation of local stress components using the structural principal stresses or corresponding components and fatigue notch factor referring to the stress component perpendicular to the weld toe. An additional benefit of the ENS method in screening critical locations is its use of a single S-N curve for the weld root and weld toe and its compatibility with the structural and nominal stress methods. The disadvantage of the ENS method is that it requires a relatively fine element mesh and an accurate model to directly determine the ENS. The ENS method requires significantly more computational resources and the work of an analyst, which restricts its applicability to screening analysis using a global FE model.

Combining the ENS and local strain approaches in the 4R method

The multiparameter novel notch stress approach, developed at Lappeenranta University of Technology, combines the ENS, Smith-Watson-Topper (SWT), and local strain methods. It takes into account applied stress ratio R, residual stresses, plastic behavior of material, and local geometry (Nykänen et al., 2017). The effect of local geometry can be considered by the appropriate fatigue notch factor K_f . Calculation of the fatigue notch factor K_f or direct calculation of the appropriate ENS range for the worst case in the as-welded condition are based on fictitious notch radius r_f = 1 mm, according to the ENS method. The 4R method is extended to consider the actual weld geometry and real notch radius for relatively smooth weld geometries by adjusting the fictitious notch radius $r_f = r_{true}$ + 1 mm (Björk et al., 2018).

The consideration of the effect of mean stress in the 4R method is based on the local stress ratio R_{loc} , which is determined taking into account the elastic-plastic behavior of the material and the parameters presented above. The local stress ratio R_{loc} of the ENS range after the set-up cycle can be calculated using Neuber's rule and the Ramberg-Osgood relationship, presented in the next section (3.1.2), relating to the local strain approach. The defined actual local stress ratio R_{loc} is used to convert the applied range of ENS to the reference range, which corresponds to $R_{loc} = 0$. Equation 3.9 presents this conversion, based on the SWT method:

$$\Delta\sigma_{\mathrm{ref}} = \frac{\Delta\sigma}{\sqrt{1 - R_{\mathrm{loc}}}} \tag{3.9}$$

where

$\Delta\sigma_{ref}$ is the converted reference stress range, corresponding to $R_{loc} = 0$
$\Delta\sigma$ is the applied (actual) ENS range
R_{loc} is the actual local stress ratio

Considering Equation 3.9, fatigue life is calculated using the following equation:

$$N = \frac{C}{\Delta\sigma_{\mathrm{ref}}{}^{m}} = \frac{C}{\left(\Delta\sigma/\sqrt{1-R_{\mathrm{loc}}}\right)^{m}} = C\left(\frac{\sqrt{1-R_{\mathrm{loc}}}}{\Delta\sigma}\right)^{m} \tag{3.10}$$

where

$\Delta\sigma$	is the applied (actual) ENS range
R_{loc}	is the actual local stress ratio
C	is the constant of 4R master S-N curve, corresponding to R_{loc}=0
m	is the exponent of 4R master S-N curve

The master S-N curve used in the 4R method is defined by statistical analysis of a large number of test results. The master curve differs from conventional standard S-N curves. The slope exponent of the master S-N curve used in the 4R method is m = 5.85; the mean and characteristic constants are, respectively, $C_{\mathrm{mean}} = 10^{21.59}$ and $C_{\mathrm{char}} = 10^{20.83}$ (Nykänen et al., 2017).

Multiaxial stress-based approaches

Findley's model is a well-known multiaxial-stress-based approach which utilizes the concept of the critical plane. According to this model, the damage criteria combine the effects of alternating shear stress and normal stress perpendicular to the shear plane (Socie & Marquis, 2000). The fatigue failure occurs in the most critical plane at the point of interest, where the failure criteria achieve the maximum value. Several planes must be considered at each point of interest in order to determine the most critical plane, and the number of recalculations required depends on the angular increment chosen for discretization. Applying the method to large element models and non-proportional loading requires time-consuming calculations and significant computer capacity (Rabb, 2017). The method is well verified and widely used for fatigue life calculations under multiaxial loading. However, the fact that calculation is required of several planes at each point of interest significantly increases computational efforts and limits the applicability of the method for overall screening of critical locations.

Another stress-based approach in wide use for multiaxial fatigue calculation is the Dang Van model, which is based on microscopic stresses at the critical volume of material. The combination of microscopic shear stress and microscopic hydrostatic stress is used as the parameter of local crack nucleation in the grains. The model assumes the certain relation between the microscopic stresses in the material grains and macroscopic stresses used in conventional engineering analyses. The macroscopic stresses correspond to the local stress and strains used in the local strain approach (Socie & Marquis, 2000). The required accuracy of analysis is quite challenging for use with global models. An additional computational challenge is related to the determination of the stabilized residual stress, which requires that the multidimensional hypersphere around the loading path formed by the stress tensor is determined (Rabb, 2017).

Some methods convert the multiaxial stress state to the equivalent uniaxial stress to simplify multiaxial fatigue calculations. The "signed von Mises" is an example of this kind of criteria, which Rabb (2017) calls "pseudo-criteria" with good reason. "Signed von Mises" utilizes the conventional equivalent von Mises stress with the addition of the sign, based on the sign of hydrostatic stress. In some cases, the criterion may appear to work. The inconsistency of the criterion is revealed in cases where an insignificant change in the multiaxial stress state changes the sign of the hydrostatic stress and causes a dramatic increasing or decreasing of the criterion, based on the "signed von Mises."

3.1.2 **Strain-based approaches**

A notch strain or local strain approach is focused on the fatigue life up to the initiation of the technical crack, considering the elastic-plastic local strain at the notch. Calculation of the fatigue life in this method is based on comparison of the actual local elastic-plastic strain amplitude and strain-life curve of the unnotched specimen. The total strain amplitude is divided into elastic and plastic portions, as presented in strain-life Equation 3.11 (Dowling, 2013):

$$\varepsilon_{\mathrm{a}} = \frac{\Delta\varepsilon}{2} = \frac{\Delta\varepsilon^{\mathrm{e}}}{2} + \frac{\Delta\varepsilon^{\mathrm{p}}}{2} = \frac{\sigma_{\mathrm{f}}'}{E}(2N_{\mathrm{f}})^{b} + \varepsilon_{\mathrm{f}}'(2N_{\mathrm{f}})^{c} \tag{3.11}$$

where

ε_{a}	is the amplitude of the local elastic-plastic strain
$\Delta\varepsilon$	is the range of the local total strain
$\Delta\varepsilon^{\mathrm{e}}$	is the range of the local elastic strain
$\Delta\varepsilon^{\mathrm{p}}$	is the range of the local plastic strain
σ_{f}', $\varepsilon_{\mathrm{f}}'$	are material parameters: fatigue strength and ductility coefficients
b, c	are exponents of the material parameters σ_{f}' and $\varepsilon_{\mathrm{f}}'$
N_{f}	is the number of cycles to failure, when $2N_f$ is a number of reversals
E	is the Young's modulus of the material

Local elastic-plastic stress and strain can be defined directly, using a FE model with an appropriate material model and fine enough element mesh. Values can also be approximated using the Ramberg-Osgood stress-strain curve in combination with Neuber's or Glinka's rules, discussed below. The monotonic form of the Ramberg-Osgood curve is presented in Equation 3.12 and the cyclic form in Equation 3.13 (Dowling, 2013):

$$\varepsilon = \varepsilon^{\mathrm{e}} + \varepsilon^{\mathrm{p}} = \frac{\sigma}{E} + \left(\frac{\sigma}{K}\right)^{\frac{1}{n}} \tag{3.12}$$

$$\varepsilon_a = \frac{\Delta\varepsilon}{2} = \frac{\Delta\varepsilon^{\mathrm{e}}}{2} + \frac{\Delta\varepsilon^{\mathrm{p}}}{2} = \frac{\Delta\sigma}{2E} + \left(\frac{\Delta\sigma}{2K'}\right)^{\frac{1}{n'}} \tag{3.13}$$

where

ε_a	is the amplitude of the local elastic-plastic strain
ε, $\Delta\varepsilon$	are the local elastic-plastic strain and strain range
ε^e, $\Delta\varepsilon^e$	are the local elastic strain and strain range
ε^p, $\Delta\varepsilon^p$	are the local plastic strain and strain range
E	is the Young's modulus of the material
σ, $\Delta\sigma$	are the local elastic-plastic stress and stress range
K, n	are the monotonic strain-hardening coefficient and corresponding exponent
$K´$, $n´$	are the cyclic strain-hardening coefficient and corresponding exponent, that can be approximated by material parameters $\sigma_f´$, $\varepsilon_f´$, b and c, explained above (Equation 3.11); $K´ = \sigma_f´/(\varepsilon_f´)^{(b/c)}$ and $n´ = b/c$

The local strain approach allows the plastic behavior and cyclic plasticity to be considered. In the case of elastic cyclic loading, the effect of residual stresses and individual plastic loading events on the true local mean stress can also be considered using the local strain approach, as implemented in the 4R method presented above. Determining the elastic-plastic stress and strain requires an additional rule for use in combination with the Ramberg-Osgood curve. Neuber's rule and Glinka's rule, presented below, are widely used.

Neuber's rule

During plastic deformation, stress concentration factor K_σ decreases and strain concentration factor K_ε, contrarily, increases. Neuber's rule is based on the assumption that in local plastic deformation, the geometric mean value of the stress and strain concentration factors K_σ and K_ε stays constant, equivalent to the theoretical elastic stress concentration factor K_t . Using this assumption, the product of the local elastic-plastic stress and strain can be formulated by elastic nominal stress (Dowling, 2013):

$$\sqrt{K_\sigma K_\varepsilon} = K_t \tag{3.14}$$

$$\sigma\varepsilon = K_\sigma S \cdot K_\varepsilon e = S \cdot e \cdot K_t^2 = \frac{(K_t S)^2}{E} \tag{3.15}$$

where

K_σ	is the stress concentration factor, defined as a ratio of local elastic-plastic stress and nominal elastic stress; $K_\sigma = \sigma / S$
K_ε	is the strain concentration factor, defined as a ratio of local elastic-plastic strain and nominal elastic strain; $K_\varepsilon = \varepsilon / e$
K_t	is the theoretical elastic stress concentration factor
σ, ε	are local elastic-plastic stress and strain
S, e	are nominal elastic stress and strain; $e = S / E$
E	is the Young modulus of the material

Equation 3.15 presents the equality of the sums of strain energy density (SED) and complementary SED in the elastic-plastic and elastic solutions. Figure 3.3 presents a graphical representation of Neuber's rule. The shaded triangles in Figure 3.3 have equal areas and present the left- and right-hand sides of Equation 3.15, divided by 2. An unknown point on the Ramberg-Osgood stress-strain curve, referenced to actual elastic-plastic stress and strain, can be defined by equating the areas of these triangles.

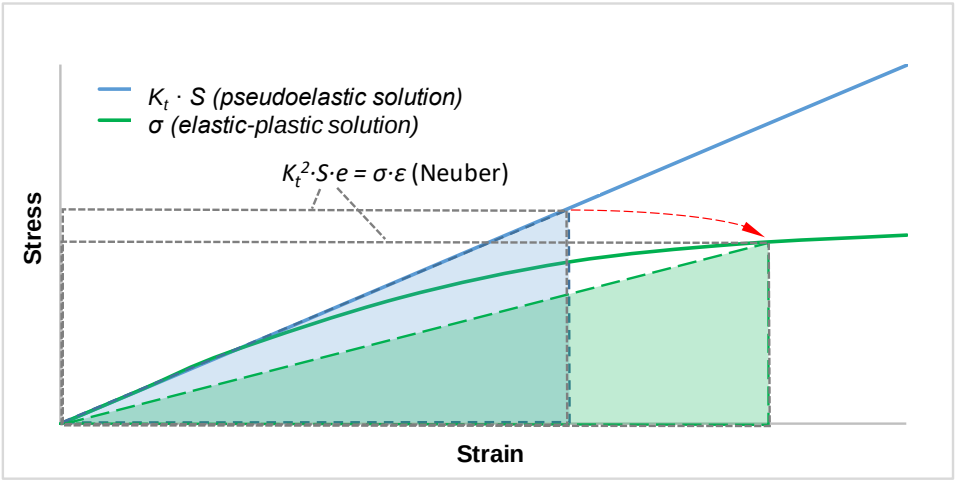

Figure 3.3: Graphical presentation of Neuber's rule. The shaded triangles with equivalent areas present the left- and right-hand sides of Equation 3.15, divided by 2.

Dowling (2013) remarks that Neuber's rule is an approximation which usually gives reasonable accuracy but has a tendency to overestimate. Overestimation of the notch strain by Neuber's rule was also noted by Moon et al. (1977) and Ellyin and Kujawski (1989b), who suggested that it overestimates notch strain for cyclic loading and that Glinka's rule gives more accurate results for predicting crack initiation life. To avoid overestimation caused by the Neuber's solution for a sharp notch, Sonsino (1982) has proposed a correction method for mild notch cases. The corrected solution uses the average of pseudoelastic strain and total strain defined using the Neuber's rule. In case of elastic-perfectly plastic material, the formulation, presented by Sonsino (1982), gives the result, which is between the Neuber's rule and the Glinka's rule presented later in this Chapter.

Use of the fatigue notch factor K_f in Neuber's rule

Topper et al. (1969) present the use of fatigue notch factor K_f instead of stress concentration factor K_t in the case of cyclic loading. The cyclic form of Equation 3.15 can be presented using fatigue notch factor K_f , which takes into account microstructural notch support effect:

$$\Delta\sigma\Delta\varepsilon = \frac{(K_f \Delta S)^2}{E} \tag{3.16}$$

where

$\Delta\sigma$ is the fatigue effective elastic-plastic stress range
$\Delta\varepsilon$ is the corresponding elastic-plastic strain range
ΔS is the elastic nominal stress range
Δe is the elastic nominal strain range; $\Delta e = \Delta S / E$
E is the Young's modulus of the material
K_f is the fatigue notch factor

Radaj et al. (2006) presented the implementation of the fatigue analysis using the Neuber's rule with the fatigue notch factor K_f, and this approach was chosen as the basis for the screening procedure.

Approximating the fatigue notch factor K_f

Fatigue notch factor K_f determines the value of the fatigue effective local stress, based on nominal elastic stress. Fatigue notch factor K_f can be calculated using stress concentration factor K_t and appropriate material parameters using, for example, the rules presented by Peterson (1974).

Alternatively, fatigue notch factor K_f can be obtained as a ratio of defined fatigue effective notch stress and corresponding elastic nominal stress:

$$K_f = \frac{\sigma}{S} \tag{3.17}$$

where

K_f is the fatigue notch factor
σ is the fatigue effective stress amplitude
S is the elastic nominal stress amplitude

According to the ENS method presented in Section 3.1.1 above, the fatigue effective local stress of the welded joint can be approximated by stress analysis using an appropriate fictitious notch radius. The fictitious notch radius r_f = 1 mm can be used for welded joints in as-welded condition as a worst-case assumption (Radaj et al., 2006). In this case, taking into account Equation 3.17, the value of fatigue notch factor K_f is equal to stress concentration factor K_t, defined using fictitious notch radius r_f = 1 mm:

$$K_f = K_t(r_f = 1 \text{ mm}) \tag{3.18}$$

Fricke and Bogdan (2001) noted that the ratio of ENS and structural stress correlates with the ratio of fatigue classes used in these approaches. The difference in the fatigue strengths used in the different methods applied to the same case can also be utilized to

approximate the corresponding fatigue notch factor K_f. Assuming that the accuracy of the methods, which are approved for use in standards and norms, has been verified by extensive testing, the fatigue life estimations of such methods should correspond to actual test results with a certain accuracy. Correspondingly, fatigue life estimations calculated by different methods for the same case must be close enough to each other. Based on this assumption, the fatigue notch factor of the welded joint can be approximated as the ratio of the fatigue classes used in the ENS approach and appropriate reference method. The idea of conversion between the nominal stress, structural stress, and ENS methods, based on the ratios of appropriate fatigue classes, is implemented in the German FKM-guideline for analytical strength assessment (Hänel et al., 2003).

Glinka's equivalent strain energy density (ESED) method

Glinka's rule (Molski & Glinka, 1981) is a widely-used alternative rule for the determination of the local notch stress and strain. This rule assumes the approximative equality of the SED at the notch root for linear elastic and elastic-plastic behavior. Figure 3.4 presents a graphical representation of Glinka's rule. An unknown point on the Ramberg-Osgood stress-strain curve, referenced to actual elastic-plastic stress and strain, can be defined by equating the area of the triangle, representing elastic strain energy density W^e, and the area under the stress-strain curve, representing elastic-plastic strain energy density W.

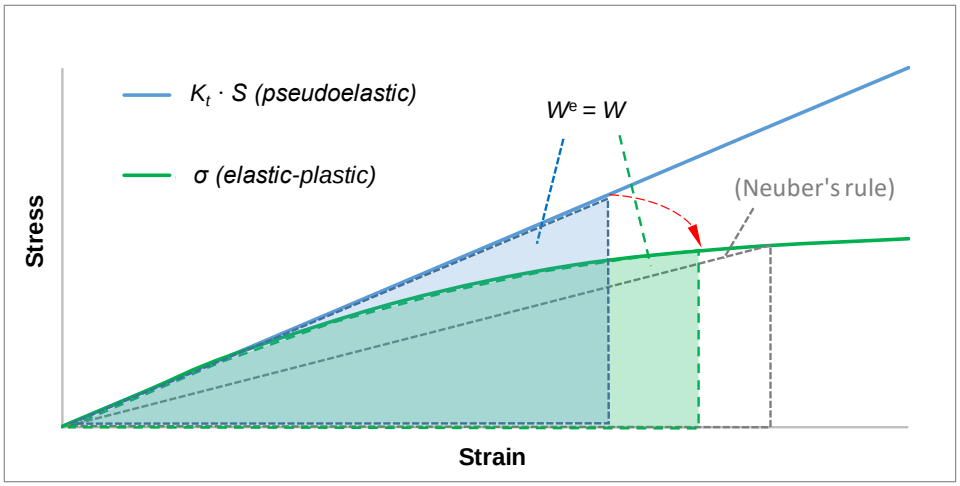

Figure 3.4: Graphical presentation of Glinka's equivalent strain energy density (ESED) method. The shaded equivalent areas represent elastic and elastic-plastic strain energy densities. The unshaded area of the triangle represents Neuber's rule for comparison.

Elastic strain energy density W^e and elastic-plastic strain energy density W can be calculated using Equations 3.19 and 3.20. The relation between local notch stress and

nominal elastic stress can be defined by the equality of the W^e and W, Equation 3.21 (Glinka, 1985):

$$W^e = \frac{(K_t S)^2}{2E} \tag{3.19}$$

$$W = \int \sigma \, d\varepsilon = \frac{\sigma^2}{2E} + \frac{\sigma}{n+1}\left(\frac{\sigma}{K}\right)^{\frac{1}{n}} \tag{3.20}$$

$$\frac{\sigma^2}{2E} + \frac{\sigma}{n+1}\left(\frac{\sigma}{K}\right)^{\frac{1}{n}} = \frac{(K_t S)^2}{2E} \tag{3.21}$$

where

W^e	is the elastic strain energy density
W	is the elastic-plastic strain energy density
σ	is the local elastic-plastic stress
E	is Young's modulus of the material
K, n	are monotonic strain-hardening coefficient and corresponding exponent
K_t	is the theoretical elastic stress concentration factor
S	is the nominal elastic stress

Singh et al. (1996) conclude that the ESED method or Glinka's rule tend to underestimate elastic-plastic notch stress and strain. The probability of underestimation increases if fatigue notch factor K_f is used in Glinka's rule instead of theoretical stress concentration factor K_t.

Generalized notch analysis

Ellyin and Kujawski (1989b) present a more generalized method to describe nonlinear stress-strain behavior at the notch. The method is applicable for monotonic and cyclic loading and for uniaxial and multiaxial states. It is based on the equality of the sum of the strain energy and complementary strain energy in theoretical linear-elastic or pseudoelastic solutions and actual elastic-plastic solutions. According to this method the relation between solutions can be presented as (Ellyin & Kujawski, 1989b):

$$\sigma_{ij}\varepsilon_{ij} = \sigma_{ij}^e \varepsilon_{ij}^e \tag{3.22}$$

or $$qW(\varepsilon) = W^e(\varepsilon) \tag{3.23}$$

where

q	is the factor dependent on the strain hardening of the material, value of which is bounded by 0.5 (for elastic-perfectly plastic material) and 1.0; $q = (1+n')/2$
n'	is the cyclic strain-hardening exponent

$W(\varepsilon)$ on actual elastic-plastic strain energy density
$W^{e}(\varepsilon)$ on theoretical linear-elastic strain energy density
σ_{ij} , ε_{ij} are the actual elastic-plastic stress and strain components
σ^{e}_{ij} , ε^{e}_{ij} are the theoretical linear-elastic stress and strain components

3.1.3 Energy based models

The primary area of application of energy-based, as well as strain-based, models is low cycle fatigue (LCF) with associated cyclic plasticity. The role of cyclic plasticity is often dominant, and some energy-based models are based on considerations of plastic work only, for example the Morrow and Garud models (Socie & Marquis, 2000). Ignoring elastic work limits the applicability of such models in the area of high cycle fatigue (HCF), which is the primary area of interest in this work. The effect of elastic work is taken into account in Liu's virtual strain energy-based model and in Ellyin's strain energy density (SED)-based model. Liu's model is a combination of the critical plane and energy-based models (Socie & Marquis, 2000). The required calculation of the virtual strain energy-based parameter for different planes limits the applicability of this method for global screening. Ellyin's SED-based model (Ellyin, 1989a) is presented in more detail below as the most interesting method for the content of this work.

Ellyin's SED-based model

The SED-based model presented by Ellyin (1989a) uses the sum of the range of plastic SED ΔW^{p} and positive portion of the range of elastic SED ΔW^{e+} as the parameter related to a fatigue damage:

$$\Delta W^{\text{Ellyin}} = \Delta W^{p} + \Delta W^{e+} \tag{3.24}$$

where

ΔW^{Ellyin} is the range of fatigue-effective SED in Ellyin's model
ΔW^{p} is the range of plastic SED
ΔW^{e+} is the positive portion of the range of elastic SED

Ellyin used the notation "total" in quotation marks for the damaging portion of the range of SED, defined by Equation 3.24. In this thesis, the notation "Ellyin" (ΔW^{Ellyin}) replaces the original notation "total" in order to prevent misunderstanding. The graphical representation of the damaging portion of the range of SED according to Ellyin's model is shown in Figure 3.5.

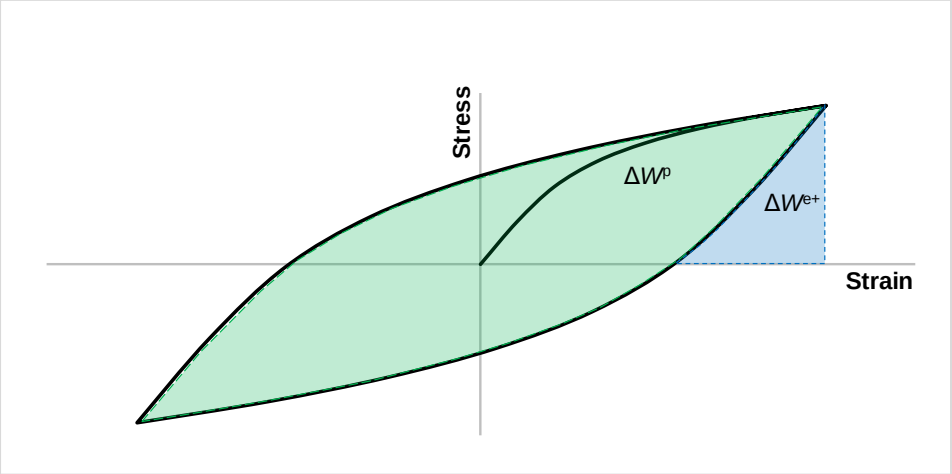

Figure 3.5: Damaging portion of the strain energy density (SED) according to Ellyin's model. The range of plastic SED is inside the hysteresis loop, and the triangle area under the right side of the hysteresis loop is the positive part of the range of elastic SED.

The plastic portion of the range of SED can be calculated by integration over the loading cycle (Ellyin, 1989a):

$$\Delta W^{\mathrm{p}} = \int_{\text{cycle}} \sigma_{ij} \mathrm{d}\varepsilon_{ij}^{\mathrm{p}} \tag{3.25}$$

where

ΔW^{p}	is the range of the plastic SED
σ_{ij}	is the stress tensor
$\varepsilon^{\mathrm{p}}{}_{ij}$	is the plastic portion of the strain tensor

The positive portion of the range of elastic SED, included in the damaging part of SED in Ellyin's model, can be calculated using principal normal components by the following equation (Ellyin & Xia, 1993):

$$\Delta W^{\mathrm{e+}} = \int_{\text{cycle}} \mathrm{H}(\sigma_i)\mathrm{H}(\mathrm{d}\varepsilon_i^{\mathrm{e}})\sigma_i \mathrm{d}\varepsilon_i^{\mathrm{e}} \tag{3.26}$$

where

$\Delta W^{\mathrm{e+}}$	is the positive part of the range of elastic SED
σ_i	is the principal stress components (i = 1, 2, 3)
$\varepsilon^{\mathrm{e}}{}_i$	is the elastic part of the principal strain components
$\mathrm{H}(x)$	is the Heaviside function; $\mathrm{H}(x) = 1$ for $x \geq 0$, $\mathrm{H}(x) = 0$ for $x < 0$

The failure criteria, based on damaging SED ΔW^{Ellyin} (Equation 3.24), consider varying severity of the different multiaxial states using the multiaxial constrain factor (MCF) ρ, according to the following equations (Ellyin & Xia, 1993):

$$\frac{\Delta W^{\text{Ellyin}}}{\rho} = \kappa_{\text{u}} N_{\text{f}}^{\alpha} + C_{\text{u}} \tag{3.27}$$

$$\rho = (1+\nu)\left[\frac{\varepsilon(T)}{\gamma(T)}\right]_{\gamma=\gamma_{max}} \tag{3.28}$$

where

ΔW^{Ellyin}	is the damaging portion of SED, defined by Equation 3.24
N_{f}	is a number of load cycles to failure
α	is the material constant, related to the slope of the fatigue curve
C_{u}	is the range of the elastic SED, which does not cause fatigue damage in the uniaxial test (corresponding to a fatigue limit)
κ_{u}	is the material constant defined by uniaxial test
ρ	is the multiaxial constraint factor (MCF), defined by Equation 3.28 at the moment when the shear strain γ in the direction 45° to the surface reaches the maximum; ρ = 1 for the uniaxial loading, ρ = 1 + ν for pure torsion and ρ = 1 - ν for equi-biaxial loading
ν	is effective Poisson's ratio
$\varepsilon(T)$	is the maximum in-plane principal strain at moment T
$\gamma(T)$	is the maximum shear strain in direction 45° to surface at moment T
T	is the moment when $\gamma = \gamma_{\text{max}}$

Considering the elastic and plastic portions of the SED makes Ellyin's model applicable for LCF and HCF. The positive elastic SED included in Ellyin's model takes into account the effect of the mean stress. The model is applicable for multiaxial stress states. The non-damaging portion of the SED related to a fatigue limit can also be taken into account, if necessary. These features provide an excellent basis for adapting Ellyin's SED-based model to screen critical points, considering the requirements and assumptions of standards and rules.

3.2 Effect of mean stress and residual stress

The mean stress has a significant effect on fatigue strength. The stress ratio R is often used to represent the mean stress:

$$R = \frac{\sigma_{\text{min}}}{\sigma_{\text{max}}} \tag{3.29}$$

where

σ_{min} is the minimum stress of the cycle
σ_{max} is the maximum stress of the cycle

The stress ratio of R = -1 corresponds to alternating loading, which is often used as a reference case in fatigue analysis of the parent metal. Increasing the stress ratio decreases fatigue strength up to a certain value, typically R = 0.5−0.7. According to Socie and Marquis (2000), on the area of R = 0.7−1.0 increasing the stress ratio has no additional effect, because full opening of the fatigue crack has already been achieved. FKM guidelines (Hänel et al., 2003) define the corresponding area when increasing the stress ratio has no additional effect as R = 0.5−1.0. The stress ratio R > 1.0 refers to the cycle with negative maximum and minimum stresses, which, in general, does not cause fatigue damage, and the mean stress has no effect.

In addition to the effect of external loading, the local residual stress at the point of interest must be considered in the mean stress and corresponding stress ratio. The influence of the residual stresses is very important, especially in the analysis of welded structures. Many authors have suggested that there are very high residual stresses acting in the weld area, up to the yield strength of the material (Fricke, 2013). The exact value of the residual stress at the welded area depends on several factors, and its reliable determination can, in some cases, be quite challenging. There is a reason for using the conservative assumptions related to the residual stress which are typical of many fatigue standards of welded structures. The residual stress equal to the yield stress of material is often assumed in these standards, and whole stress range is considered fully effective, independently of the external stress ratio. This procedure ignores the effect of mean stress, but mainly in a conservative way.

The effect of mean stress is included in some fatigue standards for welded structures by considering the lower detrimental effect of the compressive portion of the stress cycle. Standard SFS-EN 1993-1-9 (2005) permits the reduction of the compressive part of the stress range by a factor of 0.6 for non-welded and stress-relieved welded components. IIW recommendations (Hobbacher, 2008) allow the fatigue class (FAT) to be increased by an appropriate fatigue enhancement factor, which depends on effective stress ratio R and the type of structure under consideration. This factor varies between 1.0 and 1.6 for non-welded and stress-relieved components, and between 1.0 and 1.3 for small simple thin-walled elements with short welds. For complex welded structures with global residual stress, the fatigue enhancement factor is 1.0 and, consequently, increasing the fatigue strength is not allowed.

In local approaches, the residual stress can be taken into account in the set-up cycle as an additional local stress term in the theoretical fully elastic side of the following equation (Radaj et al., 2006):

$$\left(\frac{K_{\mathrm{f}}\Delta S}{1-R}+\sigma^{\mathrm{res}}\right)^2\frac{1}{E}=\sigma\varepsilon \tag{3.30}$$

where

K_{f}	is the fatigue notch factor
R	is the external stress ratio
ΔS	is the nominal stress range
E	is Young's modulus of the material
σ^{res}	is the residual stress
σ, ε	are the local elastic-plastic notch stress and strain

Local notch stress and strain at the upper point of the loading cycle can be calculated using the monotonic Ramberg-Osgood Equation 3.12 in combination with Equation 3.30. In the case of elastic stress range, $\Delta\sigma = K_f\,\Delta S \leq 2f_y$, the lower point of the loading cycle can be defined directly by subtracting the stress range from the upper point, defined above. Otherwise, the cyclic Ramberg-Osgood (Equation 3.13) in combination with the cyclic form of Neuber's rule (Equation 3.16) can be used. The defined upper and lower points of the loading cycle consider the effect of residual stress and elastic-plastic behavior. These points define the local mean stress of the cycle or true stress ratio, which can be used in the fatigue analysis. This way of considering the influence of the residual stress and local plasticity on the set-up cycle and kinematic work hardening is implemented in the 4R method (Björk et al., 2018). Accurate consideration of the actual mean stress, instead of assuming that the residual stress equals to the yield stress of the material, allows utilizing better fatigue resistance and avoids extra conservatism. However, this requires very careful consideration of the influence of various factors. For example, the significance of mean and residual stresses and, correspondingly, the benefit of thermal stress relief are much smaller under a variable-amplitude loading than under constant-amplitude loading (Sonsino 2009a).

3.3 Local plasticity

The nominal stress and structural stress methods are based on the elastic assumptions for stresses used in these methods. In fatigue standards for welded structures, the maximum allowed stress range is often limited to $1.5f_{\mathrm{y}}$ (f_{y} is the yield stress of the material) under the nominal stress method, and to $2.0f_{\mathrm{y}}$ under the structural stress method (Hobbacher, 2008). However, with these limitations, the corresponding local stresses can exceed the yield stresses of the material, and local plasticity may occur.

Pressure vessel standard SFS-EN 13445-3 (2017) includes the possibility of taking into account the local cyclic plasticity, if the calculated elastic structural stress range exceeds twice the yield strength of the material, $2.0f_{\mathrm{y}}$. The detrimental effect of cyclic plasticity can be taken into account in this case by increasing the computational elastic structural stress range, using the appropriate correction factor K_{e}:

$$\Delta\sigma_{\mathrm{corr}} = K_{\mathrm{e}}\Delta\sigma^{\mathrm{pse}} \tag{3.31}$$

$$K_{\mathrm{e}} = 1 + A_0\left(\frac{\Delta\sigma^{\mathrm{pse}}}{2f_{\mathrm{y}}} - 1\right) \tag{3.32}$$

where

K_{e}	is the elastic-plastic correction factor for the structural stress range
f_{y}	is the yield stress of the material
$\Delta\sigma^{\mathrm{pse}}$	is the computational pseudoelastic structural stress range, $\Delta\sigma^{\mathrm{pse}} > 2f_{\mathrm{y}}$
A_0	is a material parameter, $A_0 = 0.4{-}0.5$

The ENS method is based on the linear elastic assumption for the stress range without considering the elastic-plastic behavior (Fricke, 2013). The local non-linearity of the material behavior and micro-structural support effect at the notch is taken into account using the effective notch radius and corresponding master fatigue resistance curve (Hobbacher, 2008). A direct limitation of the maximum stress range is not present, but apparently the method is intended for use on the area which corresponds to the elastic structural stress outside the range of LCF.

The notch strain method is based on the local elastic-plastic strain and stress at the notch and takes into account the elastic-plastic behavior of material. The energy-based model developed by Ellyin (1989a) is based on the use of the elastic and plastic portions of SED, and consideration of elastic-plastic behavior is a basic feature of this model.

3.4 Cumulative damage and cycle counting methods

All the methods discussed above determine fatigue strength using the relation between an appropriate reference quantity and the corresponding fatigue life or number of loading cycles. The stress range of an appropriate level of accuracy, the strain range, or the range of SED can be used as reference quantity, depending on the method. In the case of constant amplitude loading, the allowable number of load cycles can be determined by direct comparison of an actual value of the appropriate reference quantity with the corresponding fatigue strength curve. The actual value can be defined by appropriate analysis or measurement. The calculation of the fatigue life in the case of variable amplitude loading is often based on the simple linear cumulative damage hypothesis known as the Palmgren-Miner rule. According to this rule, the partial damage D_i, caused by arbitrary loading block i of n_i cycles, is a ratio of the number of applied cycles and the number of allowable cycles with actual range:

$$D_i = \frac{n_i}{N_i} \tag{3.33}$$

where

D_i	is the partial damage caused by loading block i
n_i	is the actual number of cycles in block i

N_i is the allowable number of cycles for block i

The total damage D, caused by the whole loading history, is a sum of the partial damages D_i, caused by individual loading blocks i:

$$D = \sum D_i = \sum \frac{n_i}{N_i} \leq 1 \tag{3.34}$$

where

D is the total damage
and the other symbols are explained above (Equation 3.33)

According to Equation 3.34 the failure occurs if total damage D reaches the value of 1.0. In some cases, the value of total damage 1.0 is non-conservative and, for example, in the IIW recommendations (Hobbacher, 2008) the value of the total damage is limited to 0.5 or 1.0 depending on the type of multiaxial loading. The allowable value depends on the nature of the load, i.e. the constant or variable amplitude load as well as the proportionality or non-proportionality. The material can affect the allowable value as well. (Sonsino & Wiebesiek, 2007). The value of total damage 1.0 can be unsafe also in uniaxial cases, especially under variable amplitude loading as presented by Sonsino et al. (2004). However, the exact allowable value of the total damage is less critical in the screening based on a relative criterion, than in the calculations of a fatigue life.

The Palmgren-Miner linear cumulative damage hypothesis does not take into account a sequence effect of the loading blocks or cycles and interactions between events. Manson et al. (1967) present an alternative rule, which includes dividing the linear cumulative damage into two stages, crack initiation and crack propagation. Several non-linear cumulative damage models have been developed to avoid the shortcomings of linear models. However, the linear Palmgren-Miner rule is still the most used (Stephens et al., 2001).

Calculating the cumulative damage requires the individual load cycles to be extracted from the variable amplitude loading history. The cycling counting aspects have been presented very thoroughly by Köhler et al. (2017). In cases of uniaxial loading, the rainflow cycle counting method, presented by Matsuishi and Endo in 1968, is very widely known and most frequently used (Dowling, 2013). The graphical interpretation of this method is also called a “reservoir” counting method (Hobbacher, 2008).

The pressure vessel standard SFS-EN 13445-3 (2017) presents a simplified method for obtaining the cycles of uniaxial load history, consisting of a set of independent, regularly repeated individual loadings. The determination of the stress ranges and number of cycles of the loading events, based on the individual loadings, is presented in Figure 3.6. The individual loadings 1−4 are arranged from higher to smaller number of cycles n_1−n_4, and the stress ranges of the loading events A−D are defined as the sums of the appropriate stress ranges of the individual loadings 1−4. Table 4.2 in Section 4.6.3 presents the

corresponding determination of the stress ranges and number of cycles of the loading events using the stress ranges and number of cycles of the individual loadings.

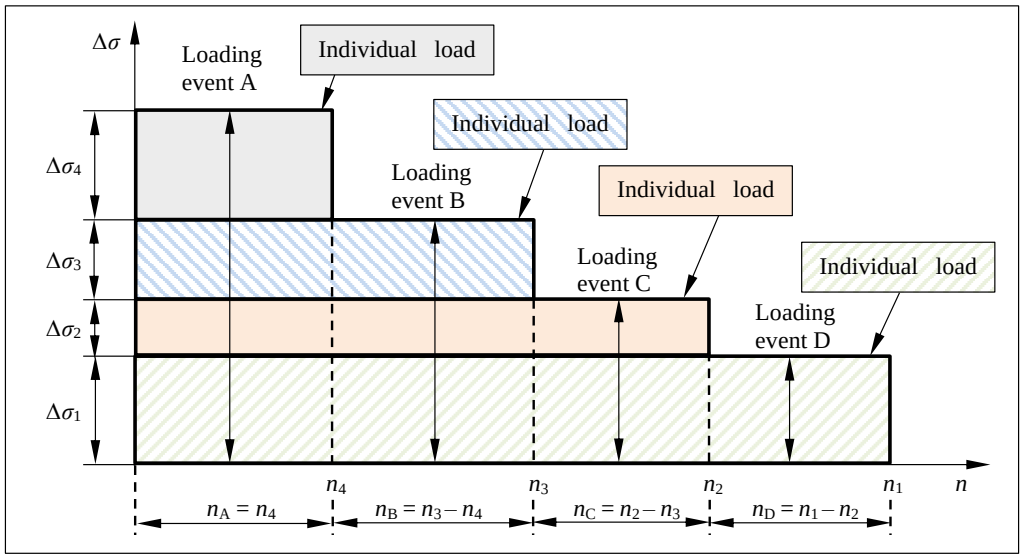

Figure 3.6: Simplified method of determining the stress ranges and number of cycles of the loading events of stress history, consisting of a set of independent individual loadings ($n_1 > n_2 > n_3 > n_4$). Vertical axis $\Delta\sigma$ is stress range and horizontal axis n is the number of loading cycles.

The same loading-related terms are used later in Chapter 4, which is a reason to clarify them in more detail. The term “load” is used primarily for individual loads or forces. The term “independent individual loading” is used for a more general entity, which may include one or more individual simultaneous loads acting at the same frequency and without a phase difference. The orientation of the principal stress axes is constant in this case and, consequently, one “individual loading” causes a proportional loading condition. Correspondingly, a combination of two or more proportional “independent individual loadings” can cause a non-proportional loading condition with varying orientation of the principal stress axis during the cycle. In the simpler case, where “loading” contains only one “load”, these terms mean the same thing. The word “independent” in this context refers to independence from other individual loadings or loads. The term “individual loading” corresponds to a separate load case in the linear static FE analysis, which may include several fully simultaneous loads. The term “loading event” refers to a combination of several individual loadings (or loads), the combined effect of which is decisive for fatigue analysis. The concept of “loading events” can be applied to loads in uniaxial cases only. In the general case, the concept is applicable only to stresses and only in a certain location. The term “loading event” corresponds in this case to a certain moment of combined stress history when a decisive situation for fatigue analysis arises at a certain point.

The cycle counting of the multiaxial non-proportional loading history must take into account the simultaneous independent varying of different components. Conventional uniaxial rainflow cycle counting is not applicable in these cases. The cycle counting methods applicable to non-proportional multiaxial loading are, for example, the Bannantine-Socie method (Bannantine & Socie, 1991) and the Wang-Brown method (Wang & Brown, 1996).

The Bannantine-Socie method relates to the application of a critical plane model. The critical plane model is based on the value of the fatigue damage which occurs on the most critical plane at the location of interest. The calculation of fatigue damages on several planes is required to obtain the most critical plane and corresponding maximum fatigue damage. One normal stress component or one shear component, depending on the expected damage model, must be considered on an individual plane, which enables the conventional uniaxial rainflow cycle counting method to be applied to the component of interest on the plane under study.

The Wang-Brown method determines the reversals of the multiaxial non-proportional loading history utilizing the relative equivalent strain. The calculation of the relative equivalent strain is based on the values of components related to the variable reference state. These relative components are the ranges between the chosen reference state and the current state of the loading history. Using the time histories of the relative components related to the certain reference state, the corresponding time history of the relative equivalent strain can be defined. The maximum value of the calculated relative equivalent strain defines the point of loading history at which the ranges of components related to the used reference state result in a higher corresponding equivalent range. This point of loading history is used in the next relative calculation as the new reference state. The use of relative ranges instead of absolute values prevents typical problems caused by equivalent-based procedures related to losing the sign. In some cases, the Wang-Brown method may fail to detect individual events, and improved versions of the method have been presented (Meggiolaro & de Castro, 2012). In addition, application of the method to peak-valley filtered data requires caution (Yanchukovich et al., 2019). However, in the comparison of the Bannantine-Socie and the Wang-Brown cycle counting methods, presented by Socie and Marquis (2000), both methods found the same major cycles and a difference was observed only in the definition of the smaller cycles.

3.5 Background summary

The nominal stress method enables the critical locations to be screened using quite a coarse element model. The challenges are to interpret the similarity of the real construction and the classified reference details, to determine the appropriate modified nominal stress and, in particular, to process the cases which cannot be compared with any classified details. The use of the detail-dependent fatigue strengths and its poor suitability for multiaxial cases also limit the applicability of the nominal stress method to global screening.

The structural stress method is less dependent on the geometry of structural detail. Due to an increased computational capacity, the accuracy of the element mesh required for the structural stress method is often achievable in a global model. However, the structural stress method is not applicable for analysis of the weld roots. The different rules for processing some types of locations pose an additional challenge in applying the method to global screening.

The effective notch stress (ENS) method enables analysis of a weld toe and weld root using a uniform procedure and the same fatigue strength. This method takes into account the local geometry of the weld and can, therefore, give more accurate results than the nominal and structural stress methods. Considering the local geometry requires very fine element meshes and accurate local models or sub-models, which is poorly suited to the global screening of critical locations. However, the exact effect of local geometry can be ignored in the preliminary screening, and the other benefits of the ENS method can be leveraged by computational conversion of the nominal or structural stresses to the level comparable with ENS. The converted stresses are close to the level of local accuracy, which improves their suitability for consideration of elastic-plastic behavior.

Ellyin's method, based on strain energy density (SED), can be applied to the screening of critical locations in a manner compatible with the ENS method. Ellyin's SED-based method is applicable for HCF and allows multiaxiality and possible elastic-plastic behavior to be considered. All general assumptions used in the conventional stress-based methods can be considered in the SED-based model, with significant extension and enhancement. The SED-based method is suitable for the implementation of the screening procedure.

4 Presentation of the developed screening method

A novel method applicable to screening the critical locations of a fatigue-loaded welded structure has been developed. The method is applicable to fatigue loading which contains a few independent proportional constant amplitude loads with different frequencies. The terms related to loading are explained in Section 3.4. The method considers a multiaxial state, a local plasticity, an actual mean stress, and the yield stresses of materials. It utilizes Ellyin's energy-based multiaxial fatigue model, modified for use in combination with the effective notch stress (ENS) approach. Approximating the ENS is based on the structural stresses at the weld toe and the nominal stresses at the weld throat, determined by the results of a linear elastic FE analysis. The computational efficiency required for global screening limits the reasonable size of the FE model, and using the plate element model is a primary assumption.

The developed screening method is compatible with the basic principles of the conventional standards and rules used for the fatigue analysis of welded structures. Its application requires compliance with certain rules and practices in relation to modelling and post-processing of results. A brief overview of the developed screening method is presented below, followed by a detailed description of each step within it.

The screening procedure consists of seven steps, including a loop to process each loading event of the case under investigation. The final step after the required loops is to calculate the total damage at different locations of a structure and estimate the corresponding fatigue lives.

The first step of the procedure involves creating the appropriate FE model, using the plate elements and element mesh applicable to determine structural or nominal stresses. The structural stresses at the weld toes and nominal stresses in the weld throats are basic input information for the screening procedure.

The second step involves calculating the ENS using the defined nominal and structural stresses. Conversion of the structural stresses to ENS is implemented using fatigue notch factor K_f, approximated as a ratio of the appropriate fatigue classes. A more accurate analysis can be obtained by more accurately determining the fatigue notch factor. Conversion of the different stress components is based on the relations presented by Radaj (2006). The conversion of both stress ranges and mean stresses to the ENS values can be implemented using the same procedure.

The loop starts in the third step of the procedure. The third step involves determining the most critical combination of the individual independent loads for each location included in the screening process. Determining the most critical combinations is based on the ranges of effective notch stress and inverse application of the Wang-Brown multiaxial cycle counting. The most critical combination of individual loads is defined for each location by the highest von Mises value, based on the ranges of ENS components. This part of the procedure determines the critical load combinations for each cycle of the

loading history under consideration. Cycles of the loading history are determined using a simplified procedure based on the summation of appropriate ranges.

Step four involves constructing a symmetric amplitude-based stress history for each location, using defined critical combinations of the individual loadings, and fitting these stress histories to the elastic region. The mean stress and residual stress can be considered when fitting the stress histories, if necessary. Several fitting iterations are used to increase accuracy. Fitted stress history is used to determine the strain energy density (SED) of the cycle, based on components of ENS and the corresponding strains using the plane stress assumption.

Calculating the SED for each location is the fifth step of the procedure. Determining SED is based on Ellyin's method, implemented with some modifications. Ellyin's original SED-based method considers plastic SED and the positive part of the elastic SED. The modified implementation enables compatibility with conventional standards and rules by partial inclusion of the compression in effective SED. The modified implementation includes an additional correction of the influence of the positive elastic mean stress. The effective value of the SED is calculated using the multiaxial constraint factor (MCF), according to Ellyin's model. The local plasticity is considered using an elastic-perfectly plastic (E-PP) material model, if necessary.

The sixth step of the procedure is the last step of the loop. The sixth step consists of estimating the fatigue damage using effective SED. The allowable number of cycles is defined by effective SED and SED-based fatigue strength, calculated from the uniaxial S-N curve of the ENS approach (FAT225), and used to calculate the partial damages.

The same loop to determine partial damages must be applied to every loading event related to the corresponding cycle of loading history. Finally, the total damage for every considered location is calculated by summing the defined partial damages after the last loop. The most critical locations can be screened by using the total damages or other corresponding quantities as relative usage factors, or number of cycles to failure, calculated from total damage.

Figure 4.1 presents the main steps of the developed screening procedure. Sections 4.1–4.7 present the developed screening method in more detail, including all steps and sub-steps in the same order as shown in Figure 4.1.

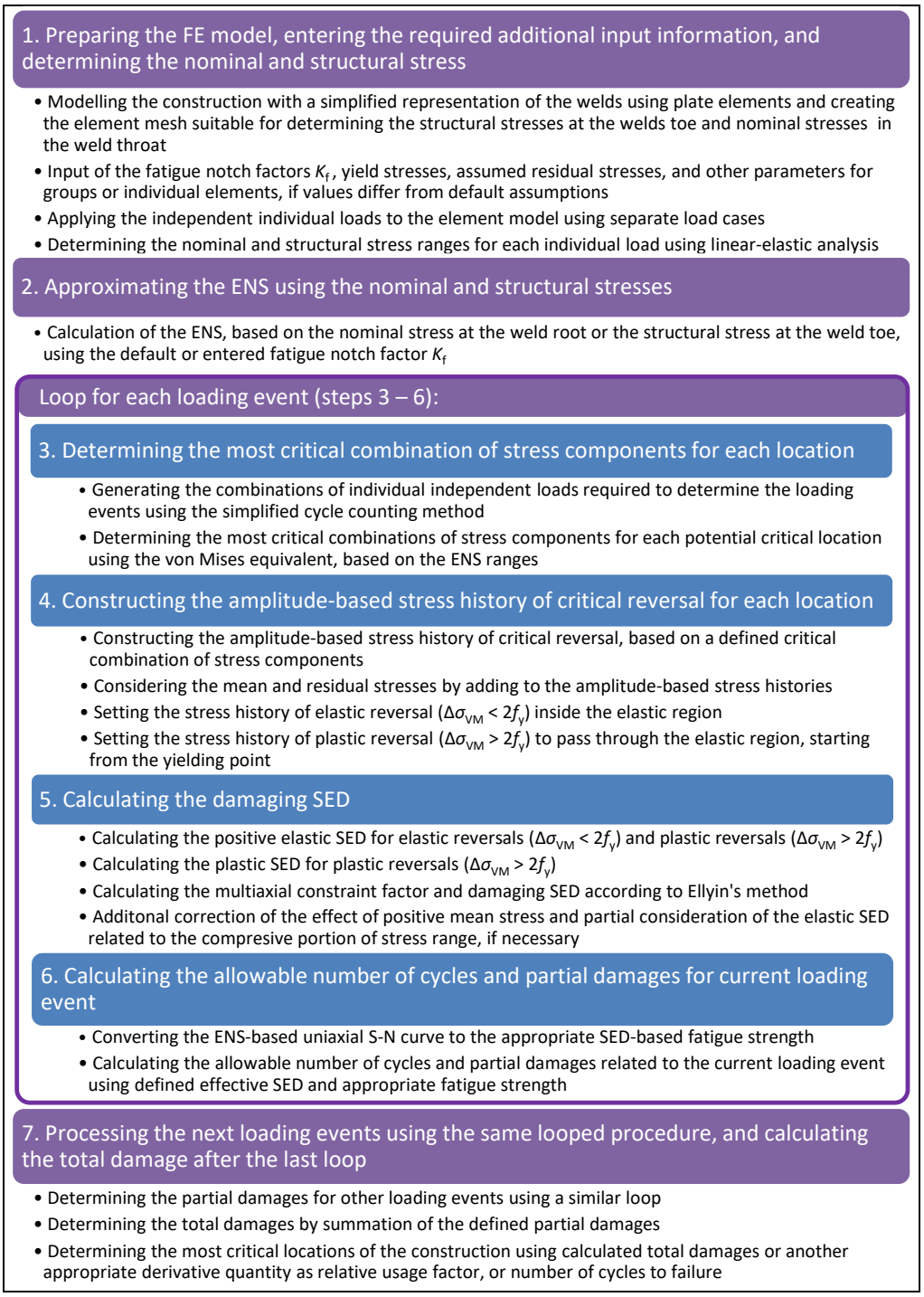

Figure 4.1: Main steps of the developed screening procedure to determine the critical locations of a welded structure, based on the strain energy density method.

4.1 Determining the nominal and structural stress using the FE model

Applying the developed screening method requires the use of FE model, which is suitable for approximating the structural stresses at the weld toes and nominal stresses in the weld throats with an appropriate degree of accuracy. This requirement can be met by different solutions, using exact determination or approximative methods. Using the mesh-insensitive methods with a constant element size at the areas adjacent to the weld toes is useful in decreasing modelling effort. Including the welds in the FE model can be simply done by using plate elements or other techniques suitable for determining nominal stresses.

4.1.1 Element mesh for the approximation of structural stress

Areas of the structure adjacent to the welds must be modelled using a mesh which is suitable for approximation of the structural stresses. Based on the results of the calibration models investigated in this thesis, the results of element corners adjacent to the weld give quite an accurate approximation of the structural stress. Five-millimeter parabolic plate elements were used in these models of the test specimens, with material thickness varying between 3 and 6 mm. Achieved accuracy is assumed when using this element size with thicker materials. The chosen element size is suitable for the mesh-size-insensitive determination of structural stresses based on nodal or sectional forces and moments, as presented by Fermér et al. (1998), Fermér and Svensson (2001), and Dong (2001). The element size of 5 mm is also applicable for the accurate determination of the structural stress on the edge of details (hot spot Type B, Figure 3.1) by extrapolation, which is an additional benefit for a more accurate analysis after preliminary screening.

Two principal cases related to the location of the element attached to the weld can be specified:

- An element is attached to a continuous weld: the structural stress on the edge of the element can be approximated by averaging the results of the two corners of the element attached to the weld.
- An element is attached to the end of the weld: the structural stress can be approximated directly by the results at one corner of the element.

The default assumption for elements adjacent to the weld toe is the first case until another is specified. In the second case, the information about the corner of the element attached to the end of the weld can be specified directly in the FE model. In this case, the structural stress can be approximated directly from the results of the individual corner of the element without averaging. Depending on the case, the same procedure defines all planar stress components (perpendicular $\sigma_{\perp}$, longitudinal $\sigma_{\parallel}$, and in-plane shear τ) of each element attached to the weld toe, either as the average stress at two corners of the element or directly as the stress at one corner of the element.

4.1.2 Modelling the welds and approximating the nominal stress

The screening procedure uses the nominal stress in the weld throat to obtain the most critical welds. The inclusion of the welds in the FE model is useful in determining the nominal stress in the weld throat and implementation of the screening procedure. Modelling and postprocessing effort can be decreased by using the plate elements to simplify the welds. However, in some cases, the simplified modelling of the welds using plate elements requires additional adjustment of the bending stiffness. The results of a separate local model of the joint under investigation or general recommendations, for example rules DNV-GL (2016), can be used for this adjustment. Additionally, the influence of the implemented correction of bending stiffness must be considered when determining the nominal stress at the weld root.

The allowed level of weld simplification depends on the dimensional properties of details and the required accuracy of the screening results. The reduction of the width or the thickness of attachment to line without physical thickness can significantly affect results in some cases. The separate rigid links between a simplified weld, modelled by one plate element, and the area of the attachment of the weld to the base metal can be used in FE models to avoid this problem, if necessary. Recommendations for weld modelling using plate elements in combination with rigid links or multipoint constraints are presented by Niemi (2018) and Fricke (2013). This solution was implemented in FE models of tested specimens, as presented in Appendix B (Figures B.6 and B.7). Using rigid links or multipoint constraints enables an accurate idealization of the welds with realistic stiffness, but modelling effort limits the applicability of this method to the overall screening of large structures. In some cases, additional correction of the weld area around the corner of the attachment is required. This correction can be implemented according to Fricke (2013), using the correction factor K_w related to the ratio of weld areas.

Modelling the welds by plate elements allows the approximation of the nominal stresses at the weld root directly by stresses at the element centroid on the appropriate surface. This procedure obtains the nominal stresses at the weld root of each weld element: normal component $\sigma_\perp$, longitudinal component $\sigma_\parallel$, in-plane shear component $\tau_\parallel$, and transversal shear component $\tau_\perp$, which must also be considered in the analysis of the weld throat (see Figure 4.2). For technical reasons explained in Section 4.3, the components $\sigma_\perp$ and $\tau_\perp$ are kept separate at this stage and processed independently, both as transversal components, using the same procedure.

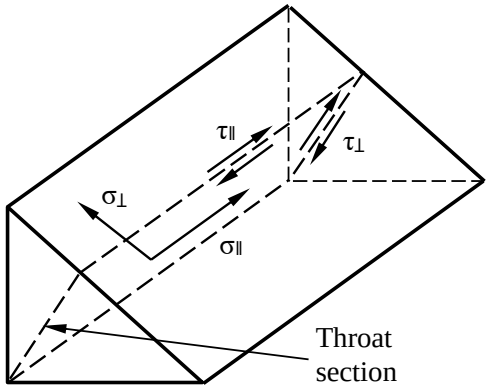

Figure 4.2: Stress components of the fillet weld.

4.1.3 **Additional input information for the screening procedure**

The input information needed to implement the screening procedure can be included directly in the FE model. The welds and areas adjacent to the weld must be grouped and separated from one another and from the rest of the model to facilitate post-processing. Appropriate information can be input for these groups of elements or for individual elements, if necessary, and utilized in the screening procedure, together with the results of the FE analysis. Required input information includes:

- List or group of elements attached to a weld toe
  - In the common case of elements adjacent to continuous welds, the averaging of the element corner results can be used as a default assumption without additional declaration
  - A preliminary approximation of the perpendicular fatigue notch factor K_f, based on the ratio of the fatigue classes, can be used as the default assumption for this group without additional declaration
  - The identification number of the element corner located at the end of the weld or other corresponding structural discontinuity must be used for direct approximation of the stress components without averaging
- List or group of elements presenting simplified welds
  - In the common case of continuous welds, the results from the appropriate surface at the element centroid can be used for the approximation of the nominal stress as a default assumption without additional declaration

  - A preliminary approximation of the perpendicular fatigue notch factor K_f, based on the ratio of the fatigue classes, can be used as the default assumption for this group without additional declaration
  - The additional cross-section correction factor K_w for special cases with the weld around a stiffener termination or other corresponding structural discontinuity
- General input information for both groups listed above: elements adjacent to the weld and elements presenting simplified welds
  - More accurate value of the fatigue notch factor K_f, if necessary
  - Yield stress of material, if necessary and available
  - Residual stress, if necessary and available

Approximation of the perpendicular fatigue notch factor K_f, based on the ratio of fatigue classes, is explained in Section 4.2.

4.1.4 Modelling the loading

The developed method is intended for the screening of critical locations under a combination of independent constant amplitude loads acting with a certain frequency. All the simultaneously acting proportional loads that are related to the same individual loading must be included in one load case. Each independent loading must be defined for the FE analysis as a separate individual load case. These separate load cases will be included in the screening procedure for quasi-static combination and determination of the stress histories, as presented in Figure 4.3. The processing of the loads and stress histories is presented in Sections 4.3 and 4.4 of this chapter. At this stage of the screening procedure, only the separate individual load cases related to the independent loadings must be generated for linear elastic FE analysis. The terms related to loads and loading are described above in Section 3.4.

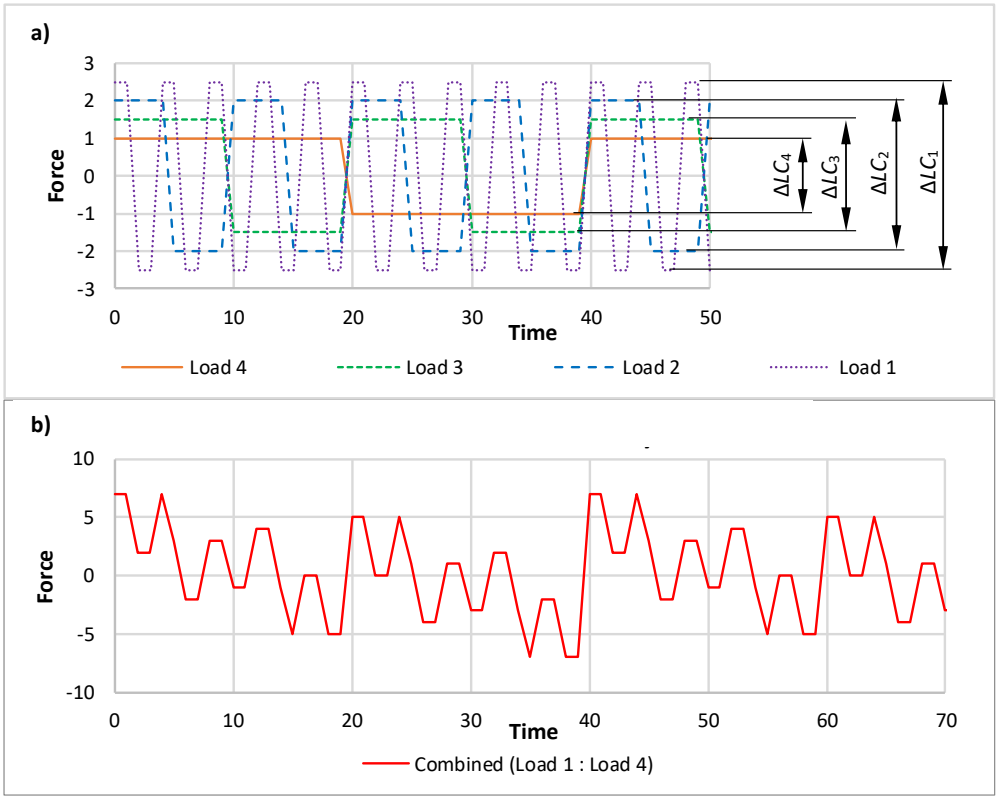

Figure 4.3: Example of the four independent constant amplitude loads (a), corresponding load ranges to generate the separate load cases and combined load history (b).

The screening procedure uses the ranges and possible mean stresses of the individual load cases to process the stress history. The individual independent loads can be defined using corresponding ranges and mean values, either directly or by loading pairs, for further calculation of the ranges and mean values after the analysis.

4.1.5 The results of the first step of the procedure

The results of this stage of the screening procedure are defined approximative values of the structural stresses and nominal stresses at each location included in the area of interest. Three components of structural stress must be obtained for each location adjacent to the weld toe:

- perpendicular component $\sigma_{\perp}$
- longitudinal component $\sigma_{\parallel}$
- in-plane shear component $\tau_{\parallel}$

Four components of nominal stress must be obtained for the weld root of each weld element (see Figure 4.2):

- perpendicular component $\sigma_\perp$
- longitudinal component $\sigma_\parallel$
- in-plane shear component $\tau_\parallel$
- transversal shear component $\tau_\perp$

These components must be obtained for each independent load case separately in a format applicable to determining the stress ranges or amplitudes and mean stresses, if necessary.

The following additional information for appropriate locations can be included in the FE-model:

- more accurate value of the fatigue notch factor K_f, if necessary
- yield stress of the material, if necessary and available
- residual stress, if necessary and available

4.2 Approximating the effective notch stresses

The ENS is approximated using structural or nominal stresses, defined by the FE analysis, and appropriate fatigue notch factors K_f. Determining structural and nominal stresses by the results of the linear elastic FE analysis is presented in the previous section. At this stage of the screening procedure, it is assumed that the required structural stresses at the weld toes and nominal stress components in the weld throat are obtained with appropriate accuracy:

- Perpendicular $\sigma_\perp$, longitudinal $\sigma_\parallel$, and in-plane shear $\tau_\parallel$ components for elements adjacent to the weld toes
- Normal component $\sigma_\perp$, longitudinal component $\sigma_\parallel$, in-plane shear component $\tau_\parallel$, and additionally transversal shear component $\tau_\perp$ as presented in Section 4.1 (see Figure 4.2)

Based on Equations 3.4–3.6, the approximation of the ENS components from appropriate structural or nominal stresses can be implemented using known fatigue notch factor $K_{f\perp}$ of a transversal stress component $\sigma_\perp$:

$$\sigma_\perp^{\mathrm{ENS}} = K_{f\perp}\sigma_\perp \tag{4.1}$$

$$\sigma_\parallel^{\mathrm{ENS}} = \sigma_\parallel + \nu\sigma_\perp(K_{f\perp} - 1) \tag{4.2}$$

$$\tau_{\parallel}^{\mathrm{ENS}} = K_{\mathrm{f}\tau} \cdot \tau_{\parallel} = \frac{1}{2}(K_{\mathrm{f}\perp} + 1)\tau_{\parallel} \tag{4.3}$$

where

$K_{\mathrm{f}\perp}$ is the known fatigue notch factor referring to the transversal nominal or structural stresses $\sigma_{\perp}$

$\sigma_{\perp}$, $\sigma_{\parallel}$, $\tau_{\parallel}$ are reference stress components in the coordinate system aligned to the weld

ν is Poisson's constant

$K_{\mathrm{f}\tau}$ is the fatigue notch factor referring to stress component $\tau_{\parallel}$

Equation 4.3 presents the approximation of the fatigue notch factor for in-plane shear $K_{\mathrm{f}\tau}$ from known fatigue notch factor $K_{\mathrm{f}\perp}$ of a transversal normal stress component, as presented by Radaj et al. (2006):

$$K_{\mathrm{f}\tau} = \frac{1}{2}(K_{\mathrm{f}\perp} + 1) \tag{4.4}$$

where the used symbols are explained above (see Equation 4.3).

In the processing of nominal stresses of welds, Equation 4.1 applies independently to normal component $\sigma_{\perp}$ and transversal shear component $\tau_{\perp}$.

The approximative value of the transversal fatigue notch factor $K_{\mathrm{f}\perp}$ can be estimated for screening purposes from the ratio of the fatigue strengths of the corresponding structural or nominal case and the ENS-based fatigue strength. After a preliminary screening, a more accurate determination of the transversal fatigue notch factor can be used for the detected point of interest, if necessary. A separate local element model with fine solid-element mesh can be used for this purpose.

4.2.1 Estimating the fatigue notch factor by ratio of fatigue classes

The value of the fatigue notch factor $K_{\mathrm{f}\perp}$ of a transversal normal stress component related to the used reference stress can be estimated as the ratio of the appropriate known fatigue classes:

$$K_{\mathrm{f}\perp}(\mathrm{ref}) = \frac{FAT^{\mathrm{ENS}}}{FAT^{\mathrm{ref}}} \tag{4.5}$$

where

$K_{\mathrm{f}\perp}(\mathrm{ref})$ is the transversal fatigue notch factor related to reference stress

FAT^{ENS} is the fatigue class (fatigue strength at $2 \cdot 10^6$ cycles) related to the ENS

FAT^{ref} is the fatigue class related to the used reference stress and case

According to IIW recommendations (Hobbacher, 2008), the fatigue classes are 225 MPa for ENS stress, 90–100 MPa for hot spot (HS) or structural stresses, and 36–50 MPa for nominal stresses of the weld throat at the weld root. Based on these fatigue classes, the transversal fatigue notch factors for screening analysis can be estimated as follows:

$$K_{f\perp}(\mathrm{HS}) = \frac{FAT^{\mathrm{ENS}}}{FAT^{\mathrm{HS}}} = \frac{225}{(90 \ldots 100)} = 2.5 \ldots 2.25$$

$$K_{f\perp}(\mathrm{root}) = \frac{FAT^{\mathrm{ENS}}}{FAT^{\mathrm{root}}} = \frac{225}{(36 \ldots 50)} = 6.25 \ldots 4.5$$

where

$K_{f\perp}$(HS)	is the transversal fatigue notch factor related to the HS or structural stress at the weld toe
$K_{f\perp}$(root)	is the transversal fatigue notch factor related to the nominal stress of the weld throat at the weld root
FAT^{ENS}	is the fatigue class for the ENS
FAT^{HS}	is the fatigue class for the HS or structural stress
FAT^{root}	is the fatigue class for the weld root, based on the nominal stresses of the weld throat

Accordingly, the fatigue notch factor $K_{f\perp}$(HS) = 2.5 can be used as the initial default value to approximate the ENS at the weld toe and $K_{f\perp}$(root) = 5.0 for the weld root. The values correspond to the use of the fatigue classes FAT90 for structural stress at the weld toe and FAT45 for nominal stress at the weld root. These values can be used as preliminary assumptions and replaced by more accurate values at the areas of interest detected by preliminary screening, if necessary.

4.2.2 The results of the second step of the procedure

The results of this stage of the screening procedure are defined approximative values of the ENS at each location included in the area of interest. Three components of the ENS must be obtained for each location attached to the weld toe and weld root:

- perpendicular component $\sigma_\perp$
- longitudinal component $\sigma_\parallel$
- in-plane shear component $\tau_\parallel$

Additionally, to be compatible with common standards and rules, the fourth ENS component, transversal shear $\tau_\perp$, must be defined for the weld root of each weld element.

These components must be obtained for each independent load case separately in a form suitable to determine the stress ranges or amplitudes and mean stresses, if necessary. The

following steps of the screening procedure utilize the stress ranges or amplitudes and mean stresses calculated using these converted components.

4.3 Determining the most critical load combinations

Determining the most critical load combination is the third step of the screening procedure. This step starts the processing loop, which includes steps 3–6 of the procedure. The loop must be repeated for each existing loading event.

4.3.1 Determining the loading cycles using the simplified method

Critical locations under a combination of the constant amplitude loads can be screened using the simplified method to determine stress ranges according to standard SFS-EN 13445-3 (2017), as presented in Section 3.4. The simplified method defines the load cycles directly as combinations of known separate load ranges or amplitudes. However, this method defines the cycles of the stress history directly related to the load history. In multiaxial cases, the different relation between external loading and the histories of the individual stress components must be considered.

Under a combination of constant amplitude loads, the histories of the stress components include all possible combinations of positive or negative load amplitudes (see Figure 4.4). On the other hand, the ratio between stress components is fixed in the individual load, and the selected direction of the load amplitude must be applied to all related stress components simultaneously. The following equation presents how the stress cycle of the individual component σ is obtained, based on a combination of the known individual constant amplitude loads:

$$\sigma_{ij}^{\mathrm{comb}} = \sum_{p=1}^{p_{\max}} K(p) \cdot \sigma_{ij}(p) \tag{4.6}$$

where

- $\sigma_{ij}^{\mathrm{comb}}$ are amplitudes of the stress components under a combination of the independent constant amplitude loads
- $p_{\max}$ is the number of the considered independent load cases
- $\sigma_{ij}(p)$ is the amplitude of the stress component under individual independent constant amplitude load p
- $K(p)$ is the combination factor, which defines the phase of the individual load p in the combination. The same value of the coefficient $K(p)$ must be used for each stress component related to the individual load case p; $K(p)$ = -1 or 1

4.3.2 Determining the critical combination of stress components

The load ranges or amplitudes forming the cycle are known when the simplified method according to standard SFS-EN 13445-3 (2017) is used. The issue in multiaxial cases is to define the point of the cycle related to a most critical or determinative combination of the included components. The critical combination of the component amplitudes during the cycle can be defined using the von Mises equivalent amplitude by analogy with the Wang-Brown multiaxial cycle counting method, based on the equivalent strain (Wang & Brown, 1996). The processing of loading, based on the stress ranges, corresponds to the use of peak-valley filtered data. This solution is common in quasi-static FE analysis but it may complicate defining the cycles when applying the Wang-Brown cycle counting method (Yanchukovich et al., 2019). However, in the screening procedure the cycles are already defined using the simplified calculation method and the Wang-Brown method has been utilized only to maximize the range of the known cycle.

Combining the components and obtaining the determinative combination is presented in Figure 4.4. The left-hand side of the figure is a visual representation of Equation 4.6, applied separately to three separate stress components. The right-hand side presents the corresponding von Mises equivalent amplitude used to obtain the determinative combination of these components. Steps 0–1 in Figure 4.4 present the unloaded condition, and Steps 2–3 include only one applied load with lower frequency (LC4). Steps 4–5 present two alternative conditions formed by the fluctuation of the second load (LC3) in combination with the applied first load (LC4). Correspondingly, the fluctuation of the next load (LC2) is added at Steps 6–7 and the last load, with the highest frequency (LC1), is added at Steps 8–9. In this example, the determinative combination related to the one reversal is +LC4-LC3+LC2+LC1, presented by the yellow curve. The combined loading history of the cycle (Figure 4.3) includes all these combinations. For different locations of the construction, the determinative combination of the stress components occurs at different points of the cycle. The determinative combination must be obtained separately for each location of the construction under consideration.

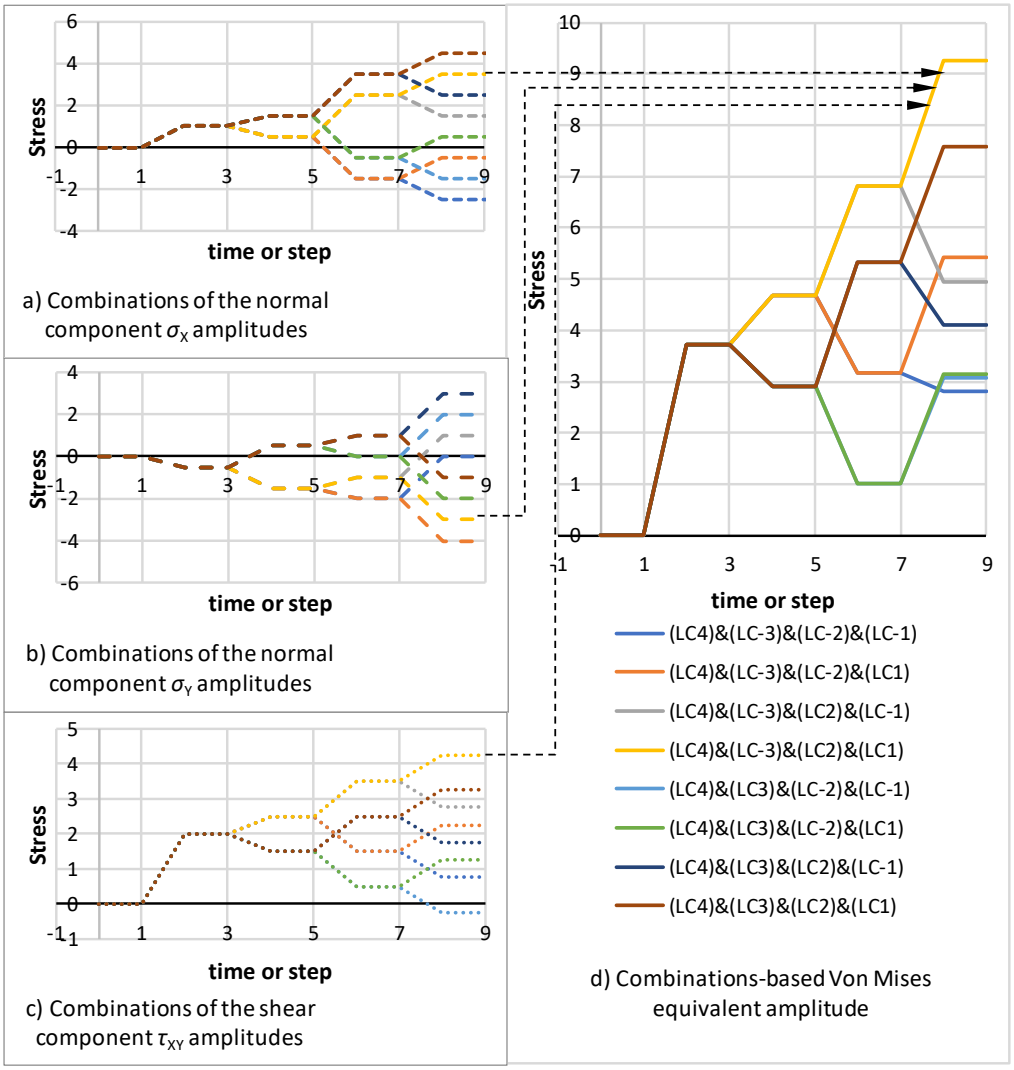

Figure 4.4: Example of the cycle formed by four independent constant amplitude loads. The possible combinations of the stress component are presented on the left-hand side of the figure (a–c). The right-hand side of the figure presents the corresponding von Mises equivalent amplitude (d). The yellow curve represents the determinative combination of the stress amplitudes in this example.

Using the von Mises equivalent and, correspondingly, excluding the hydrostatic stress from obtaining the determinative combination is debateable. This analogy with the Wang-Brown multiaxial cycle counting method was chosen because it is quite well-known and considers all components, instead of reducing the multiaxial history to uniaxial projection. The critical combination of stress components can be determined using alternative criteria to the von Mises equivalent, as presented below.

The developed screening procedure utilizes the SED approach, which considers the distortion energy associated with von Mises stress and energy of the volumetric changes associated with hydrostatic stress. The elastic SED of a proportional case starting from zero can be calculated using the following equation (Ellyin, 1989a):

$$W^{\mathrm{e}} = W^{\mathrm{D}} + W^{\mathrm{V}} = \frac{1}{6E}\{3(1+\nu)s_{ij}s_{ij} + (1-2\nu)(\sigma_{kk})^2\} \tag{4.7}$$

where

W^{e} is the total elastic energy
W^{D} is the elastic energy of distortion
W^{V} is the elastic energy of volumetric change
E is Young's modulus of the material
ν is Poisson's ratio
s_{ij} is the deviatoric stress tensor
σ_{kk} is the sum of the normal stress components

The first term of Equation 4.7 presents the elastic energy of distortion and is related to the von Mises stress. The second term presents the elastic energy of the volumetric change and is related to hydrostatic stress. These parts of a total SED can be presented using the following equations (Timoshenko, 1983):

$$W^{\mathrm{D}} = \frac{1+\nu}{3E}(\sigma_{\mathrm{VM}})^2 \tag{4.8}$$

$$W^{\mathrm{V}} = \frac{1-2\nu}{6E}(3\sigma_{\mathrm{H}})^2 \tag{4.9}$$

where

σ_{VM} is the equivalent von Mises stress; $(\sigma_{\mathrm{VM}})^2 = 3/2\ s_{ij}s_{ij}$
σ_{H} is the hydrostatic stress, defined as the average of three normal components
and the other symbols are explained above

One more possible alternative means to determine the critical combination of stress components is to combine the von Mises stress and hydrostatic stress with an appropriate scale factor, defined by analogy with the method presented by Ottosen et al. (2008).

The most critical combination in these cases can be defined by the maximum value of the total SED or parameter based on an appropriate combination of the von Mises and hydrostatic stresses. Considering the hydrostatic stress in determining the critical combination of the stress components by using total energy (Equation 4.7) or a corresponding stress-based parameter, instead of just the von Mises equivalent, can be more reasonable when the SED-based approach is used. The presented alternative criteria

require additional study but using them does not change the procedure. These criteria can be included in the same screening procedure as alternatives to the von Mises equivalent.

A computationally efficient analytical solution to define the most critical combination of stress components has not yet been found. Utilizing the built-in tools of conventional FE software to generate all possible combinations of the partial load cases is quite an effective solution of this problem. The most critical combination of stress components can be obtained by the maximum value of the von Mises equivalent amplitude or other appropriate parameter, for example total energy, using an envelope over all generated combinations. The information about the combination factors $K(p)$ (see Equation 4.6), used in the generation of the most critical load combination, must be kept for later use. Determining the most critical combination using overall amplitude, including all the individual loadings, ignores the non-proportionality. However, this is presumed to be acceptable considering the approximative purpose of the screening.

4.3.3 Considering the transversal shear at the weld throat

Compatibility with common standards requires consideration of the transversal shear stress at the weld throats. Common standards and rules consider the transversal shear component by using the resultant-based nominal stress of the weld throat $\sigma_{w\perp}$ instead of just a normal component $\sigma_\perp$ (see Figure 4.2). Calculating the nominal stress of the weld throat $\sigma_{w\perp}$ as a resultant of the normal stress $\sigma_\perp$ and transversal shear stress $\tau_\perp$ is presented, for example, by Fricke (2013):

$$\sigma_{w\perp} = \sqrt{{\sigma_\perp}^2 + {\tau_\perp}^2} \tag{4.10}$$

where

$\sigma_{w\perp}$ is the nominal resultant stress of the weld throat
$\sigma_\perp$ is the normal stress of the weld throat
$\tau_\perp$ is the transversal shear stress of the weld throat

Using the resultant stress $\sigma_{w\perp}$, defined by Equation 4.10, instead of just normal component $\sigma_\perp$, confirms compatibility with common standards, rules, and recommendations. However, using Equation 4.10 to calculate the resultant stress loses the sign of normal stress. This does not cause any problem in standard uniaxial calculation with assumed fully effective stress ranges; however, in other cases, it is unsuitable. The transversal shear can be considered for this reason on the assumption that a possible shear component increases the influence of an actual normal component, and the sign of the normal component remains. This solution maximizes the range or amplitude of resultant stress to ensure compatibility with common standard rules, based on the assumption of fully effective stress ranges. Simultaneously saving the original sign of the normal component enables appropriate combining with other components in a multiaxial state. However, considering the mean stresses complicates the application of this solution.

The screening procedure utilizes Equation 4.10 using the stress components at the root side of the plate elements representing welds in the FE model. These stress components include a combination of linear membrane and bending stresses, considering correct signs of the components at the root side. The calculated resultant stress $\sigma_{w\perp}$ replaces the normal component $\sigma_{\perp}$, keeps the same input formats for the weld toe and weld root, and allows the same procedure to be used for both cases.

4.3.4 The results of the third step of the procedure

Third step of the screening procedure is a part of the loop, which must be repeated for each loading event. The results of this stage of the screening procedure are critical combinations of the amplitudes of separate load cases defined for each location of interest. The information about signs applied to the separate load cases to achieve the critical combination can be saved as a group of appropriate positive or negative unit combination factors $K_{crit}(p)$ for later use. Critical combinations must be obtained for each loading event included in the simplified determination of the load cycles:

- The results of the first run of the loop are p pieces of combination factors $K_{crit}(p)$ for critical reversal, including all separate independent loads
- The results of the second run of the loop are p-1 pieces of combination factors $K_{crit}(p)$ for critical reversal, including all separate loads except the load of lowest frequency
- The results of the third run of the loop are p-2 pieces of combination factors $K_{crit}(p)$ for critical reversal, including all separate loads except two loads of lowest and the next lower frequency, and so on, until only one load of highest frequency is left

4.4 Constructing the stress history of critical reversal

4.4.1 Constructing the amplitude-based alternating stress history

Constructing the anti-symmetric amplitude-based alternating stress history of the critical reversal of current loading event is the first step in this part of the screening algorithm. The anti-symmetric amplitude-based stress history based on a combination of p independent separate load cases includes $2p$+1 points. The midpoint of this alternating stress history (T = 0) is zero, and the other points can be defined by adding or subtracting appropriate amplitudes. Only those stress histories related to the critical combination of amplitudes of separate independent load cases are needed in a further screening procedure. This stress history of the critical reversal must be constructed using the combination factors $K_{crit}(p)$, defined for the most critical combination of amplitudes in Section 4.3.

The following equation defines the first point of the critical reversal using the amplitudes related to separate independent load cases and combination factors $K_{crit}(p)$:

$$\sigma_{ij}(T = -p_{\max}) = \sigma_{ij}(T = 0) - \sum_{p=1}^{p_{\max}} \left(K_{\text{crit}}(p) \cdot \sigma_{ij}(p) \right) \tag{4.11}$$

where

$\sigma_{ij}(T = -p_{max})$	are stress components at the first point of the stress history, marked as time or step $T = -p_{max}$
$\sigma_{ij}(T = 0)$	are stress components at the midpoint of the stress history; for anti-symmetric alternating loading the values are zero
p_{max}	is the number of independent load cases included in the reversal under consideration
$\sigma_{ij}(p)$	are the amplitude of the stress components under individual independent constant amplitude load p
$K_{crit}(p)$	is the combination factor of critical reversal defined in the previous step of the procedure (Section 4.3); $K_{crit}(p)$ = -1 or 1

The next point of the anti-symmetric alternating stress history can be defined by adding the appropriate amplitude to the previous point, according to the following equation:

$$\sigma_{ij}(T = -p_{\max} + 1) = \sigma_{ij}(T = -p_{\max}) + K_{\text{crit}}(1) \cdot \sigma_{ij}(1) \tag{4.12}$$

where

$\sigma_{ij}(T = -p_{max}+1)$	are stress components at the second point of the stress history, marked as time or step $-p_{max}+1$
$\sigma_{ij}(T = -p_{max})$	are stress components at the previous point of stress history, defined above by Equation 4.11
$\sigma_{ij}(1)$	are amplitudes of the stress components related to individual load cases with highest frequency, numbered here as $p = 1$
$K_{crit}(1)$	is the combination factor related to individual load cases with higher frequency, numbered here as $p = 1$, defined in the previous step of the procedure (Section 4.3), $K_{crit}(1)$ = -1 or 1

The same procedure must be continued until all $2p+1$ points of the critical reversal are defined. The points of the stress history must be obtained in a similar manner until the midpoint of reversal $T = 0$ is reached, after which the same amplitudes must be added in reversed order (from the lowest frequency to the highest) to determine the points of the second half of the stress history until the last point, marked as time or step $T = p_{max}$, is defined. Figure 4.5 shows the stress history of the critical reversal based on the example presented in Figure 4.4. The critical reversal of each location included in the screening procedure must be defined.

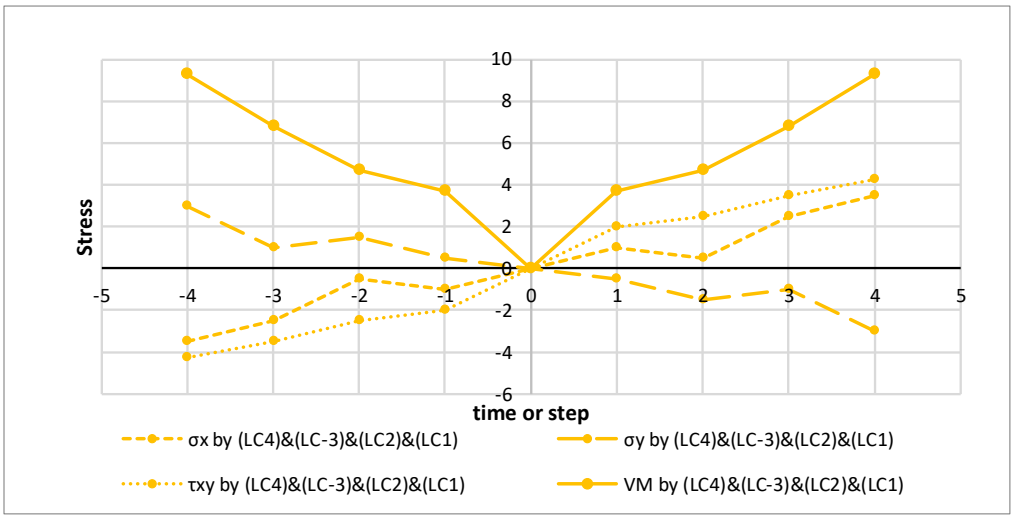

Figure 4.5: The stress history of the anti-symmetric alternating reversal formed by four independent constant amplitude loads. The example is based on the critical combination defined by the yellow curve in Figure 4.4. The continuous curve presents the amplitude-based value of the von Mises equivalent, symmetric for the left and right halves of the stress history.

4.4.2 Considering mean and residual stresses

The replacing of the whole alternating stress history constructed above is used to consider the effect of the mean stress and residual stress, by moving the midpoint of stress history from origo to an appropriate point. Possible mean stresses must be converted to ENS using the same algorithm presented in Section 4.2. The following equation presents a preliminary combination of the mean and residual stress and alternating stress history defined above:

$$\sigma_{ij}^{\mathrm{R}}(T) = \sigma_{ij}(T) + \left(\sigma_{ij}^{\mathrm{mean}} + \sigma_{ij}^{\mathrm{res}}\right) \tag{4.13}$$

where

$\sigma_{ij}{}^{\mathrm{R}}(T)$	are the stress components at point T of the stress history, including appropriate mean and residual stresses
$\sigma_{ij}(T)$	are the corresponding stress components of the alternating stress history, defined above (Section 4.4.1)
$\sigma_{ij}{}^{\mathrm{mean}}$	are the components of the total mean stress of loading cycle, presented as ENS
$\sigma_{ij}{}^{\mathrm{res}}$	are the components of the residual stress

The high residual stress equivalent to the yield stress of material, ignoring the mean stress, can be used as a preliminary assumption for compatibility with common standards and rules related to fatigue of welded structures. The yield stress of the material is the only

information required in this case. This default assumption can be replaced by more accurate values for existing mean and residual stress, if necessary and if such information is available. However, consideration of the actual values of mean and residual stress may be incompatible with standard requirements. A preliminary replacement of the stress history to the equi-biaxial yield point of the material is presented in Figure 4.6.

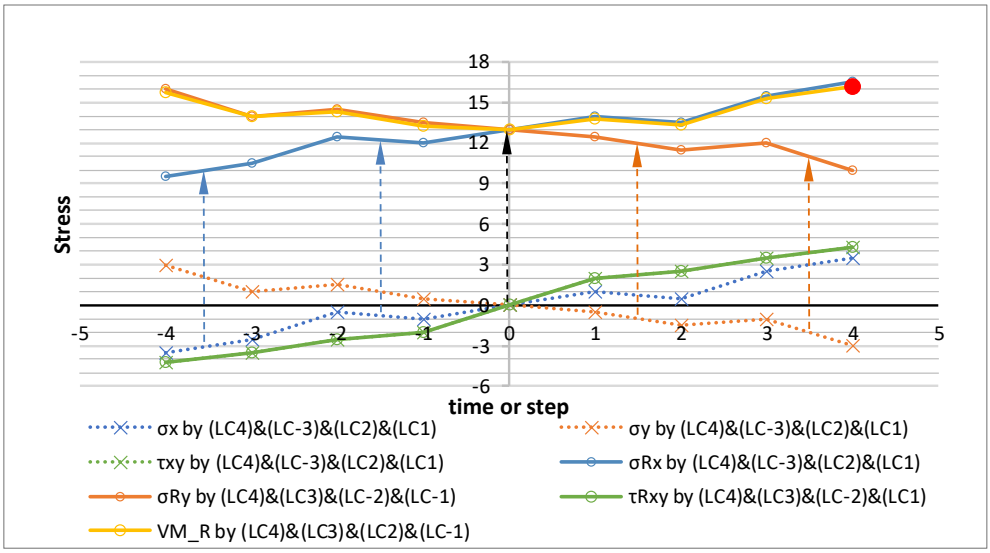

Figure 4.6: Preliminary replacement of the stress history by moving the midpoint from origo to the equi-biaxial yielding point of material. The assumed yield stress of the material and residual stress is 13 units. Index R in the component's names refers to "replaced". The example is based on the critical combination defined by the yellow curve in Figures 4.4 and 4.5.

4.4.3 Fitting the stress history to the elastic area

The next step is fitting the moved stress history of the considered set-up cycle inside the yielding surface. The use of E-PP material model is assumed to be accurate enough for screening purposes, because the primary area of interest is HCF. The von Mises stress calculated for every step of the stress history under consideration detects possible material yielding. Two main cases must be considered: potentially elastic stress history, in which the total amplitude does not exceed the yield stress of material f_y; and plastic stress history, in which the total amplitude exceeds the yield stress of the material.

Potentially elastic stress history can be forced on the elastic area by using scale factor q, defined as the ratio of the yield stress of the material and maximum von Mises stress, and applying corresponding offsets to the whole history of stress components. The calculation of the component offsets is based on component values at the point of maximum von

Mises stress, shown in Figure 4.6 by a red circle. The following equations define the scale factor q and appropriate offsets of the stress components:

$$q = \frac{f_{\mathrm{y}}}{\sigma_{\mathrm{VM,max}}} \tag{4.14}$$

$$\sigma_{ij}^{\mathrm{offset}} = (q-1) \cdot \sigma_{ij}(\sigma_{\mathrm{VM,max}}) \tag{4.15}$$

where

$\sigma_{\mathrm{VM,max}}$	is the maximum von Mises stress of the stress history
f_{y}	is the yield stress of the material
q	is the scale factor, defined above by Equation 4.14
$\sigma_{ij}(\sigma_{\mathrm{VM,max}})$	are the stress components at the point of the stress history with maximum von Mises stress $\sigma_{\mathrm{VM,max}}$
$\sigma_{ij}^{\mathrm{offset}}$	are the offset components for the current fitting iteration

The stress history is replaced by adding the component offsets to the appropriate components of the stress history:

$$\sigma_{ij}^{\mathrm{new}}(T) = \sigma_{ij}^{\mathrm{old}}(T) + \sigma_{ij}^{\mathrm{offset}} \tag{4.16}$$

where

$\sigma_{ij}^{\mathrm{new}}(T)$	are the stress components of the stress history after the fitting iteration
$\sigma_{ij}^{\mathrm{old}}(T)$	are the stress components of the stress history before the fitting iteration
$\sigma_{ij}^{\mathrm{offset}}$	are the offset components defined above by Equation 4.15

Forcing the potentially elastic stress history onto the elastic area can require a few iterations. The two iterations of the fitting procedure presented above are shown in Figure 4.7, while Figure 4.8 demonstrates obtaining the appropriate scale factors. In some cases, the whole stress history cannot be fitted inside the elastic area, even if the total amplitude is below the yield stress of the material. The maximum allowed number of fitting iterations must be limited to avoid infinite loops. After reaching the iteration limit, these cases can be classified as plastic and processed like other plastic cases in which the total amplitude exceeds the yield stress of the material. For plastic cases, same fitting procedure is used to force the stress history of plastic reversal to pass through the elastic region, starting from the yielding point for technical reasons explained below in Section 4.5.

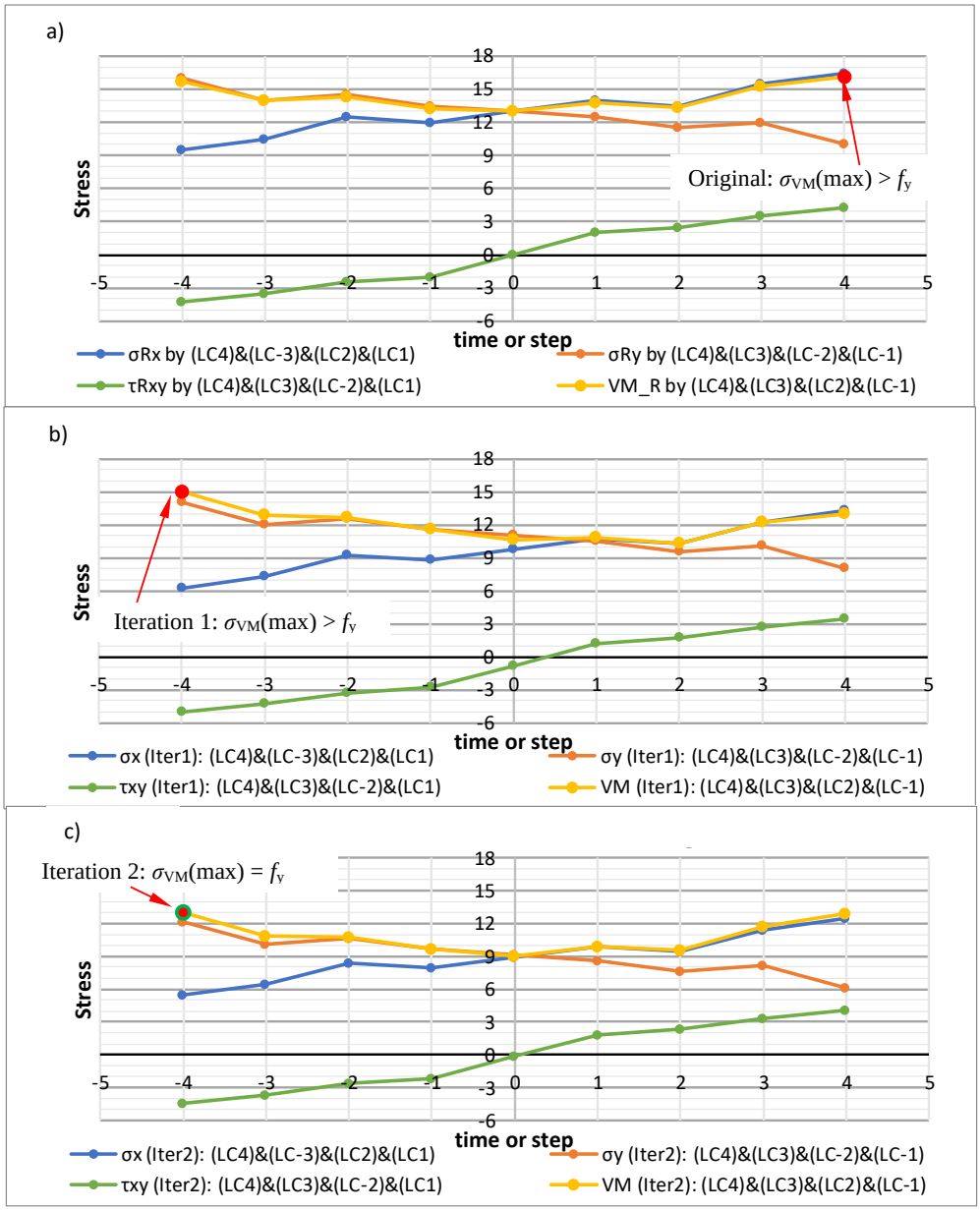

Figure 4.7: Fitting the elastic stress history to the elastic area in two iterations: a) Original history of reversal, replaced from origo to yielding point; b) History of reversal after first fitting iteration; c) History of reversal after second fitting iteration. The assumed yield stress of material is f_y = 13 units.

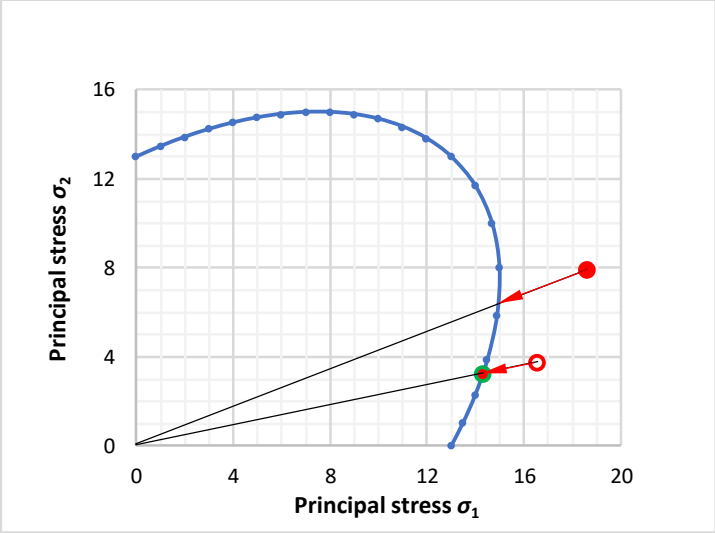

Figure 4.8: Obtaining the scale factor to fit the elastic stress history to the elastic area. The assumed yield stress of the material is f_y = 13 units.

4.4.4 The results of the fourth step of the procedure

Fourth step of the screening procedure is a part of the loop, which must be repeated for each loading event. The result of this stage of the screening procedure is a stress history based on a critical combination of the amplitudes of separate load cases. This stress history of critical reversal, first obtained as anti-symmetrical alternating load, can be used later to determine the MCF needed to calculate the effective strain energy density. The possible mean and residual stresses were considered by appropriate replacement of the alternating stress history and fitting to the elastic area. In plastic cases with a total amplitude in excess of the yield stress of the material, the stress history of plastic reversal is forced to pass through the elastic region, starting from the yielding point. These stress histories of the critical reversal are obtained for each location included in screening procedure.

4.5 Calculating SED using Ellyin's model with modifications

According to Ellyin's original SED-based model, effective SED includes plastic SED and positive elastic SED, as presented above in Section 3.1.3:

$$\Delta W^{\text{Ellyin}} = \Delta W^{\text{p}} + \Delta W^{\text{e+}} \tag{4.17}$$

where

ΔW^{Ellyin} is the range of the effective SED in Ellyin's model

ΔW^{p} is the range of the plastic SED
ΔW^{e+} is the positive part of the range of the elastic SED

The effective SED of the cycle can be calculated using the appropriate plastic and elastic SED of the individual steps. Calculations of the SED of individual steps of the reversal and the total effective SED of the cycle, with some modifications and extensions, are presented later in this section. These modifications and extensions are related to the ability to adjust the effect of mean stress and consider an appropriate portion of the elastic compression to ensure compatibility with different standards and rules.

Total effective SED is determined based on the elastic stress history of the critical reversal, obtained as presented in Section 4.4 above. The stress history contains all the existing independent loads. Each individual load is divided into two separate amplitude-based individual steps, located symmetrically in the constructed stress history. Two different types of reversal must be processed depending on the results of the fitting procedure, presented above in Section 4.4.3:

1) fully elastic
2) plastic (or actually elastic-plastic)

The stress history of an elastic reversal is located inside the elastic area. Fully elastic behavior is assumed in this case after the set-up cycle, and all individual steps of the reversal are elastic. The von Mises stress at the start and the end of any step are below the yield stress of the material. The same procedure can be used to determine the elastic SED of every step of the reversal in this case. The procedure is presented later in this section.

A part of the stress history of a plastic reversal is located outside the elastic area. Local plasticity is assumed in this case and must be considered in calculating the SED for the screening procedure. In this case, the stress history of reversal includes elastic steps and, additionally, plastic or semi-plastic load steps:

- At the beginning and end of the elastic step, the elastic von Mises stress is below the yield stress of the material. The processing of the individual elastic steps of the plastic reversal is similar to elastic reversal.
- The semi-plastic step starts in the elastic area, and the yield stress of the material is exceeded at the end of the step. The semi-plastic step is a combination of the elastic and plastic steps, with yielding occurring during the step.
- At the beginning and end of the plastic step, the pseudoelastic von Mises stress exceeds the yield stress of the material, and the value increases during the step. A special case involves decreasing the pseudoelastic von Mises stress on the plastic area of the step. This special case, related to temporal elastic unloading, is considered in Appendix E.

The SED of a reversal is calculated by separately processing each step of the reversal. The total effective SED of the loading cycle can be calculated using appropriate partial values of SED, defined for individual steps. The calculations of the different portions of SED for different types of individual steps are presented below.

4.5.1 Calculating the SED of the individual step

Elastic SED of the individual elastic load step

According to Ellyin's original SED-based approach, in addition to plastic SED, only the positive elastic SED affects fatigue. For this reason, the positive and negative elastic SED must be separated from each other. The total range of the positive elastic SED over the complete cycle can be obtained by summing the partial values calculated for each individual step of the reversal. The stress components change linearly during the individual step and, in general, the principal directions at the start and the end of the step are different. Transforming the stress components into a specific coordinate system, presented below, simplifies the separation of positive and negative elastic energy.

Transforming the stresses of an individual step into a principal coordinate system based on the stress ranges of the step leads to a constant value of the shear stress and strain during the step. Correspondingly, the range of the SED related to the shear component is zero. The range of the positive elastic strain energy of the individual step can be calculated in this coordinate system considering normal stress components only. According to assumed plane stress condition, the transformation to the range-based principal coordinate system can be implemented using the following equations:

$$\varphi = \frac{1}{2}\arctan\left(\frac{2\Delta\sigma_{12}(T)}{\Delta\sigma_{11}(T) - \Delta\sigma_{22}(T)}\right) \tag{4.18}$$

$$\sigma'_{11} = \sigma_{11}\cos^2\varphi + \sigma_{22}\sin^2\varphi + \sigma_{12}\sin\varphi\cos\varphi \tag{4.19}$$

$$\sigma'_{22} = \sigma_{22}\cos^2\varphi + \sigma_{11}\sin^2\varphi + \sigma_{12}\sin\varphi\cos\varphi$$

$$\sigma'_{12} = -(\sigma_{11} - \sigma_{22})\sin\varphi\cos\varphi - \sigma_{12}(\sin^2\varphi - \cos^2\varphi)$$

where

$\Delta\sigma_{ij}(T)$	are the original components of the stress ranges over the step T
φ	is the range-based principal angle for step T
σ'_{ij}	are transformed components of the stresses calculated at the start and end of step T
σ_{ij}	are original components of the stresses at the start and end of step T

The corresponding transformed strain components required to determine the SED can be calculated using Hooke's law and the transformed stress components defined above:

$$\varepsilon'_{ij} = \frac{1}{E}\left[(1+\nu)\sigma'_{ij} - \nu\sigma'_{kk}\delta_{ij}\right] \tag{4.20}$$

where

ε'_{ij}	is the transformed strain tensor at the start and end of step T
E	is Young's modulus of the material
ν	is Poisson's ratio
σ'_{ij}	is the transformed stress tensor at the start and end of step T
σ'_{kk}	is the trace of the stress tensor at the start and end of step T
δ_{ij}	Kronecker delta ($\delta_{ij} = 1$ if $i = j$; $\delta_{ij} = 0$ if $i \neq j$)

The result of the proposed transformation is a constant value of the shear stress during the step and zero range of the SED related to the shear component. Excluding the shear component from the calculation of the elastic SED prevents issues related to the interpretation of its sign. After the transformation, the positive elastic SED of the individual step can be calculated based on the normal components only, analogically with Equation 3.26, presented by Ellyin and Xia (1993) for principal stresses and strains:

$$\Delta W_{ij}^{e+}(T) = \int_{\text{step } T} \mathrm{H}\left(\sigma'_{ij}\right)\sigma'_{ij}\, d\varepsilon'^{e}_{ij} \tag{4.21}$$

where

$\Delta W_{ij}^{e+}(T)$	are components of the positive elastic SED of step T
σ'_{ij}	are normal components of the stress tensor, transformed according to Equation 4.19
ε'^{e}_{ij}	is the elastic part of the transformed strain tensor, calculated according to Equation 4.20
H(x)	is the Heaviside function; H(x) = 1 for $x \geq 0$, H(x) = 0 for $x < 0$

The Heaviside function of the elastic strain used in Equation 3.26 is excluded from Equation 4.21 considering the positive elastic SED related to the loading or unloading during the individual step. Both values are required for the subsequent approximation of the positive elastic SED over the complete elastic cycle, based on one reversal, as presented later in this section.

In addition to the positive elastic SED, the negative elastic SED must be obtained to consider the compressive loading. Ellyin's original model ignores the negative elastic SED related to compression, and only the positive elastic SED and plastic SED are required. However, common fatigue standards and rules for welded structures consider the whole or, at least, a significant portion of the compressive loading and related part of the stress range. Compatibility with these assumptions can be ensured by partially considering the negative elastic SED related to the compression. The required negative elastic SED can be calculated similarly to the positive elastic SED, except that the Heaviside function H(x) must be used in inverse form [1-H(x)]:

$$\Delta W_{ij}^{e-}(T) = \int_{\text{step } T} \left[1 - \mathrm{H}\left(\sigma'_{ij}\right)\right] \sigma'_{ij} d\varepsilon'^{e}_{ij} \tag{4.22}$$

where the symbols are explained above (see Equation 4.21)

Determining the total effective SED over a complete elastic cycle using incremental results, defined by Equations 4.21 and 4.22 for the individual steps, is presented later in this section.

Plastic SED of the individual plastic load step

The elastic-perfectly plastic (E-PP) material model is chosen for an approximative consideration of local plasticity in the screening procedure. The relation between pseudoelastic and actual elastic-plastic SED is based on the principle presented in Section 3.1.2. The plastic SED is approximated using the generalized form of Neuber's rule and E-PP material model, as presented in Figure 4.9. According to the relations presented in Figure 4.9, the plastic SED W^{p} can be defined by following equations:

$$2 \cdot W^{pse} = W^{p} + 2 \cdot W^{e} \quad \Rightarrow$$

$$W^{p} = 2 \cdot [W^{pse} - W^{e}] = k_{pl} \cdot W^{pse/p} \tag{4.23}$$

where

W^{pse}	is the total pseudoelastic SED
W^{e}	is the elastic SED before yielding
W^{p}	is the plastic SED after yielding using an E-PP material model
$W^{pse/p}$	is the portion of the pseudoelastic SED after yielding related to the plastic behavior; $W^{pse/p} = [W^{pse} - W^{e}]$
k_{pl}	is the ratio of plastic SED W^{p} and part of the pseudoelastic SED $W^{pse/p}$ related to plastic behavior, explained above; default value k_{pl} =2.0 corresponds to Neuber's rule and the E-PP material model

Neuber's rule and the corresponding ratio $k_{pl} = 2.0$ is chosen as default. Oher assumptions can be implemented by using appropriate k_{pl} values, for example $k_{pl} = 1.0$ corresponds to a combination of Glinka's rule and an E-PP material model.

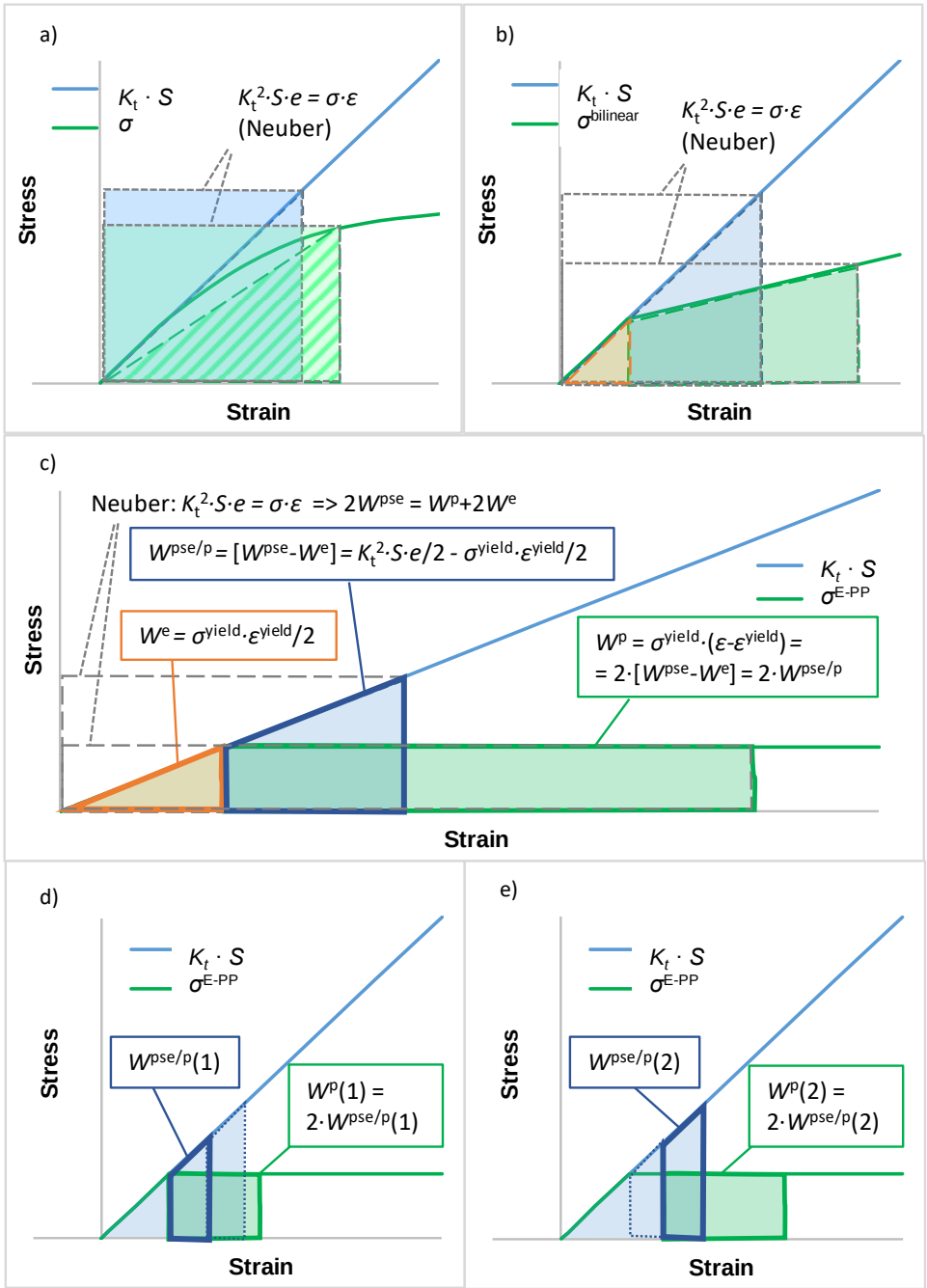

Figure 4.9: Applying Neuber's rule to different material models: a) continuous nonlinear; b) bilinear; c) elastic-perfectly plastic (E-PP); followed by incremental application of Neuber's rule to the E-PP material model (Figures d and e for increments 1 and 2, respectively). In the figure, W^e is elastic SED, W^p is plastic SED, $W^{pse/p}$ is the incremental plastic portion of the pseudoelastic SED.

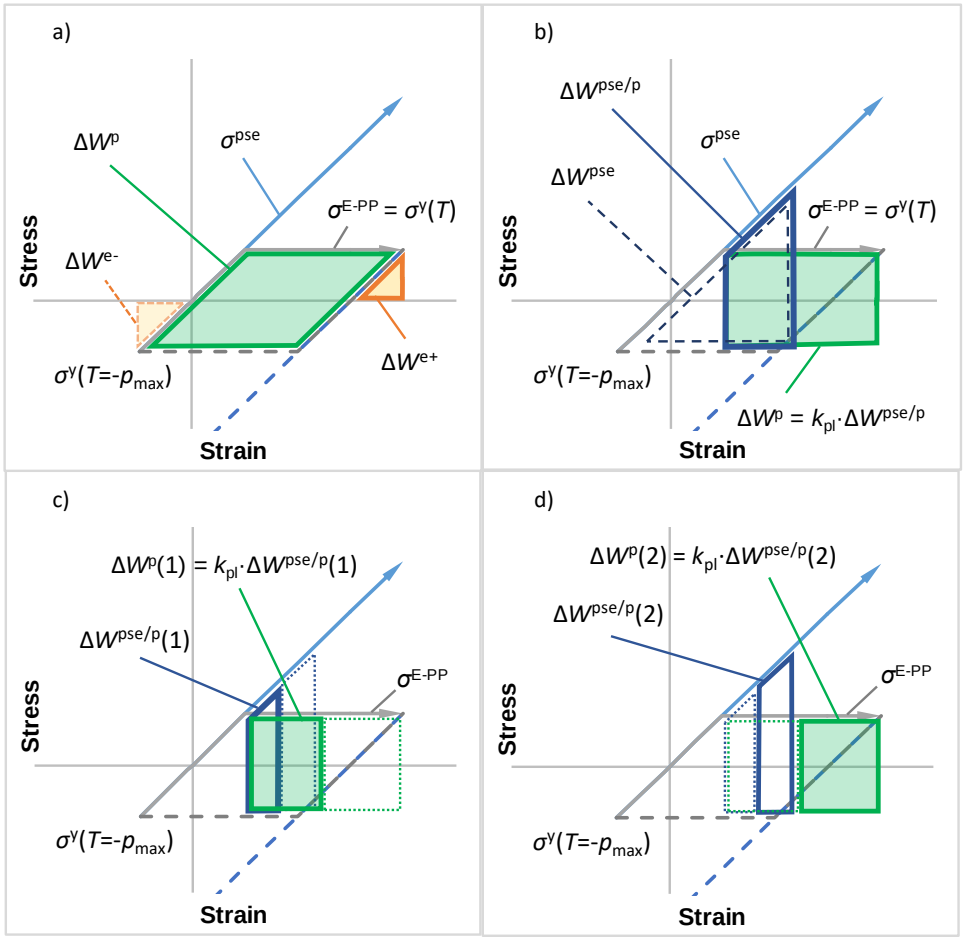

Figure 4.10: Total SED of the plastic cycle (a), plastic SED ΔW^{p} of the cycle (b) and incremental calculation of the plastic SED of the plastic cycle (c and d) using the elastic-perfectly plastic (E-PP) material model. The symbols in the figure are: ΔW^{e+} and ΔW^{e-} are positive and negative elastic SED; ΔW^{pse} is the total pseudoelastic SED; $\Delta W^{pse/p}$ is a part of the pseudoelastic SED related to the plastic behavior; k_{pl} is the ratio of ΔW^{p} and $\Delta W^{pse/p}$; $\sigma^{y}(T=-p_{max})$ is the stress component value at the start of the reversal, forced to the yielding point; $\sigma^{y}(T)$ is the stress component value at the other yielding point of reversal.

Figure 4.10 presents the corresponding relation for cyclic loading applicable for the incremental calculation of the plastic SED of the individual plastic step. The plastic SED $\Delta W_{ij}^{p}(T)$ of the individual plastic step T can be calculated by using an appropriate incremental value of the pseudoelastic SED $\Delta W_{ij}^{pse/p}(T)$:

$$\Delta W_{ij}^{p}(T) = k_{pl} \cdot \Delta W_{ij}^{pse/p}(T) \tag{4.24}$$

where

$\Delta W_{ij}^{\mathrm{pse/p}}(T)$ is the incremental pseudoelastic SED of the plastic step T related to the plastic behavior

k_{pl} is the ratio of plastic SED ΔW^{p} and part of the pseudoelastic SED $\Delta W^{\mathrm{pse/p}}$ related to plastic behavior, as explained above; default value k_{pl} =2.0 corresponds to Neuber's rule and an E-PP material model

As presented above in Section 4.4, the stress history of the plastic reversal was forced to start from the yielding point and pass through the elastic region towards the yielding at the other end of the reversal. Hence, the component value at the start of the stress history is already set to the appropriate yielding point (see Figure 4.10), and the incremental pseudoelastic SED of the plastic step T is:

$$\Delta W_{ij}^{\mathrm{pse/p}}(T) = \left[\frac{\sigma_{ij}^{\mathrm{pse}}(T+1) + \sigma_{ij}^{\mathrm{pse}}(T)}{2} - \sigma_{ij}^{y}(\mathrm{start})\right] \cdot \left(\varepsilon_{ij}^{\mathrm{pse}}(T+1) - \varepsilon_{ij}^{\mathrm{pse}}(T)\right) \tag{4.25}$$

where

$\sigma_{ij}^{\mathrm{pse}}(T)$ is the stress component value at the start of current plastic step T

$\sigma_{ij}^{\mathrm{pse}}(T+1)$ is the stress component value at the end of current plastic step T

$\sigma_{ij}^{y}(\mathrm{start})$ is the stress component value at the start of current reversal, forced to the yielding point

$\varepsilon_{ij}^{\mathrm{pse}}(T)$ is the strain component value at the start of current plastic step T

$\varepsilon_{ij}^{\mathrm{pse}}(T+1)$ is the strain component value at the end of current plastic step T

Equation 4.25 defines the pseudoelastic SED of the plastic step based on the results of the linear elastic analysis. An increase in the pseudoelastic von Mises stress during the plastic step is assumed. A decrease in the pseudoelastic von Mises stress on the area above the yield stress of the material constitutes a special case, considered in Appendix E, related to temporal elastic unloading.

SED of the individual semi-plastic load step

The semi-plastic load step includes elastic and plastic parts. The step starts from the elastic area with a von Mises stress below the yield stress of material. At the end of the step, the pseudoelastic von Mises stress exceeds the yield stress of the material, and the yielding point is reached during the semi-plastic step. This step can be divided into elastic and plastic sub-steps, each of which can be processed using the appropriate algorithm, elastic or plastic, as presented above. The starting point of the elastic sub-step is the same as the starting point of the whole semi-plastic step, and its end point is a point where yielding occurs. Correspondingly, this yielding point is the start point of the plastic sub-step, whose end point is the same as the end point of the whole semi-plastic step. An additional operation required for this type of step is to obtain the yielding point inside the

semi-plastic step. The yield point can be determined in several different ways, one of which is shown in Appendix D.

4.5.2 Calculating the fatigue effective SED of the complete cycle

The SED of the complete elastic cycle consists of elastic incremental SED only. The SED of the complete plastic cycle includes the elastic and plastic incremental SED of the individual elastic, semi-plastic, and plastic steps.

Elastic SED of the elastic cycle

The stress history, constructed as presented in Section 4.4, includes only one reversal of a complete cycle assumed to be symmetric. A step in the reversal with negative strain range related to the unloading during the considered reversal has a symmetric pair with positive strain range on the second reversal and vice versa (Figure 4.11). Based on the assumed symmetry of the cycle, the positive elastic SED of the complete elastic cycle ΔW^{e+} can be defined using the incremental positive elastic SED $\Delta W_{ij}^{e+}(T)$ of one reversal. The incremental values of the positive elastic SED $\Delta W_{ij}^{e+}(T)$, calculated by Equation 4.21, must be summed as magnitudes without regard to their sign. The elastic SED can be first summed by the components *ij* of each step *T* and then by the steps during the reversal:

$$\Delta W^{e+} = \sum_{T} \text{abs}(\Delta W_{ij}^{e+}(T)) \tag{4.26}$$

where

ΔW^{e+} is the positive elastic SED over the complete elastic cycle
$\Delta W_{ij}^{e+}(T)$ are the components of the positive elastic SED of the individual step *T*, defined by Equation 4.21
T is the index number of the step in the considered reversal

The negative elastic SED is required in considering the effective portion of the compression. The calculation of the negative elastic SED ΔW^{e-} is similar to that of positive elastic SED:

$$\Delta W^{e-} = \sum_{T} \text{abs}(\Delta W_{ij}^{e-}(T)) \tag{4.27}$$

where

ΔW^{e-} is the negative elastic SED over the complete elastic cycle
$\Delta W_{ij}^{e-}(T)$ are the components of the negative elastic SED of the individual step *T*, defined by Equation 4.22
T is the index number of the step in the considered reversal

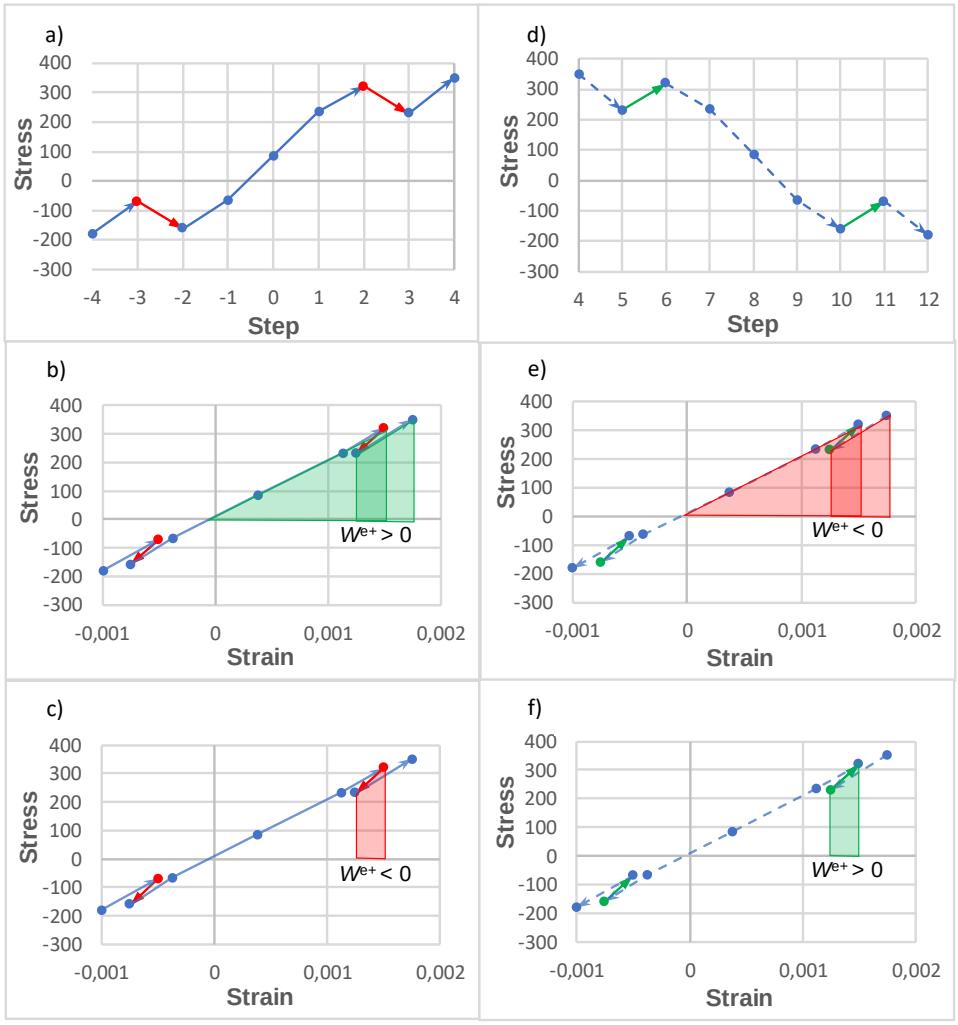

Figure 4.11: Stress history of reversal 1, under investigation (a), corresponding stress-strain path and positive elastic SED W^{e+} (b and c). Green-shaded areas relate to the needed loading phase (b) and red-shaded ones to the unloading phase (c), which must be excluded from the calculation of total SED of current reversal. The corresponding quantities of the second reversal are presented in Figures d−f. The negative portion of the positive elastic SED W^{e+} related to the unloading during the considered reversal 1 (c) is equivalent to the positive portion of the positive elastic SED W^{e+} on the second reversal (f).

Compatibility with common fatigue standards and rules for welded structures assumes the possibility of considering the appropriate compressive portion of the elastic stress ranges as fatigue effective. The complete or partial inclusion of the compressive portion of the stress range in the effective stress range cannot be applied directly to the appropriate portions of the elastic SED. Increasing the effective stress range in the stress-based

approach corresponds to offsetting the stress history in the SED-based approach, which must be implemented differently to achieve a comparable effect. The effect of including the compressive portion of the stress range related to the standard effectivity factor k_{comp} can be approximated using the following equation:

$$\Delta W^{\mathrm{e}}_{\mathrm{eff}} = \left(1 + k_{\mathrm{comp}}\sqrt{\frac{\Delta W^{\mathrm{e}-}}{\Delta W^{\mathrm{e}+}}}\right)^2 \Delta W^{\mathrm{e}+} \tag{4.28}$$

where

- $\Delta W^{\mathrm{e}+}$ is the positive elastic SED of the cycle (Equation 4.26)
- $\Delta W^{\mathrm{e}-}$ is the negative elastic SED of the cycle (Equation 4.27)
- $\Delta W^{\mathrm{e}}_{\mathrm{eff}}$ is the effective elastic SED, including the assumed effective part of the negative elastic SED
- k_{comp} is the conventional standard effectivity factor of the negative stress range
  $k_{\mathrm{comp}} = 0$ corresponds to Ellyin's original approach
  $k_{\mathrm{comp}} = 0.6$ corresponds to the confirmed compression, according to standard SFS-EN 1993-1-9 (2005)
  $k_{\mathrm{comp}} = 1.0$ corresponds to the fully effective compression as the default assumption of standard SFS-EN 1993-1-9 (2005) and similar rules

In the uniaxial case, increasing the effective SED, defined by Equation 4.28, is similar to including the negative part of the stress range, multiplied by factor k_{comp}, in the effective stress range. Equation 4.28 is applicable only for positive elastic SED greater than zero. To be fully compatible with standard assumptions, Equation 4.28 can be extended to cases with completely negative stress ranges by the conditional equation for $\Delta W^{\mathrm{e}+} = 0$:

$$\Delta W^{\mathrm{e}}_{\mathrm{eff}} = k^2_{\mathrm{comp}} \Delta W^{\mathrm{e}-} \tag{4.29}$$

where the symbols are explained above (see Equation 4.28)

However, reasonability of using Equation 4.29 and the fatigue effectivity of the completely negative stress range are debatable.

Elastic SED of the plastic cycle

The positive and negative elastic SED during the complete plastic cycle can be approximated similarly to the elastic cycle, using the incremental elastic SED of the elastic steps and Equations 4.26 and 4.27. The elastic portion of the semi-plastic step must be included in the elastic SED of the plastic cycle. The incremental elastic SED of the elastic steps, including the elastic portion of the semi-plastic step, can be calculated using Equations 4.21 and 4.22. Correspondingly, the compressive loading of the plastic cycle can be considered, if necessary, using Equation 4.28.

The elastic SED of a plastic cycle can be more accurately calculated by extending the stress history from one reversal to a complete cycle and including only positive values of the incremental elastic SED over the complete cycle.

Plastic SED of the plastic cycle

The range of the plastic SED over a complete cycle is a sum of the incremental plastic SED of the plastic steps of the considered reversal, including the plastic portion of the semi-plastic step:

$$\Delta W^{\mathrm{p}} = \sum_{T} \Delta W_{ij}^{\mathrm{p}}(T) \tag{4.30}$$

where

ΔW^{p}	is the plastic SED of the complete plastic cycle
$\Delta W^{\mathrm{p}}{}_{ij}(T)$	is the incremental plastic SED of the individual plastic steps, defined by Equation 4.24
T	is the index number of the step in the considered reversal

Effective SED of the complete cycle

The effective SED ΔW_{eff} of the complete elastic cycle is the effective elastic SED $\Delta W^{\mathrm{e}}{}_{\mathrm{eff}}$, defined by Equation 4.28 or 4.29. The effective SED ΔW_{eff} of the complete plastic cycle is a sum of the effective elastic SED $\Delta W^{\mathrm{e}}{}_{\mathrm{eff}}$, defined using Equations 4.28 or 4.29, and plastic SED ΔW^{p}, defined using Equation 4.30. In general form, the effective SED ΔW_{eff} of the complete cycle is:

$$\Delta W_{\mathrm{eff}} = \Delta W_{\mathrm{eff}}^{\mathrm{e}} + \Delta W^{\mathrm{p}} \tag{4.31}$$

where

$\Delta W^{\mathrm{e}}{}_{\mathrm{eff}}$	is the effective elastic SED of the complete elastic or plastic cycle
ΔW^{p}	is the plastic SED of the complete plastic cycle; $\Delta W^{\mathrm{p}} = 0$ for the elastic cycle

4.5.3 Correcting the effect of mean stress in the SED-based method

According to investigations presented in Appendix C, Ellyin's SED-based method estimates a higher influence of the mean stress than the Smith-Watson-Topper (SWT) damage parameter for cycles with positive minimum stress. The results of some implemented tests also indicate a possible overestimation of the means stress effect by Ellyin's SED-based method in cases with positive minimum stress. Based on these observations, the capability to adjust the effect of the mean stress in cases with positive minimum stress is included in the screening procedure, as presented below. The possibility to adjust the effect of the mean stress is also required to ensure compatibility

with fatigue standards and rules, which typically assume a fully effective stress range without direct consideration of the mean stress. This correction of the mean stress is not related to the varying mean stress sensitivity of different materials and the corresponding material properties. The correction takes into account the differences between the methods, related to consideration of the mean stresses. The correction factor k_{mean} (see Equation 4.32) allows adjusting the consideration of mean stress according to a certain method, such as the SWT or the original Ellyin's approach, or to ignore the effect of mean stress completely.

As presented in Appendix C, the independent componential correction of the mean stress effect can be implemented in a principal coordinate system using the following equation:

$$\Delta W_i^{\text{e+}} = \frac{\Delta\sigma_i \Delta\varepsilon_i}{2} + k_{\text{mean}} \cdot \sigma_{i,\text{min}} \Delta\varepsilon_i \tag{4.32}$$

where

$\Delta\sigma_i$ is the range of the principal stress component
$\Delta\varepsilon_i$ is the range of the principal strain component
$\sigma_{i,\text{min}}$ is the positive minimum value of the principal stress component
i is the index related to the principal components (i =1,2 for plane stress condition)
k_{mean} is the factor for correcting the effectiveness of the portion of SED located below positive minimum stress;
k_{mean} = 1.0 relates to Ellyin's original model without correction
k_{mean} = 0.5 for correction based on a uniaxial SWT parameter
k_{mean} = 0 for correction based on the standard SFS-EN 1993-1-9 (2005), DNV rules and IIW recommendations

Equation 4.32 presents the direct reduction of that portion of the SED located below the positive minimum stress, using correction factor k_{mean}. However, for technical reasons, the capability to correct the mean stress effect is implemented by subtracting the overestimated portion of the SED located below the positive minimum stress from the total SED (Figure 4.12).

The corrected value of the fatigue effective SED ΔW_{corr} in cases with positive minimum stress can be calculated using the following equations:

$$\Delta W_{\text{corr}} = \Delta W_{\text{eff}} - \Delta W_{i,\text{over}} \tag{4.33}$$

$$\Delta W_{i,\text{over}} = (1 - k_{\text{mean}}) \cdot \text{H}(\sigma_{i,\text{min}}) \cdot \sigma_{i,\text{min}} \cdot \Delta\varepsilon_{i,\text{tot}} \tag{4.34}$$

where

ΔW_{eff} is the effective SED of the cycle, defined by Equation 4.31

$\Delta W_{i,\text{over}}$ are the overestimated portions of the SED related to the positive minimum stress in a principal coordinate system (Equation 4.34).
$H(x)$ is the Heaviside function; $H(x) = 1$ for $x > 0$; $H(x) = 0$ for $x < 0$
$\Delta\varepsilon_{i,\text{tot}}$ is the total range of the strain component, defined as a sum of the incremental strain ranges of this component over the reversal in the range-based principal coordinate system
and the other symbols are explained above (Equation 4.32)

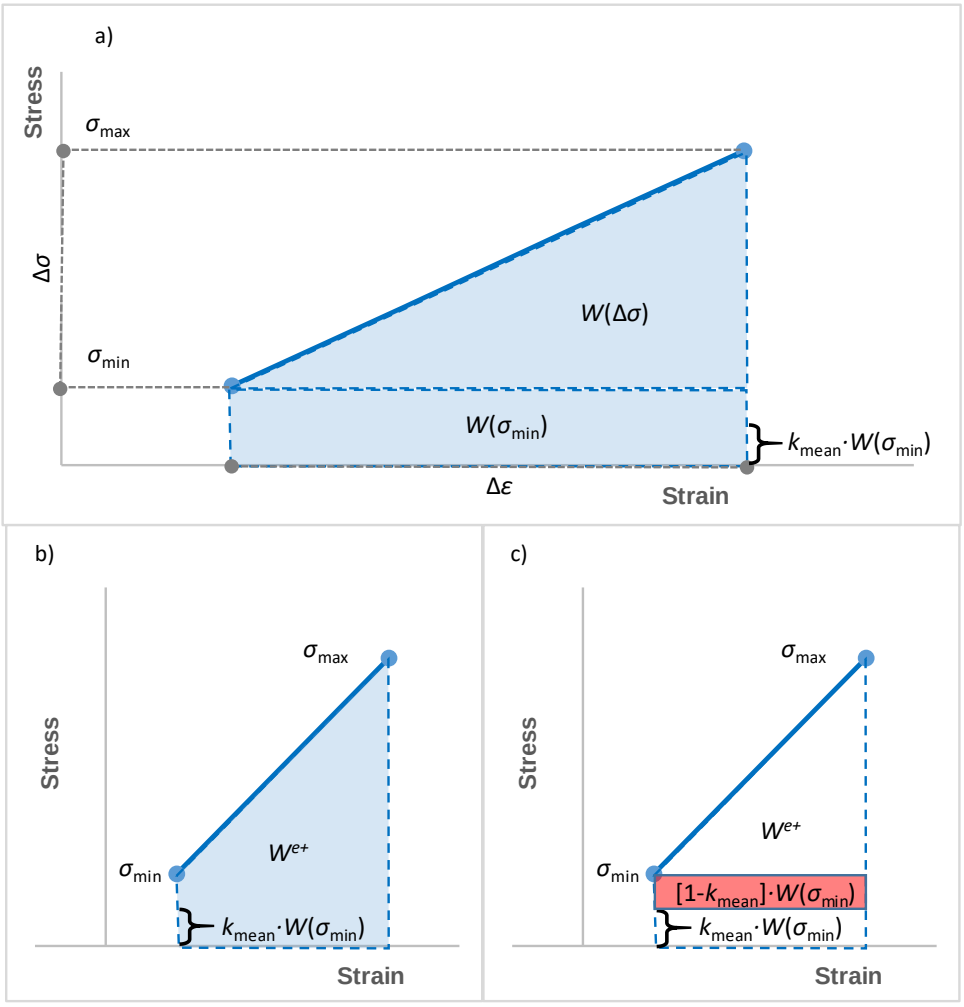

Figure 4.12: a) The strain energy density (SED) W^{e+} of a cycle with positive minimum stress $\sigma_{\min}$; b) correction of the mean stress effect by reduction of the SED below the stress range $W(\sigma_{\min})$ using correction factor k_{mean}; c) the corresponding correction by subtracting the overestimated portion $[1\text{-}k_{\text{mean}}]\cdot W(\sigma_{\min})$ from the total SED W^{e+}.

For the purpose of a screening analysis, the mean stress effect was approximately corrected using a principal coordinate system based on the stress ranges over the whole cycle. In the assumed plane stress condition, the required transformation angle is defined using the stress values at the start and end of the reversal and an equation similar to Equation 4.18:

$$\Delta\sigma_{ij,\mathrm{tot}} = \sigma_{ij}(\mathrm{start}) - \sigma_{ij}(\mathrm{end}) \tag{4.35}$$

$$\varphi = \frac{1}{2}\arctan\left(\frac{2\Delta\sigma_{12,\mathrm{tot}}}{\Delta\sigma_{11,\mathrm{tot}} - \Delta\sigma_{22,\mathrm{tot}}}\right) \tag{4.36}$$

where

$\Delta\sigma_{\mathrm{ij,tot}}$ are the total ranges of the stress components over the reversal in the original coordinate system
σ_{ij}(start) are the stress components ij at the start of the reversal
σ_{ij}(end) are the stress components ij at the end of the reversal

The stress history is transformed to the overall principal coordinate system defined by Equations 4.35 and 4.36 by using Equation 4.19. The corresponding strains are defined using Equation 4.20. The range of the shear stress and strain between the start and end points of the reversal is zero in this range-based principal coordinate system. This leads to zero energy associated with the shear component, regardless of the non-zero value of the shear stress itself. Only normal components have non-zero energy in this coordinate system. These transformed normal stresses and strains are used in Equation 4.34 to approximate the possible overestimated portion of the SED related to the positive minimum stress below stress ranges. The solution is approximative, because incremental ranges of shear strain can be non-zero. However, sufficient accuracy for screening purposes is assumed.

4.5.4 Calculating the multiaxial constraint factor or energy coefficient

Ellyin's SED-based method considers varying damage impacts of the different multiaxial cyclic loadings using the multiaxial constraint factor (MCF), as presented in Section 3.1.3. MCF for screening analysis is calculated according to Ellyin and Xia (1993), using the maximum in-plane principal strain and maximum shear strain in the plane, inclined at 45° to the surface. This maximum shear strain can be determined by subtracting the out-of-plane normal strain from one or the other in-plane normal strain. Calculation of the MCF requires the out-of-plane strain to be known, which can be determined by using Hook's law for known in-plane components (out-of-plane normal stress $\sigma_\perp = 0$ is assumed for plane stress condition):

$$\varepsilon_{\perp} = \frac{1}{E}[\sigma_{\perp} - \upsilon(\sigma_1 + \sigma_2)] = -\frac{\upsilon}{E}(\sigma_1 + \sigma_2) = -\frac{\upsilon}{1-\upsilon}(\varepsilon_1 + \varepsilon_2) \tag{4.37}$$

where

υ	is Poisson's ratio
$\sigma_{\perp}$	is out-of-plane stress component; $\sigma_{\perp} = 0$ in plane stress condition
σ_1, σ_2	are normal in-plane stress components in a principal coordinate system
ε_1, ε_2	are normal in-plane strain components in a principal coordinate system

Outside the low cycle fatigue (LCF) area, the elastic Poisson's constant can be used, instead of the effective value, with sufficient accuracy for the purposes of screening analysis. The required strains are calculated for each step of the amplitude-based reversal in the case of non-proportional loading. The normal strain value used for calculation of the MCF is taken at the moment when the inclined maximum shear strain reaches the maximum value:

$$\rho = (1 + \nu)\left[\frac{\varepsilon(T)}{\gamma(T)}\right]_{\gamma=\gamma_{max}} \tag{4.38}$$

where

ρ	is the multiaxial constraint factor (MCF); $\rho = 1$ for the uniaxial loading $\rho = 1 + \nu$ for pure torsion $\rho = 1 - \nu$ for equi-biaxial loading
ν	is effective Poisson's ratio
$\varepsilon(T)$	is maximum in-plane principal strain; $\varepsilon = \max(\varepsilon_1, \varepsilon_2)$ at the moment T
$\gamma(T)$	is maximum shear strain in direction 45° to the surface; $\gamma = \max(\lvert\varepsilon_1 - \varepsilon_{\perp}\rvert$ or $\lvert\varepsilon_2 - \varepsilon_{\perp}\rvert)$ at the moment T

4.5.5 The results of the fifth step of the procedure

Fifth step of the screening procedure is a part of the loop, which must be repeated for each loading event. The results of this stage of the screening procedure are corrected effective SED ΔW_{corr} and value of the multiaxial constraint factor ρ, defined for a processed loading event. Both values are required at the next stage to calculate the allowable number of cycles and are defined for each location of interest. Corrected effective SED includes positive elastic SED and possible plastic SED, according to Ellyin's original method. Additionally, the effect of the mean stress can be corrected, and that portion of the SED related to the compression can be considered, if necessary.

4.6 Determining the allowable number of cycles and fatigue damage

4.6.1 Calculating the allowable number of cycles

The allowable number of cycles, based on the strain energy density (SED), is determined using an equation similar to that presented by Ellyin and Xia (1993). The corrected value of the SED ΔW_{corr}, defined by Equation 4.33 and other related equations (Section 4.5), is used to calculate the allowable number of cycles, instead of Ellyin's original SED ΔW^{Ellyin} (see Equation 3.27 in Section 3.1.3):

$$\frac{\Delta W_{\text{corr}}}{\rho} = \kappa_u N_f^{\alpha} + C_u \quad \Rightarrow$$

$$N_f = \left[\frac{1}{\kappa_u}\left(\frac{\Delta W_{\text{corr}}}{\rho} - C_u\right)\right]^{\frac{1}{\alpha}} \tag{4.39}$$

where

ΔW_{corr} is the corrected SED, calculated according to Equation 4.33 in Section 4.5
N_f is the number of the considered cycles to failure
α is the material constant
C_u is the range of elastic SED which does not cause fatigue damage in a uniaxial test, that is, the SED related to the fatigue limit
κ_u is the material constant defined by the uniaxial test
ρ is the MCF defined by Equation 4.38

An infinitely long fatigue life is assumed if the effective SED stays below value C_u.

4.6.2 Determining the required parameters

Calculating the allowable number of cycles using Equation 4.39 requires definition of the appropriate material parameters κ_u, C_u and α. These parameters are obtained using the appropriate uniaxial S-N curve. The standard uniaxial S-N curve is defined by the exponent related to the slope of the S-N curve in the logarithmic scale and by fatigue class, that is, the allowable stress range at the fatigue life of $2 \cdot 10^6$ cycle. The allowable number of cycles, based on the standard S-N curve, can be defined by the following equation:

$$N_f = \frac{C}{\Delta\sigma^m} = 2 \cdot 10^6 \cdot FAT^m \cdot \Delta\sigma^{-m} \tag{4.40}$$

where

C is a constant related to the S-N curve; $C = 2 \cdot 10^6 \cdot FAT^m$
$\Delta\sigma$ is the applied uniaxial stress range
m is the exponent related to the slope of the S-N curve

FAT is the fatigue class of the used S-N curve, that is, the allowable uniaxial stress range at $2 \cdot 10^6$ cycles

Fully elastic behavior is assumed in the reference uniaxial constant amplitude test on the HCF area. In the case of uniaxial elastic loading with assumed stress ratio $R = 0$, the corresponding SED ΔW can be defined using the following equation:

$$\Delta W = \frac{\Delta\sigma^2}{2E} \tag{4.41}$$

where

$\Delta\sigma$ is the stress range used in the reference test
E is Young's modulus of the material

The fatigue standards and rules often ignore fatigue limit $\Delta\sigma_{th}$, and corresponding material constant C_u can be assumed to be zero. Considering, additionally, that $\rho = 1$ for uniaxial cases, Equations 4.39, 4.40 and 4.41 give:

$$N_f = \left[\frac{1}{\kappa_u}\left(\frac{\Delta\sigma^2}{2E}\right)\right]^{\frac{1}{\alpha}} = 2 \cdot 10^6 \cdot FAT^m \cdot \Delta\sigma^{-m} \tag{4.42}$$

where

N_f is the number of the considered cycles to failure
α, κ_u are the material constants in the SED-based calculation
$\Delta\sigma$ is the uniaxial stress range
m is the exponent related to the slope of the S-N curve
FAT is the fatigue class of the used S-N curve, that is, the allowable uniaxial stress range at the $2 \cdot 10^6$ cycles

The value of the material constant α can be defined by setting equal exponents of the stress range to the left and right of Equation 4.42:

$$\Delta\sigma^{2/\alpha} = \Delta\sigma^{-m} \quad \Rightarrow$$

$$\alpha = -\frac{2}{m} \tag{4.43}$$

where the symbols are explained above (see Equation 4.42)

Correspondingly, the material constant κ_u can be defined by Equations 4.42 and 4.43:

$$[2E\kappa_u]^{\frac{m}{2}} = 2 \cdot 10^6 \cdot FAT^m \quad \Rightarrow$$

$$\kappa_u = \frac{1}{2E}[2 \cdot 10^6 \cdot FAT^m]^{\frac{2}{m}} \tag{4.44}$$

where the symbols are explained above (see Equation 4.42)

The fatigue class of the characteristic S-N curve commonly used with the ENS method is FAT225; that is, the allowable uniaxial stress range at the $2 \cdot 10^6$ cycles is 225 MPa. The corresponding fixed exponent related to the inverse slope of the S-N curve in the logarithmic scale is $m = 3$. The characteristic fatigue class can be converted to the mean value using safety factor 1.37 (Sonsino et al., 2012). Table 4.1 shows values of the material constants α and κ_u related to the characteristic and mean S-N curves for the ENS method. If necessary, the material parameters corresponding to the alternative S-N curve can be defined by Equations 4.43 and 4.44.

Table 4.1: The material parameters for SED-based method based on the ENS S-N curves.

Curve	m	FAT	α	κ_u
characteristic	3	225	-0.667	1913
mean	3	308	-0.667	3591

The allowable number of cycles for current loading event can be calculated using defined material parameters and Equation 4.39.

4.6.3 Calculating the partial damage

The partial damage $D_i(q)$, related to the considered loading event i can be calculated using linear Palmgren-Miner rule as a ratio of the applied and allowable number of cycles for each element or location q:

$$D_i(q) = \frac{n_i}{N_i(q)} \tag{4.45}$$

where

- n_i is the actual number of cycles of the loading event i
- $N_i(q)$ is the allowable number of cycles for the element or location q for the loading event i
- q is the index number of the element or location
- i is the index of the loading event (A, B, C, D in table 4.2)

The simplified cycle counting method (see Section 3.4) can be utilized to obtain the actual number of cycles of the different loading events, as presented in Table 4.2. The actual number of cycles of the first loading event A, which includes all individual loads, is equal to the lowest number of cycles of the included individual loads, which is the individual

load 4 with number of cycles n_4. The next loading event, B, includes all the individual loads except the individual load 4 with the lowest number of cycles. The number of cycles of loading event B can be defined as the difference between the lowest number of cycles of the individual load included in the current loading event, which is the individual load 3 with number of cycles n_3, and the number of cycles n_4 of the individual load 4, excluded from the current loading event B. The same principle can be applied to the next loading event and can be continued until the last loading event, D, which includes only one individual load, 1, is reached. Figure 3.6 in Section 3.4 can be used to visualize the presented procedure.

Table 4.2: Actual number of cycles of the loading events, based on individual loads

Individual loadings	Stress range	No. of cycles[1]
4	$\Delta\sigma_4$	n_4
3	$\Delta\sigma_3$	n_3
2	$\Delta\sigma_2$	n_2
1	$\Delta\sigma_1$	n_1
Loading events	**Stress range**	**No. of cycles**
A	$\Delta\sigma_4 + \Delta\sigma_3 + \Delta\sigma_2 + \Delta\sigma_1$	$n_A = n_4$
B	$\Delta\sigma_4 + \Delta\sigma_3 + \Delta\sigma_2$	$n_B = n_3 - n_4$
C	$\Delta\sigma_2 + \Delta\sigma_1$	$n_C = n_2 - n_3$
D	$\Delta\sigma_1$	$n_D = n_1 - n_2$

[1)] $n_1 > n_2 > n_3 > n_4$

4.6.4 The results of the sixth step of the procedure

The sixth step of the screening procedure is the last step of the calculation loop, which must be repeated for each loading event. The results of this stage of the screening procedure are the allowable number of cycles and partial damage defined for each location of interest for the processed loading event. The calculation is based on fatigue strength parameters obtained using the chosen appropriate uniaxial S-N curve. The same loop must be repeated for each loading event, as presented in Section 4.6.5. The total damage used to define the critical locations of the structure can be calculated using the partial results of these loops, according to Section 4.7.

4.6.5 Processing other loading events using a similar loop

Sections 4.3−4.6 present a complete calculation loop for an individual loading event and corresponding loading cycle. The loading event with a higher stress range, which includes the sum of all independent loads, is used to present the calculation procedure. The reversal of this event, represented in Figure 4.13 by a dotted blue line, includes four individual loads or 8 amplitude-based steps. The same calculation loop can be used for other loading events. According to the simplified cycle counting method, the other loading events can

be defined by excluding the individual load with the lowest number of cycles (or lowest frequency) from the combination used in the previous loading event. The reversal of the second event includes three individual loads or six amplitude-based steps, and so on.

After the next loading event is defined by excluding the individual load with the lowest number of cycles, the critical combination of individual loads must be redefined for this second loading event, using the procedure explained in Section 4.3. Considering the mean stress of this subsequent loading event differs from considering the mean stress of the first loading event. The mean stress of the subsequent loading event depends on the set-up cycle and stress range of the previous loading events. The total number of cycles of the second loading event can be divided into appropriate equivalent portions of similar reversals with different midpoints. The points of the previous reversal related to the currently excluded individual load with the lowest number of cycles can be used as midpoints of symmetric amplitude-based reversals of the second loading event, as presented in Figure 4.13.

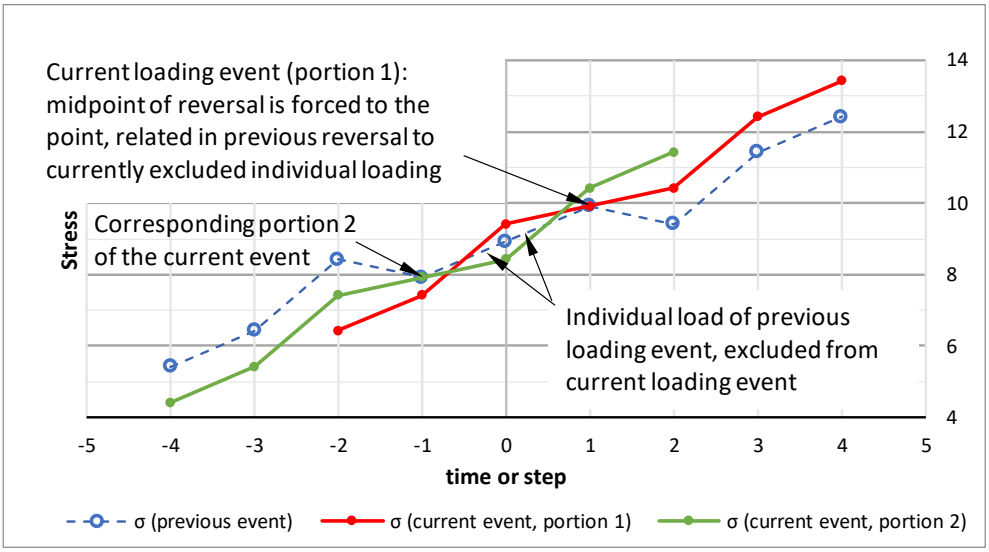

Figure 4.13: Approximation of the mean stress of second and subsequent loading events. The dotted blue line represents the reversal of the previous loading event. The number of current reversals is divided into equivalent portions with similar symmetric reversals, represented in the figure by red and green continuous lines. The midpoints of each portion of these reversals are forced to the points related in the previous reversal to the currently excluded load.

Otherwise, the other steps of the procedure explained in Sections 4.3−4.6 must be applied to the defined critical combination of the individual loads related to the loading event under processing. The same looped calculation procedure must be continued until only the load with the highest number of cycles is left.

4.7 Calculating the total damage and relative screening parameter

After processing all the loading events and related cycles, the total damage $D(q)$ can be calculated for each element or location q by summing the corresponding partial damages $D_i(q)$:

$$D(q) = \sum D_i(q) = \sum \frac{n_i}{N_i(q)} \tag{4.46}$$

where

- n_i is the actual number of cycles in the loading event i
- $N_i(q)$ is allowable number of cycles for the element or location q in the loading event i
- q is index number of the element or location
- i is the index of the loading event (A, B, C, D in table 4.2)
- $D_i(q)$ is the partial damage at the element or location q related to the loading event i (Equation 4.45)

The total damage defined by Equation 4.46 can be used directly for screening analysis, especially if the real number of actual cycles is used. As an alternative, the defined total damage can be normalized to the obtained maximum value and used as a relative screening parameter $D_{rel}(q)$:

$$D_{\mathrm{rel}}(q) = \frac{D(q)}{D_{\max}} = \frac{D(q)}{\max[D(q)]} \tag{4.47}$$

where

- $D_{rel}(q)$ is the relative damage at the element or location q, normalized to the obtained maximum value of the total damage D_{max}
- $D(q)$ is the total damage at the element or location q (Equation 4.46)
- D_{max} is the obtained maximum value of the total damage $D(q)$, including all elements or locations

5 Experimental tests

The accuracy of the screening method was investigated by laboratory tests. Figure 5.1 presents the principal scheme of the test system. The test specimen consists of a 100x80x5 rectangular hollow section (RHS) and tube Ø42.4x6.3 welded to the wider side of the RHS, as presented in Figure 5.2. The RHS is made of structural steel S420MH with a nominal yield stress of f_y = 420 MPa and an actual yield stress of 506 MPa, according to the inspection certificate. The tube is made of structural steel S235JRH with a nominal yield stress of f_y = 235 MPa and an actual yield stress of 345 MPa, according to the inspection certificate. The welding around the tube was implemented using robotized gas metal arc welding (GMAW). A total of eight test specimens were manufactured using a fillet weld or by partially penetrating a fillet weld prepared using a single bevel with root face with weld throat thicknesses of 4–6 mm. The welding start-stop point is located on the sides, which are compressed by transversal cylinder loading, and local HFMI treatment was used to prevent fatigue failure at the start-stop location.

The tests were implemented using different combinations of the two independent loadings: the vertical vibration of the RHS profile in the specimen's plane caused by a vibration motor with eccentric mass; and the transversal hydraulic cylinder force applied to the upper end of the tube. The frequency of the vertical vibration varies between 25 and 50 Hz and the frequency of the transversal load is near 5 Hz. A more detailed description of the test system and test specimens is given in Appendix B.

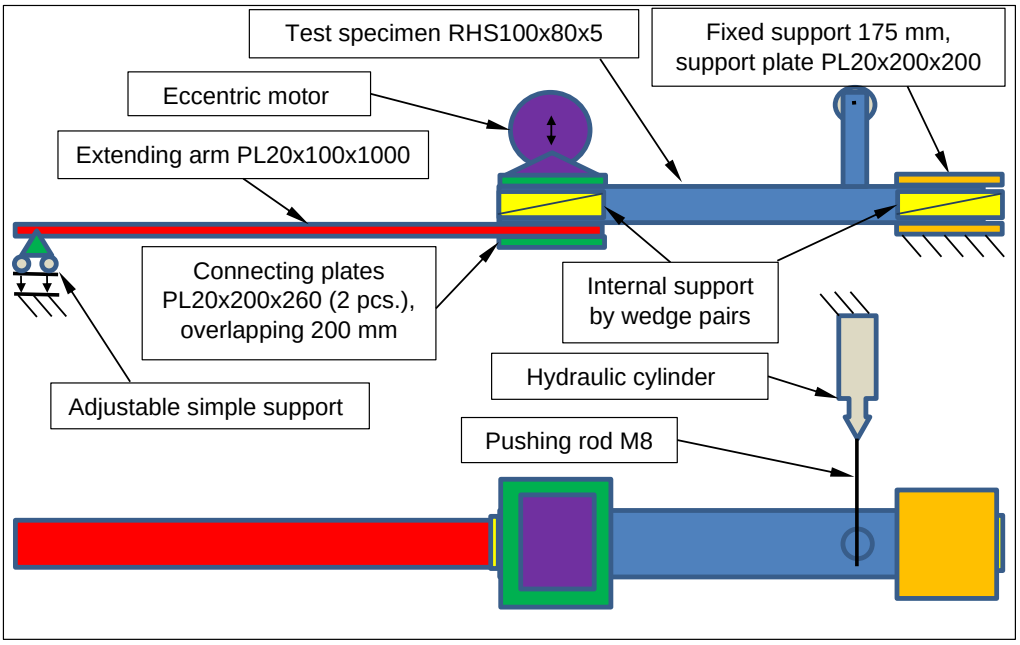

Figure 5.1: The principal scheme of the test system.

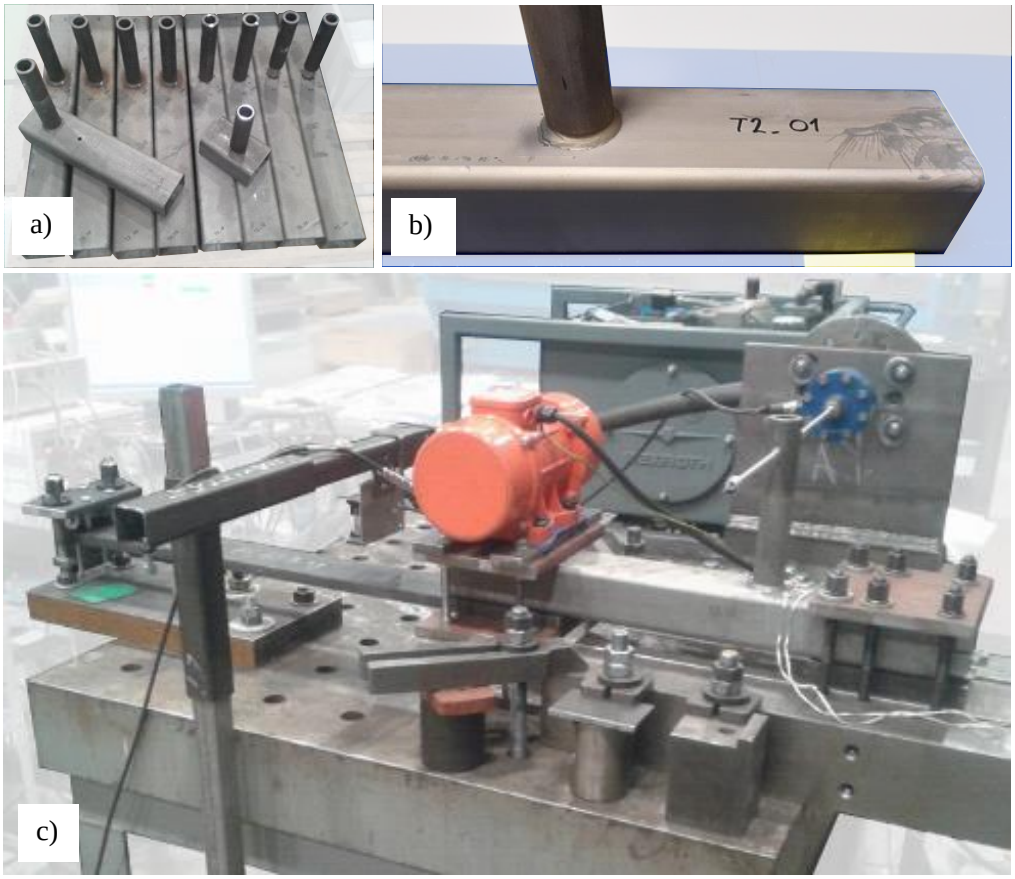

Figure 5.2: Test specimens (a, b) and test system used to verify the screening method (c).

The failure location estimated by the developed screening procedure, using the results of FE analysis, was compared to the corresponding test results. The mean values (FAT_{mean} = 308 MPa with probability of survival P_s = 50%) of the S-N curve related to the ENS method is used to estimate the failure locations and calculate corresponding fatigue lives. The material parameters for calculations based on the strain energy density concept are presented in Section 4.6 (Table 4.1). The failure location was estimated using the mean stress correction factor k_{mean} = 0.5, which corresponds to SWT parameter, as explained in Section 4.2.5. The effectivity of the negative portion of the elastic stress range is considered using factor k_{comp} = 0.6, which corresponds to standard SFS-EN 1993-1-9 (2005).

The failure of the specimens in the tests is defined as decreasing the strain range by 50%, measured by strain gauges. The estimation of the failure in the test, based on decreasing the strain range by 50%, is presented in Figure 5.3. The results of specimen T1_01 are used as an example in the figure.

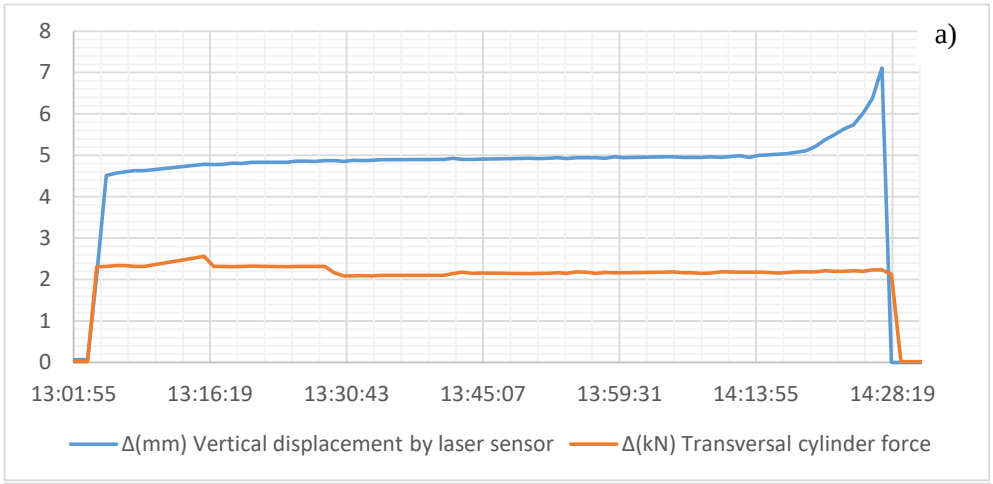

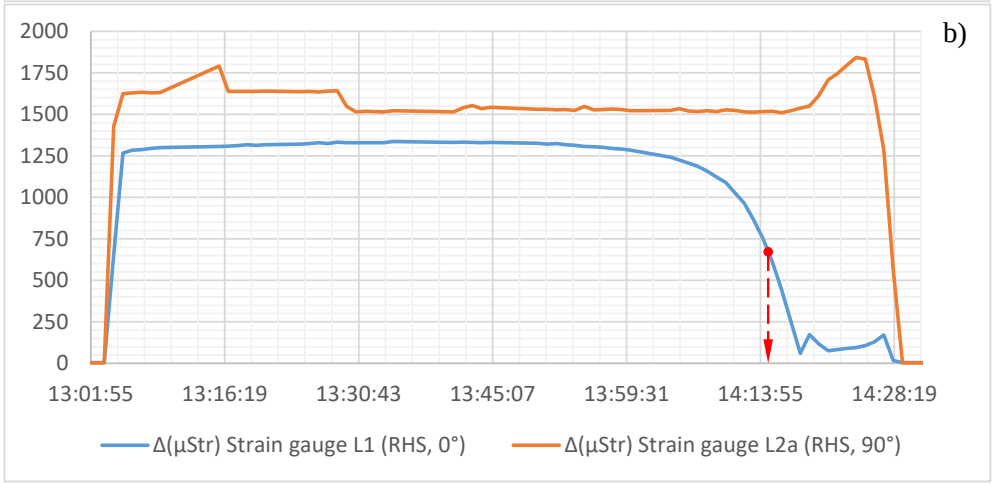

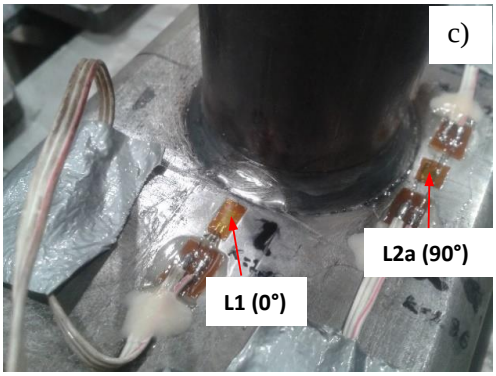

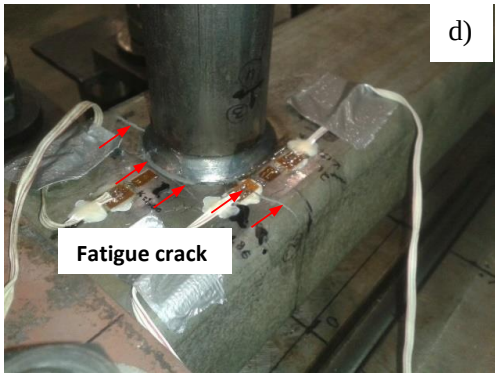

Figure 5.3: The measured loads (a) and strain ranges (b) of Specimen T1_01 (c,d). The 50% decrease in the range, measured by strain gauge L1, is used as an indicator of failure.

The comparison of the estimated failure locations and mean fatigue lives with the test results is presented in Figures 5.4 and 5.5. Figure 5.4 presents the first preliminary estimation, using a coarse approximation of the fatigue notch factor K_f = 2.5 for any locations at the weld toe. This coarse approximation is based on load-carrying fillet welds and corresponding hot spot (HS) fatigue class FAT90 (Hobbacher, 2008). Figure 5.5 presents a more accurate estimation, using two different values of the fatigue notch factor K_f for the weld toe, which is applicable to the studied case. The fatigue notch factor K_f = 2.25 is used in this case for any locations at the weld toe under vertical vibration, based on the non-load-carrying assumption and corresponding HS fatigue class FAT100 (Hobbacher, 2008). However, the fatigue notch factor K_f = 2.5 is used for any locations at the weld toe under transversal cylinder force, again based on the load-carrying assumptions.

Based on the results presented in Figures 5.4 and 5.5, the estimation of the most critical location was quite accurate in most cases. The only exception is Specimen T2_04: according to the estimation, the criticality of locations RHS 0 and RHS 90 was almost similar, but in the test, failure occurs clearly at location RHS 90. This is shown in Figure 5.4 by the red border of the green bar. As concerns Specimens T2_21 and T2_22, the estimated critical locations correspond to the tests. The calculated fatigue life is underestimated by 24–35% for Specimen T2_21 and overestimated by 23–51% for Specimen T2_22. For other cases, the correlation between the estimated mean fatigue life and the test results was surprisingly good, although the priority was to determine the critical point in relative terms.

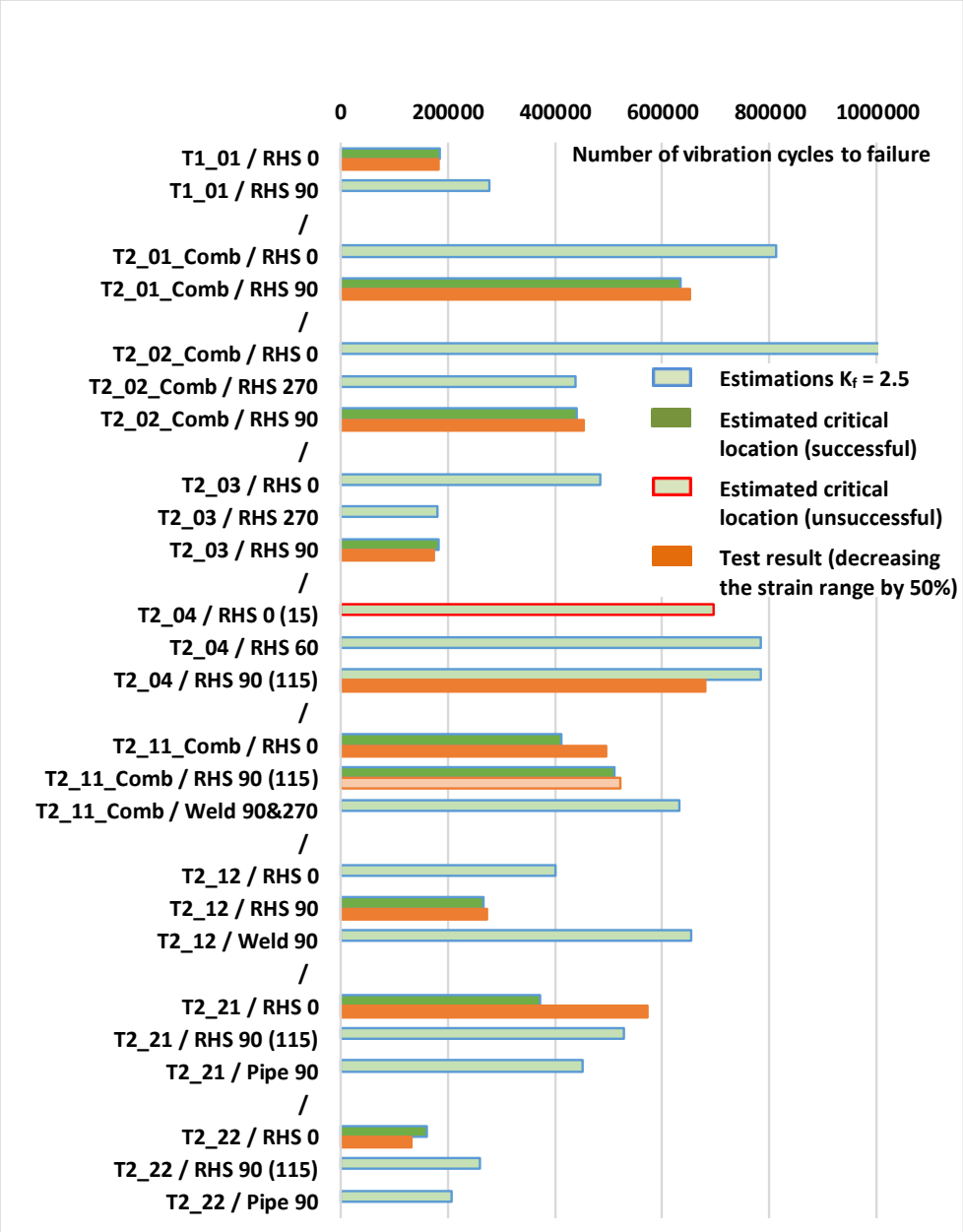

Figure 5.4: A comparison of the estimated failure locations and mean fatigue lives with the test results, using a coarse approximation of the fatigue notch factor $K_f = 2.5$ for any locations at the weld toe. The number of vibration cycles to failure is presented on the horizontal axis. The names of specimens and considered locations are presented on the vertical axis. "RHS" refers to the weld toe on the rectangular hollow section, "Pipe" – the weld toe on the tube, and "Weld" – the root of the weld between the RHS and the tube. The number refers to the angular location on the weld – 0° is directed towards the support and 90° is directed towards the hydraulic cylinder.

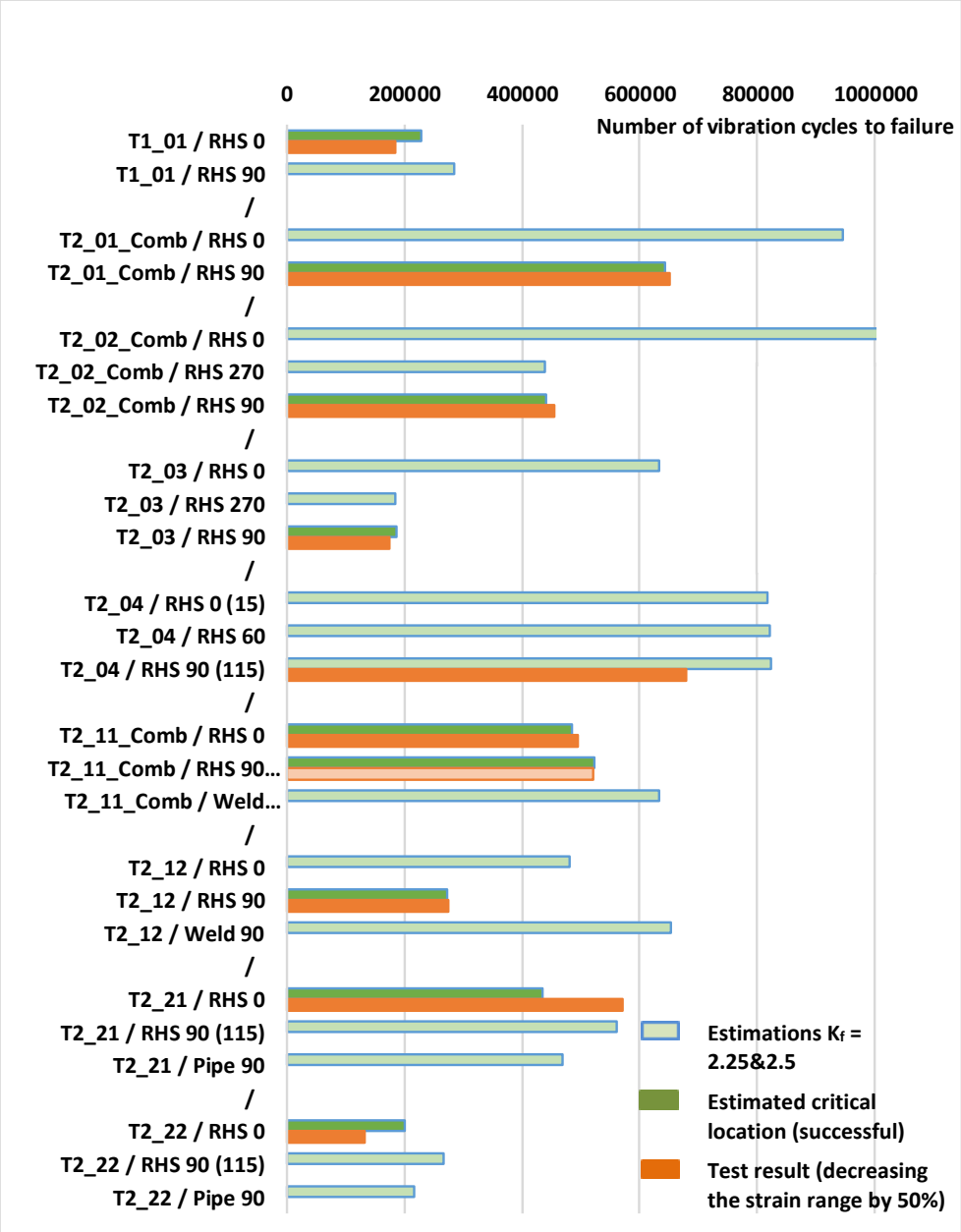

Figure 5.5: A comparison of the estimated failure locations and mean fatigue lives with the test results, using the fatigue notch factor K_f = 2.25 for vibration and 2.5 for cylinder loading. The number of vibration cycles to failure is presented on the horizontal axis. The names of specimens and considered locations are presented on the vertical axis. “RHS” refers to the weld toe on the rectangular hollow section, “Pipe” – the weld toe on the tube, “Weld” – the root of the weld between the RHS and the tube. The number refers to the angular location on the weld – 0 is directed towards the support and 90 is directed towards the hydraulic cylinder.

Figure 5.6 presents the correlation of the experimental results and the estimations defined for probability of survival P_s = 50% using the developed screening procedure. The estimations based on assumed fatigue notch factor K_f = 2.5 (Figure 5.6a) correspond to results presented on Figure 5.4. The estimations based on fatigue notch factors K_f = 2.25 for vertical vibration loading and K_f = 2.5 for transversal cylinder loading (Figure 5.6b), correspond to results presented on Figure 5.5.

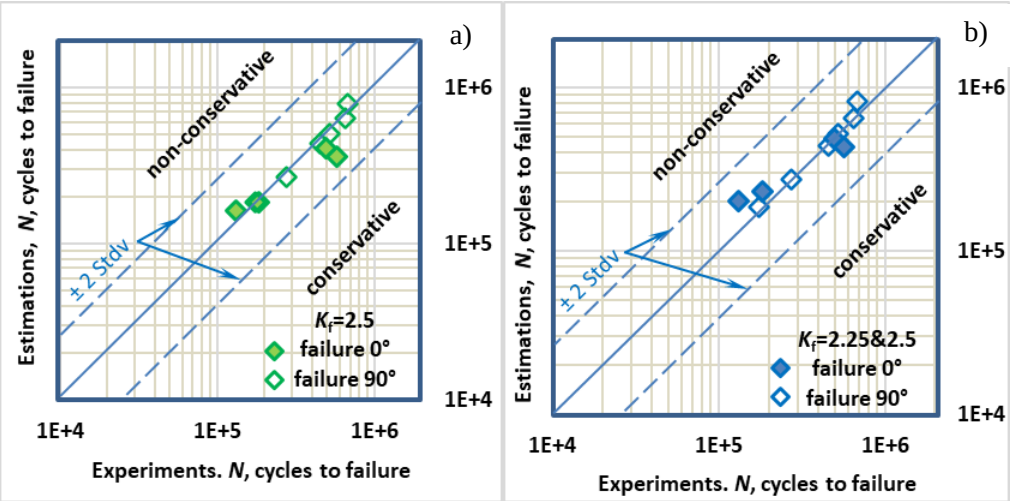

Figure 5.6: The correlation of the experimental results and the estimations defined using the fatigue notch factor K_f = 2.5 (a) and using the fatigue notch factors K_f = 2.25 for vibration and K_f = 2.5 for cylinder loading (b). The estimations are based on FAT_{mean} = 308 MPa with probability of survival P_s = 50%.

Figure 5.7 presents the failures observed in the test and the corresponding estimation of the critical location using the developed screening method. The results of Specimen T1_01 are used as an example in the figure.

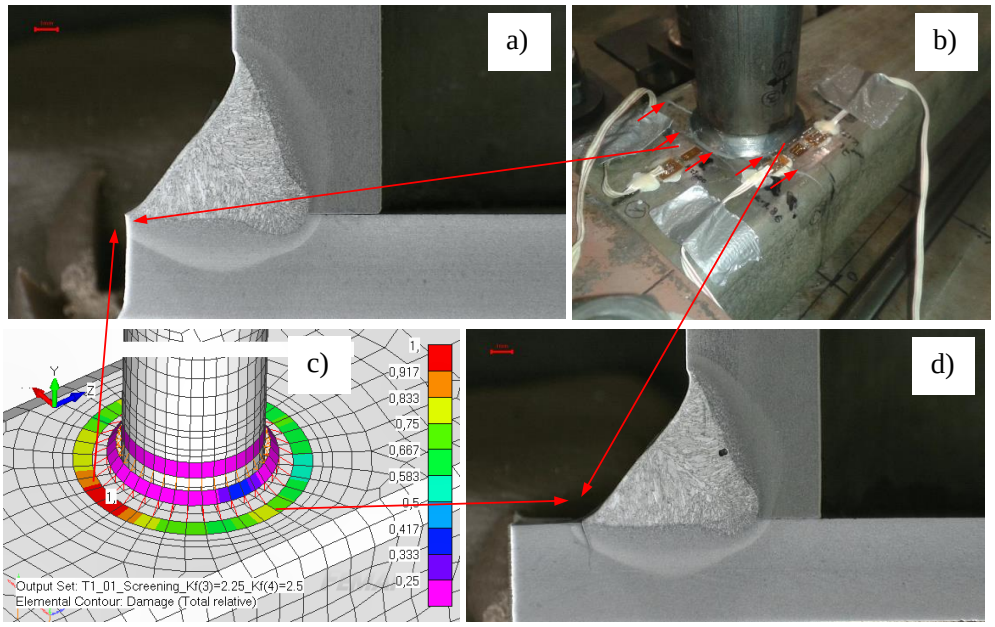

Figure 5.7: Test specimen T1_01 (b). The weld toe failure at location RHS 0° (a, strain gauge L1), initiated the crack growth at location RHS 90° (d, strain gauge 2a) and estimated the most critical location using the developed screening method (c).

6 Discussion

The aim of this thesis was to develop a screening method to determine the critical locations of welded structures. The method's primary area of applicability is high cyclic fatigue (HCF) under a combination of independent constant amplitude loads. The developed screening procedure utilizes conventional stress-based methods in combination with the strain energy density (SED)-based method, which significantly extends the flexibility of the method and its applicability to different situations.

The results of the linear elastic stress analysis are used as input information for the screening procedure. The analysis of the weld toe is based on the structural stress method. The analysis of the weld roots utilizes the nominal weld stress, which can be determined directly using the same accuracy as that required for the structural stress method. The initial stress results are converted to effective notch stresses (ENS), which are used to determine the most critical combinations of individual loads for different locations of the structure and to calculate the corresponding SED. The obtained SED is used to determine the critical locations of the structure. Different steps of the screening procedure require certain input information and use some additional adjustable parameters, which increases the compatibility of the method with different norms and assumptions. This chapter discusses the influence of the different parameters, possibilities, and limitations related to the developed screening method.

6.1 Sensitivity of the method to the different steps and parameters

Using the structural stress method as a basis for the stress analysis of the weld toes determines the required accuracy of modelling. Using a relatively fine element mesh, applicable for the direct approximation of the structural stress, allows the inclusion of welds in the global element model. This solution confirms the accuracy and comparability of the results obtained for different locations, which is of primary importance for the screening procedure. Mesh-insensitive methods can be used as an alternative solution, which reduces computational effort and requirements related to the accuracy of element mesh but requires an additional postprocessing step. Both solutions are useful, and the priority is determined as a compromise between the computing capacity and additional postprocessing. Theoretically, the less accurate stresses obtained by coarser element mesh can also be used as a relative screening parameter directly; however, the required similar level of "relative accuracy" is a significant problem, which complicates practical implementation.

The conversion of the structural and nominal stresses to the ENS can be implemented using fatigue notch factors, approximated as the ratio of ENS-based fatigue strength (FAT225), and corresponding fatigue strengths related to the original stresses, for example FAT90 and FAT45. This approximative solution significantly simplifies the screening procedure. However, better accuracy can be achieved by increasing the number of considered structural and nominal fatigue classes. More accurate results can be

obtained using the fatigue notch factors determined by analysis of actual weld geometry according to the ENS procedure or another corresponding method, if necessary. Using more precise fatigue notch factors instead of the simplified approximation by fatigue strengths increases the accuracy of the screening procedure, but requires additional work.

Determining the most critical combination of individual loads is the next important step of the procedure after converting the initial stresses to ENS stresses. The combination of individual loads, which causes the most critical combination of corresponding ENS ranges (or amplitudes), is determined using the range-based von Mises equivalent by analogy with the Wang-Brown multiaxial cycle counting method. However, this criterion, related to the distortion energy, excludes the influence of the hydrostatic stress range, which can be reasonable in plastic cases, but is, at the least, questionable in area of HCF with predominantly elastic behavior. For example, criteria based on total energy, including the distortion energy and energy of volumetric changes, may be a better option for HCF. The current distortion energy-based criteria may be replaced by others without significant changes in the screening algorithm.

Considerations of the local plasticity during the set-up cycle or the possible occasional local cyclic plasticity are based on the elastic-perfectly plastic (E-PP) material model and yield stress of the material. However, accurate screening results require the use of the actual yield stress of material, instead of the nominal value which is conventional in engineering practice. Considering the local plasticity during the set-up cycle using the nominal yield stresses in cases with relatively small stress ranges can decrease the stress ratio unjustifiably, which leads to non-conservative results. On the other hand, in cases with relatively large stress ranges, the yield stress, underestimated by the nominal value, leads to an earlier initiation of the cyclic plasticity and, correspondingly, to conservative results. Consequently, the nominal value of the yield stress may lead to either conservative or non-conservative results, depending on the situation, and its use requires special care.

Residual stress is another important parameter closely related to the local plasticity and yield stress of the material. In combination with possible mean stresses, the residual stresses and yield stress of the material define the stress ratio after the set-up cycle. A high residual stress, equal to the yield stress of the material, can be assumed if more accurate information is unavailable. This possibly conservative approximation increases the stress ratio, and the obtained screening results correspond to the assumed state instead of the unknown actual condition. However, this kind of inaccuracy is often acceptable in conventional design cases; moreover, the influence of the possible inaccuracy in the stress ratio is quite limited, especially for the SWT method, based on consideration of the mean stresses, as discussed below.

The screening procedure is implemented including the capability to adjust the efficiency of the mean stress for cases with a positive minimum stress of the cycle. Only the effective portion of SED related to the area below the positive minimum stress can be taken into account using the appropriate reduction coefficient. The reduction coefficient 1.0

corresponds to the original SED-based approach without any reduction in the efficiency of the SED below positive minimum stress. The SED related to the stress range is less detrimental in this case than SED related to a similar value of permanent positive minimum stress, which is poorly consistent with both other theories and the test results. The reduction factor 0.5 corresponds to considering the mean stress according to the widely used SWT method. This reduction factor was used to estimate the critical locations presented in this work. The reduction factor 0.0 can be applied to ignore the effect of mean stress, while simultaneously considering the whole stress range, which corresponds to conventional standard assumptions.

The developed screening procedure also includes the capability to consider the partial efficiency of the SED related to the negative portion of an elastic stress range. Totally ignoring this portion of the SED corresponds to the original SED-based approach but is not compatible with conventional fatigue standards and rules. Especially in combination with an E-PP material model, it may be necessary to consider the negative portion of the SED to avoid non-conservative results and conflicts with standard assumptions. The partial efficiency of the SED related to the negative portion of an elastic stress range can be reasoned, in this case, as compensation of the work hardening ignored in the E-PP material model. The estimations of critical locations presented in this work were made using the efficiency factor for negative elastic SED which corresponds to the factor 0.6 for the negative portion of the stress range, used in fatigue standard SFS-EN 1993-1-9 (2005). Based on the good correlation between estimations and test results presented in this thesis, this value can be recommended as the default initial value for general cases.

6.2 **Alternative approaches**

It is quite difficult to compare the developed screening method with traditional approaches due to the different purposes and specific requirements of the area of applicability. The applicability of the method to general cases is one of the most important criteria. A multiaxial condition must be assumed as the general case for overall screening, which instantly limits the applicability of conventional uniaxial methods for this purpose.

Simplified considerations of the multiaxial state using different applications of von Mises stress are not suitable for non-proportional loading (Sonsino, 2009b) and can lead to significant problems, even in much simpler cases, as presented by Rabb (2017). The more advanced methods, such as different versions of critical plane approaches, are applicable to general multiaxial cases and for the analysis of individual locations of interest. However, the required postprocessing efforts limit their applicability for the global screening of complex welded structures with a very large number of locations to be checked. An additional challenge for this kind of method is the potentially undefined exact combination of loadings, which multiplies the required postprocessing efforts by a number of different possible combinations of loadings and corresponding stress histories. Another group of potentially applicable methods are fracture mechanic, but, as with the previous group, the required accuracy and postprocessing efforts limit their applicability

to the global screening of complex welded structures. The different versions of methods based on SED often consider plastic energy only, which limits their applicability to the chosen primary area of interest, namely HCF with dominant elastic behavior and insignificant cyclic plasticity.

Ellyin's SED-based approach, chosen as a basis for the developed screening procedure, enables consideration of both portions of energy, elastic and plastic, which have paramount importance for use on an area of HCF. Additionally, processing the stress components according to this method is very efficient and corresponds well to the observed correlation between the results of the multiaxial tests and estimations, based on the sum of the squares of the stress components (Sonsino, 2009b). Ellyin's SED-based approach also includes many other benefits related to different aspects of implementation of the screening procedure. However, the original method completely ignores the SED related to a negative portion of the elastic range, which is incompatible with conventional fatigue standards for welded structures. Ellyin's energy-based approach is well suited to implementing the necessary modifications and aligns with other methods and procedures. The implemented modifications enable adjustability in relation to the negative portion of the elastic energy and effect of the mean stress, which increases compatibility with different rules and assumptions. A further very important benefit of the used method is its suitability for using the strength criteria converted directly from the corresponding data of common fatigue standards and rules. This, in turn, leads to the direct compatibility of the screening method with standard evaluations, at least on the principal level, which increases the reliability of the method and its suitability for practical design work. The implemented test program showed a good correlation between failure locations estimated using the developed screening procedure and results of the experiments. Additionally, the correlation of the estimated and observed absolute fatigue life was also quite good, being mainly within +/- 25%. The achieved accuracy of estimated absolute fatigue life enables the direct use of the results of the screening procedure for preliminary decisions about approximative fatigue resistance of structures and the rationality of further detailed analyses.

6.3 Future work

The combination of individual loads, which causes the most critical combination of corresponding ENS ranges, is determined using the range-based von Mises equivalent and the analogy with the Wang-Brown multiaxial cycle counting. Currently, all possible combinations of individual loads are generated for this purpose with the following direct comparison of von Mises equivalents, based on the corresponding combinations of component ranges. The efficiency of conventional postprocessing tools is sufficient for this purpose, when a few independent loads are considered. The analytical solution of this problem, which would be more efficient than the use of postprocessing tools, was not found in the context of this thesis, and remains to be investigated in later studies. Additionally, determining the most critical combinations using the range-based von Mises equivalent considers only the distortion energy associated with deviatoric stresses,

but ignores the energy related to volumetric changes and the fluctuation of hydrostatic stress, which can be questionable in areas of HCF with predominantly elastic behavior. The criteria based on total energy, which include distortion energy and the energy of volumetric changes, may be better suited for areas of HCF. The development of the method related to using the alternative criteria requires additional investigation in future studies.

An E-PP material model is currently used to consider the effect of monotonic and cyclic plasticity. The use of this simple material model increases the efficiency of the screening procedure and confirms its compatibility with conventional fatigue standards and rules for welded structures. However, it limits the accuracy, especially in cases with significant plasticity. Including more accurate material models in addition to the currently used E-PP material would extend the applicability of the method to more advanced cases, which must be investigated in future studies.

Another promising target for the further development of the screening method is including the capability of distinguishing the bending and membrane stress components to consider their different detrimental effect, as suggested in research by Ahola et al. (2017). Some standards and rules include consideration of the difference between bending and membrane components, and the addition of such a capability would increase the compatibility of the method with them. This capability can be included in the developed method without significant additional efforts, by using considerations of the degrees of bending (DOB) and corresponding correction of either the stress range or fatigue strength.

An effect of the longitudinal stress is currently considered part of the stress state at the weld in the screening of critical locations related to the transversal to the weld discontinuities and notches. Considering discontinuities which determine the fatigue strength of the weld under purely longitudinal loading is another area for development.

The implemented test program has shown successful estimation of failure locations and a good correlation between estimated and observed absolute fatigue life, which was mainly within +/- 25%. However, the test program was limited, and additional tests are needed for extensive confirmation of the accuracy of the developed screening method and its applicability to different cases and situations. Experimental verification is required for the possible additional features presented in this section.

7 Conclusions

Fatigue is one of the most common causes of structural damage, so fatigue analysis is an important part of the design process. Reliable fatigue analysis can be challenging, but several different methods have been developed for the successful analysis of individual locations. The chosen method defines the amount of computational resources required, but, in general, a detailed analysis of every location of the structure is not a viable option. This is especially relevant for large welded structures with a large number of potential failure locations that are not directly comparable with each other to determine critical locations.

The aim of this work was to develop a method to reliably determine the critical locations for a subsequent detailed fatigue analysis, and such a screening method was developed. The method allows the systematic screening of critical locations of welded structures, which is lacking in the available guidelines and rules for the fatigue design of welded structures. The developed screening procedure can be used to obtain the critical locations at the weld toes and weld roots of welded structures loaded by a combination of a few independent constant amplitude fatigue loadings. The combined effect of different loads, typical for this quite general loading condition, can result in a multiaxial non-proportional state which can be considered using the developed screening method.

The input information required for the screening procedure is structural stresses at the weld toe and nominal stresses in the weld throats, which can be obtained by conventional linear elastic analysis. The required level of accuracy can be achieved nowadays using the global FE models of complete structures or large parts of them.

The developed screening method includes the capability to consider or ignore different factors, depending on available data, desired accuracy, and the requirements of the used standards and rules. More accurate screening, without the simplifications caused by standard assumptions, can be achieved by increasing the number of considered parameters and using more detailed data. The detrimental effect of the local cyclic plasticity, monotonic local plasticity, residual and mean stresses, actual local geometry of weld, and other specific parameters can all be taken into account in the advanced screening. However, for purposes of compatibility with certain fatigue standards and rules, these advanced parameters can be ignored or adjusted to the appropriate level, and the partial efficiency of the compressive stress range can be considered according to standard requirements, if necessary. This renders the developed method suitable for both basic design work and more advanced research use.

The screening procedure determines the critical locations using fatigue criteria modified from Ellyin's energy-based model. The required strain energy density (SED) is defined by effective notch stresses (ENS) calculated using appropriate fatigue notch factors. The usage of the SED-based fatigue criterion significantly increases the flexibility of the screening method and its capability to consider different factors and parameters, which extends its applicability beyond the conventional assumptions of fatigue guidelines for

welded structures. The multiaxial fatigue strength parameters for the screening procedure can be determined using appropriate uniaxial S-N curves of related standards or other fatigue data available in the literature, or defined by appropriate fatigue tests. The threshold values related to the non-damaging level of cyclic loading can also be considered or ignored, depending on the actual requirements. The capability to utilize the fatigue data available in the conventional fatigue standards increases the compatibility of the developed screening method with the guidelines and rules, as well as its applicability to practical design work.

Based on the tests implemented in this work to verify the developed screening method, the estimated failure locations correlate with those observed by experiments. Additionally, there was a good correlation of estimated and observed absolute fatigue lives, which improves the reliability of the screening procedure and increases the value and usability of the results. In addition to determining the critical locations for a subsequent detailed analysis, which is the primary purpose, preliminary decisions about the fatigue resistance of the current structure and the rationality of further analysis can be made based on the results of the developed screening procedure. However, the implemented test program was limited, and additional experiments are necessary for further verification. A reasonable target for further development of the screening method is extending the area of applicability by including the more accurate material models and other capabilities, required for more sophisticated use.

References

Ahola, A., Nykänen, T., Björk, T. (2017), Effect of loading type on the fatigue strength of asymmetric and symmetric transverse non-load carrying attachments. *Fatigue & Fracture of Engineering Materials and Structures*, Vol. 40, pp. 670–682. DOI: 10.1111/ffe.12531

Ahola, A., Björk, T., Barsoum, Z. (2019), Fatigue strength capacity of load-carrying fillet welds on ultra-high-strength steel plates subjected to out-of-plane bending. *Engineering structures*, Vol. 196, 109282. DOI: https://doi.org/10.1016/j.engstruct.2019.109282

Björk, T., Mettänen, H., Ahola, A., Lindgren, M., Terva, J. (2018), Fatigue strength assessment of duplex and super-duplex stainless steels by 4R method. Welding in the World 62: 1285. DOI: https://doi.org/10.1007/s40194-018-0657-8

Bannantine, J. and Socie, D. (1991). A variable amplitude fatigue life prediction method. In: Kussmaul K, McDiarmid D, Socie D, editors. *Fatigue under biaxial and multiaxial loading*, ESIS 10. London: Mechanical Engineering Publications, p. 36–51.

Bäckström, M. (2003). *Multiaxial fatigue life assessment of welds based on nominal and hot spot stresses*: Dissertation. Espoo: VTT Technical Research Centre of Finland, (VTT Publications; 502). ISBN: 951-38-6234-8 (electronic). URL: http://www.vtt.fi/inf/pdf/publications/2003/P502.pdf

Chattopadhyay, A., Glinka, G., El-Zein, M., Qian, J. and Formas, R. (2011). Stress analysis and fatigue of welded structures. *Welding in the World*, Vol. 55, Issue 7-8, pp. 2–21 (Doc. IIW-2201). DOI: http://dx.doi.org/10.1007/BF03321326

DNV-GL (2016). *Fatigue design of offshore steel structures.* Recommended practice DNVGL-RP-C203, DNV GL AS

Doerk, O., Fricke, W. and Weissenborn, C. (2003). Comparison of different calculation methods for structural stresses at welded joints. *International Journal of Fatigue*, Vol. 25, pp. 359-369. doi:10.1016/S0142-1123(02)00167-6

Dong, P. (2001). A Structural Stress Definition and Numerical Implementation for Fatigue Analysis of Welded Joints. *International Journal of Fatigue*, Vol. 23, pp. 865–876

Dong, P., Prager, M. and Osage, D. (2007). The Design Master S-N Curve in ASME div 2 rewrite and its validations. *Welding in the World*, Vol. 51, Issue 5-6, pp. 53–63 (Doc. IIW-1802-07). DOI: https://doi.org/10.1007/BF0326657

Dowling, N.E. (2013). *Mechanical behavior of materials: Engineering methods for deformation, fracture, and fatigue*. 4th edn., international edition. Pearson Education, Harlow. ISBN 10: 0-273-76455-1; ISBN 13: 978-0-273-76455-7.

Ellyin, F. (1989a). Cyclic strain energy density as a criterion for multiaxial fatigue failure. *Biaxial and multiaxial fatigue,* EGF 3 (Edited by Brown, M.W. and Miller, K.J.), 1989, Mechanical Engineering Publications, London, pp. 571-583, ISBN 0-85298-669-6

Ellyin, F. and Kujawski, D. (1989b). Generalization of notch analysis and its extension to cyclic loading. *Engineering Fracture Mechanics*, Vol. 32, Issue 5, pp. 819-826, DOI: https://doi.org/10.1016/0013-7944(89)90178-1

Ellyin, F. and Xia, Z. (1993). A General Fatigue Theory and Its Application to Out-of-Phase Cyclic Loading. *Journal of Engineering Materials and Technology*, Vol. 115, Issue 4, pp. 411-416. doi:10.1115/1.2904239.

fe-safe (2002). *Fatigue Theory Reference Manual*, Software documentation Vol. 2, safe technology limited.

fe-safe (2017). *fe-safe User Guide*, Software documentation Vol. 1, Dassault Systèmes Simulia Corp.

Fermér, M., Andréasson, M., & Frodin, B. (1998). Fatigue Life Prediction of MAG-Welded Thin-Sheet Structures. *SAE Transactions*, Vol. 107, Section 5: Journal Of Materials & Manufacturing, 1280-1286. Retrieved from http://www.jstor.org/stable/44724267. SAE Technical Paper 982311. DOI: https://doi.org/10.4271/982311.

Fermér, M. and Svensson, H. (2001). Industrial experiences of FE-based fatigue life predictions of welded automotive structures. *Fatigue & Fracture of Engineering Materials and Structures*, Vol. 24, No. 7, pp. 489–500. DOI: https://doi.org/10.1046/j.1460-2695.2001.00409.x

Fricke, W. and Bogdan, R. (2001). *Determination of Hot Spot Stress in Structural Members with In-Plane Notches Using a Coarse Element Mesh.* Conference paper: Annual Assembly of International Institute of Welding, IIW Doc. XIII-1870-01 [Retrieved March. 12, 2019], url: https://www.researchgate.net/publication/283462099

Fricke, W. (2013). IIW guideline for the assessment of weld root fatigue. *Welding in the World*. Vol. 57, pp. 753-791. doi:10.1007/s40194-013-0066-y

Heuler, P. and Seeger, T. (1986). A Criterion for Omission of Variable Amplitude Histories. *International Journal of Fatigue,* Vol. 8, Issue 4, pp. 225-230. doi: 10.1016/0142-1123(86)90025-3

Hobbacher, A. (2008). *Recommendations for Fatigue Design of Welded Joints and Components.* International Institute of Welding, Paris. doc. XIII-2151r4-07/XV-1254r4-07

Hänel, B., Haibach, E., Seeger, T., Wirtgen, G. and Zenner, H. (2003), *Analytical Strength Assesment of components in mechanical engineering*, FKM-Guideline, 5th ed., ISBN 3-8163-0425-7

Ince, A., Glinka, G. (2016). Innovative computational modelling of multiaxial fatigue analysis for notched components. *International Journal of Fatigue,* Vol. 82, Part 2, pp. 134-145. https://doi.org/10.1016/j.ijfatigue.2015.03.019

Jussila, J., Holopainen, S., Kaarakka, T., Kouhia, R., Mäkinen, J., Orelma, H., Ottosen, N., Ristinmaa, M. and Saksala, T. (2017). A new paradigm for fatigue analysis - evolution equation based continuum approach. *Rakenteiden Mekaaniikka (Journal of Structural Mechanics),* Vol. 50(3), pp. 333-336. DOI: 10.23998/rm.65096

Glinka, G. (1985). Calculation of Inelastic Notch-tip Strain-stress Histories Under Cyclic Loading. *Engineering Fracture Mechanics,* Vol. 22(5), pp. 839-854. DOI: 10.1016/0013-7944(85)90112-2

Kyuba, H and Dong, P. (2005). Equilibrium-equivalent structural stress approach to fatigue analysis of a rectangular hollow section joint. *International Journal of Fatigue*, Vol. 27, pp. 85–94

Köhler, M., Jenne, S., Pötter, K. and Zenner, H. (2017). *Load Assumption for Fatigue Design of Structures and Components*. Springer Verlag. Berlin. ISBN 978-3-642-55248-9 (eBook). DOI:10.1007/978-3-642-55248-9.

Manson, S., Freche, J. and Ensign, C. (1967). *Application of a double linear damage rule to cumulative fatigue.* NASA technical note TN D-3839 [Retrieved March. 28, 2019], url: https://ntrs.nasa.gov/archive/nasa/casi.ntrs.nasa.gov/19670013955.pdf

Marin, T. and Nicoletto, G. (2009), Fatigue design of welded joints using the finite element method and the 2007 ASME Div. 2 Master curve, *Frattura ed Integrità Strutturale*, Vol. 3, No. 9, pp. 76 - 84; DOI: 10.3221/IGF-ESIS.09.08

Meggiolaro, M. and de Castro, J. (2012). An improved multiaxial rainflow algorithm for non-proportional stress or strain histories – Part II: The Modified Wang–Brown method. *International Journal of Fatigue*, Vol. 42, 194–206. DOI: 10.1016/j.ijfatigue.2011.10.012

Molski, K. and Glinka, G. (1981). A method of elastic-plastic stress and strain calculation at a notch root. *Materials Science and Engineering,* Vol. 50(1), pp. 93-100. DOI: 10.1016/0025-5416(81)90089-6

McDiarmid, D. (1989). The effect of mean stress on biaxial fatigue where the stresses are out-of-phase and at different frequencies. *Biaxial and Multiaxial Fatigue,* EGF3 (Edited by Brown, M. and Miller, K.), Mechanical Engineering Publications, London. ISBN: 0-85298-669-6

Moon, J., Perret, B. and Edwards, P. (1977), *A Study of Local Stress Histories in Loaded and Unloaded Holes and their Implications for Fatigue Life Estimation*. Aeronautical Research Council, Paper C.P. No. 1374, London.

nCode (2018). *DesignLife Theory Guide*, NC-DLTH 18.1.01 (HBM United Kingdom Limited)

Niemi, E. (1995). *Stress Determination for Fatigue Analysis of Welded Components.* International Institute of Welding, Abington Publishing, Cambridge, Doc. IIS/IIW-1221-93. ISBN 1 85573 213 0

Niemi, E., Fricke, W. and Maddox S. (2018). *Structural Hot-Spot Stress Approach to Fatigue Analysis of Welded Components Stress: Designer's Guide.* 2nd ed., IIW collection, Springer Nature Singapore Pte Ltd., ISBN 978-981-10-5568-3 (eBook). doi:10.1007/978-981-10-5568-3

Nykänen T., Mettänen H., Björk T., Ahola A. (2017). Fatigue assessment of welded joints under variable amplitude loading using a novel notch stress approach. *International Journal of Fatigue*, Vol. 101, pp. 177-191. https://doi.org/10.1016/j.ijfatigue.2016.12.031

Ottosen, N., Stenström, R. and Ristinmaa, M. (2008). Continuum approach to high-cycle fatigue modeling. *International Journal of Fatigue*, Vol. 30, Part 6, pp. 996-1006. https://doi.org/10.1016/j.ijfatigue.2007.08.009

Peterson, R. (1974), *Stress Concentration Factors: Charts and Relations Useful in Making Strength Calculations for Machine Parts and Structural Elements*. John Wiley, New York. ISBN 0-471-68329-9

Ping, Z., Jun, H. and Jin, M. (2008). Fatigue life analysis of the autobody in a sports utility vehicle and its improvement using the homogenization method. *Proceedings of The Institution of Mechanical Engineers*, Vol. 222, Part D-journal of Automobile Engineering, pp. 2291-2305. doi: 10.1243/09544070JAUTO916

Rabb, R. (2017). *Väsyminen ja todennäköisyysteoria (in finnish)*, Juvenes Print. Oulu. ISBN 978-952-62-1639-3

Radaj, D. (1984). Notch effect of welded joints under biaxial oblique loading. *Schweissen und Schneiden/Welding and Cutting*, Vol. 36, Issue 6, pp. E86-E88 (English version).

Radaj, D., Sonsino, C. and Fricke, W. (2006). *Fatigue assessment of welded joints by local approaches*, Second ed., Woodhead Publishing. Cambridge. ISBN 978-1-85573-948-2

SFS 2378 (1992, repealed), *Welding. Load capacity of welded joints in fatigue loaded steel structures.* Helsinki: Finnish Standards Association SFS.

SFS-EN 10025-2 (2019), *Hot rolled products of structural steels. Part 2: Technical delivery conditions for non-alloy structural steels*, Finnish standards association (SFS), Helsinki

SFS-EN 1993-1-9 (2005), *Eurocode 3: Design of steel structures. Part 1-9: Fatigue*, Finnish standards association (SFS), Helsinki

SFS-EN 13001-3-1 (2018), *Cranes. General Design. Part 3-1: Limit States and proof competence of steel structure*, Finnish standards association (SFS), Helsinki

SFS-EN 13445-3 (2017), *Unfired pressure vessels. Part 3: Design*, Finnish standards association (SFS), Helsinki

Singh, M., Glinka, G. and Dubey, R. (1996). Elastic-plastic stress-strain calculation in notched bodies subjected to nonproportional loading. *International Journal of Fracture*, Vol. 76, pp. 39-60. DOI: 10.1007/BF00034029

Socie, DF. and Marquis, GB. (2000). *Multiaxial Fatigue*. SAE International, Warrendale. ISBN 0-7680-0453-5

Sonsino, C.M. (1982). *Einfluß von Kaltverformungen bis 5% auf das Kurzzeitschwingfestigkeitsverhalten metallischer Werkstoffe (Influence of cold forming up to 5% on the low-cycle fatigue behaviour of metallic materials)*, LBF-Bericht FB-161, (Doctoral dissertation, Darmstadt, Fraunhofer-Institut für Betriebsfestigkeit)

Sonsino, C.M., Maddox, S.J. and Hobbacher, A. (2004). Fatigue life assessment of welded joints under variable amplitude loading − State of present knowledge and recommendations for fatigue design regulations. In: *Proceedings of the Annual IIW-assembly and Int. Conference*, Osaka/Japan, pp. 87-102.

Sonsino C.M., Wiebesiek J. (2007). *Assessment of multiaxial spectrum loading of welded steel and aluminium joints by modified equivalent stress and Gough-Pollard algorithms. IIW-Doc. No. XIII-2158r1-07/XV-1250r1-07*

Sonsino C.M. (2009a). Effect of residual stresses on the fatigue behaviour of welded joints depending on loading conditions and weld geometry. *International Journal of Fatigue*, Vol. 31, pp. 88-101. doi:10.1016/j.ijfatigue.2008.02.015

Sonsino C.M. (2009b). Multiaxial fatigue assessment of welded joints – Recommendations for design codes. *International Journal of Fatigue,* Vol. 31, pp. 173-187. doi:10.1016/j.ijfatigue.2008.06.001

Sonsino C.M., Fricke W., de Bruyne F., Hoppe A., Ahmadi A., Zhang G. (2012). Notch stress concepts for the fatigue of welded joints –background and applications. *International Journal of Fatigue,* Vol. 34, pp. 2-16. doi: 10.1016/j.ijfatigue.2010.04.011

Stephens, R.I., Fatemi, A., Stephens, R.R. and Fuchs, H.O. (2001). *Metal fatigue in engineering*. 2nd edn. Wiley-Interscience, New York. ISBN 0-471-51059-9

Timoshenko, S. (1983, original edition 1956). *Strength of Materials. Part 2, Advanced Theory and Problems*. 3. ed., repr. Krieger, Malabar, Florida. ISBN 0-88275-421-1

Topper, T., Wetzel, R. and Morrow, J. (1969). Neubers rule applied to fatigue of notched specimens. *J. Materials*, Vol. 4(1), pp. 200-209.

Veltri, M. (2016). FEM Techniques for High Stress Detection in Accelerated Fatigue Simulation. *Journal of Physics: Conference Series*, Vol. 744, Number 1. doi:10.1088/1742-6596/744/1/012137

Wang, C. and Brown, M. (1996). Life Prediction Techniques for Variable Amplitude Multiaxial Fatigue – Part 1: Theories. *Journal of Engineering Materials and Technology* (Transactions of the ASME), Vol.118 (3), pp. 367-370.

Yan, J.H., Zheng, X.L. and Zhao, K. (2001). Experimental investigation on the small-load-omitting criterion. *International Journal of Fatigue*, Vol. 23, Issue 5, pp. 403-415. https://doi.org/10.1016/S0142-1123(01)00005-6

Yanchukovich, A., Ahola, A. and Björk, T. (2019). Cycle counting of the peak-valley filtered multiaxial loading history using Wang–Brown method (*in finnish*). *Rakenteiden Mekaniikka (Journal of Structural Mechanics)*, Vol. 52, Issue 2, pp. 61-76. https://doi.org/10.23998/rm.75618

Appendix A: The yield stress of the material and the cyclic plasticity

In the case of constant amplitude loading, the cyclic plasticity at the level of the effective notch stress (ENS) occurs when the amplitude exceeds the yield stress of the material. The number of cycles related to beginning the cyclic plasticity can be calculated using the corresponding stress range and appropriate fatigue strength:

$$N = 2 \cdot 10^6 \cdot \left(\frac{FAT^{ENS}}{2 f_y} \right)^3 \quad \text{(A.1)}$$

where

f_y is the yield stress of the material
FAT^{ENS} is the ENS fatigue class, typically FAT^{ENS} = 225 MPa

Figure A.1 presents the number of cycles related to beginning the cyclic plasticity at the level of the ENS, depending on the yield stress of the materials. Corresponding calculations for constant amplitude loading are presented in Table A.1.

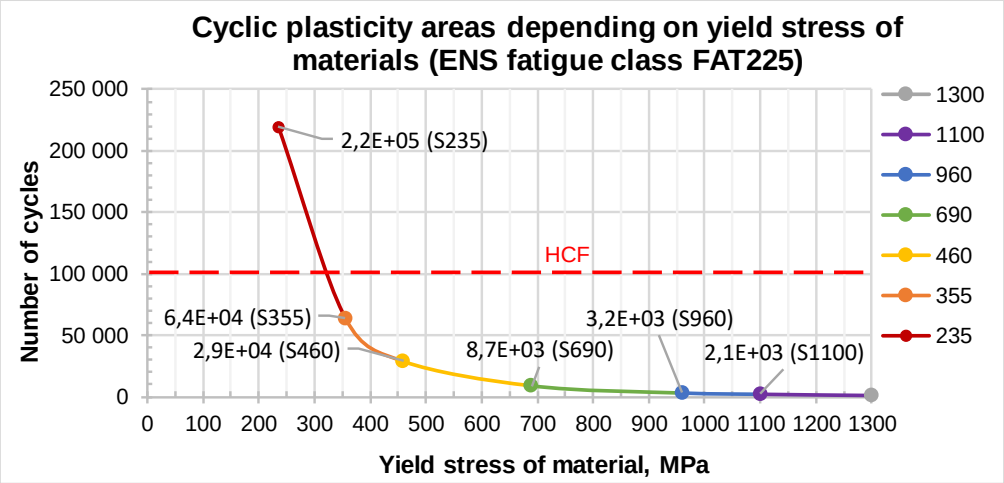

Figure A.1: The number of cycles related to the beginning of cyclic plasticity, depending on the yield strengths of the materials.

Based on these results, the yield stress of f_y = 325 MPa is the limit for beginning the cyclic plasticity on an area of high cycle fatigue (HCF, $N > 10^5$). The most common structural steels have a yield stress of over 325 MPa up to the thickness of 80 mm (SFS-EN 10025-2, 2019); thus, elastic behavior is expected on an area of HCF under constant amplitude loading. However, due to the variable amplitude loading, occasional local plasticity can

occur in some combination of the independent loads, as explained in Section 2.1, or on the transition area below 10^5 cycles. Additionally, for structural steel S235 with a yield stress of f_y = 235 MPa, the limit of cyclic plasticity under constant amplitude loading is $2.2 \cdot 10^5$ cycles on an area of the HCF defined as the area of interest. Therefore, the ability to consider local elastic-plastic behavior is not the primary purpose; however, it is very beneficial for the developed screening method.

Table A.1: The beginning of cyclic plasticity, depending on the yield stress of materials.

Material	Yield stress f_y	FAT^{ENS}	$N_{el/pl}$
EN10025-2,3,4,5,6	MPa	MPa	cycles
S235	235	225	2,19E+05
S355	355	225	6,37E+04
S460	460	225	2,93E+04
S690	690	225	8,67E+03
S960	960	225	3,22E+03
S1100	1100	225	2,14E+03
S1300	1300	225	1,30E+03

Appendix B: Verification of the FE model

Test system

Figure B.1 presents the principal scheme of the test system. A motor with eccentric mass was used to generate the vertical vibration loading and hydraulic cylinder to generate the cyclic transversal loading. Vibration frequencies ranged from 25 to 50 Hz, mostly near 45 Hz. The frequency of the cylinder loading was approximately 5 Hz, in general 1/10 the frequency of vibration. An extending arm and adjustable roller support were used to preload the test specimen in a vertical direction.

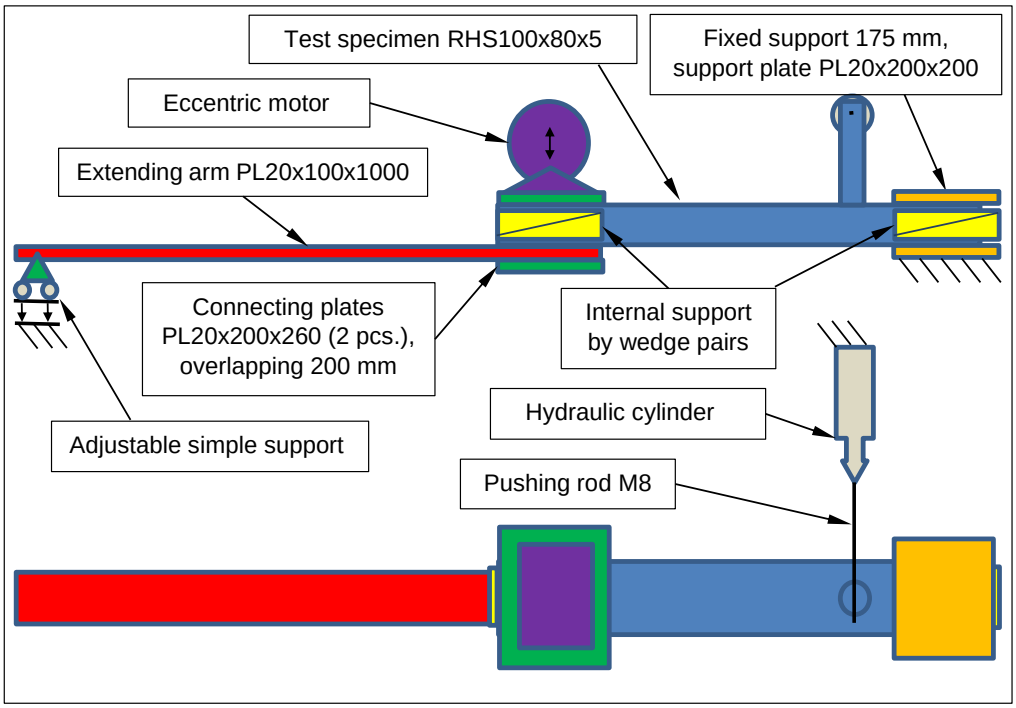

Figure B.1: The principal scheme of the test system.

The test specimen was manufactured by welding the circular tube D42.4x6.3 to the wider flange of the rectangular hollow section (RHS) 100x80x5, as presented in Figure B.2. The RHS tube was 750 mm long and the circular tube was 230 mm high. Details of the test specimen were welded using robotized gas metal arc welding (GMAW). A total of eight test specimens were manufactured. Four specimens were welded by partially-penetrating fillet weld, prepared using a single-bevel with root face with a total weld size of 6 mm (semi-V3 and fillet a3). Four other specimens were welded using a fillet weld of 4.5 mm, two with the original thickness of the pipe (6.3 mm), and two with the thickness of the

pipe decreased to 3.3 mm. The start-stop point of all specimens was located on the compression side related to the transversal cylinder loading. Avoiding fatigue failure at the start-stop location was confirmed by local high frequency mechanical impact (HFMI) treatment. The RHS tube was made of fine-grain steel S420MH (SSAB DOMEX) and the circular tube was made of steel P235GH (S235JRH).

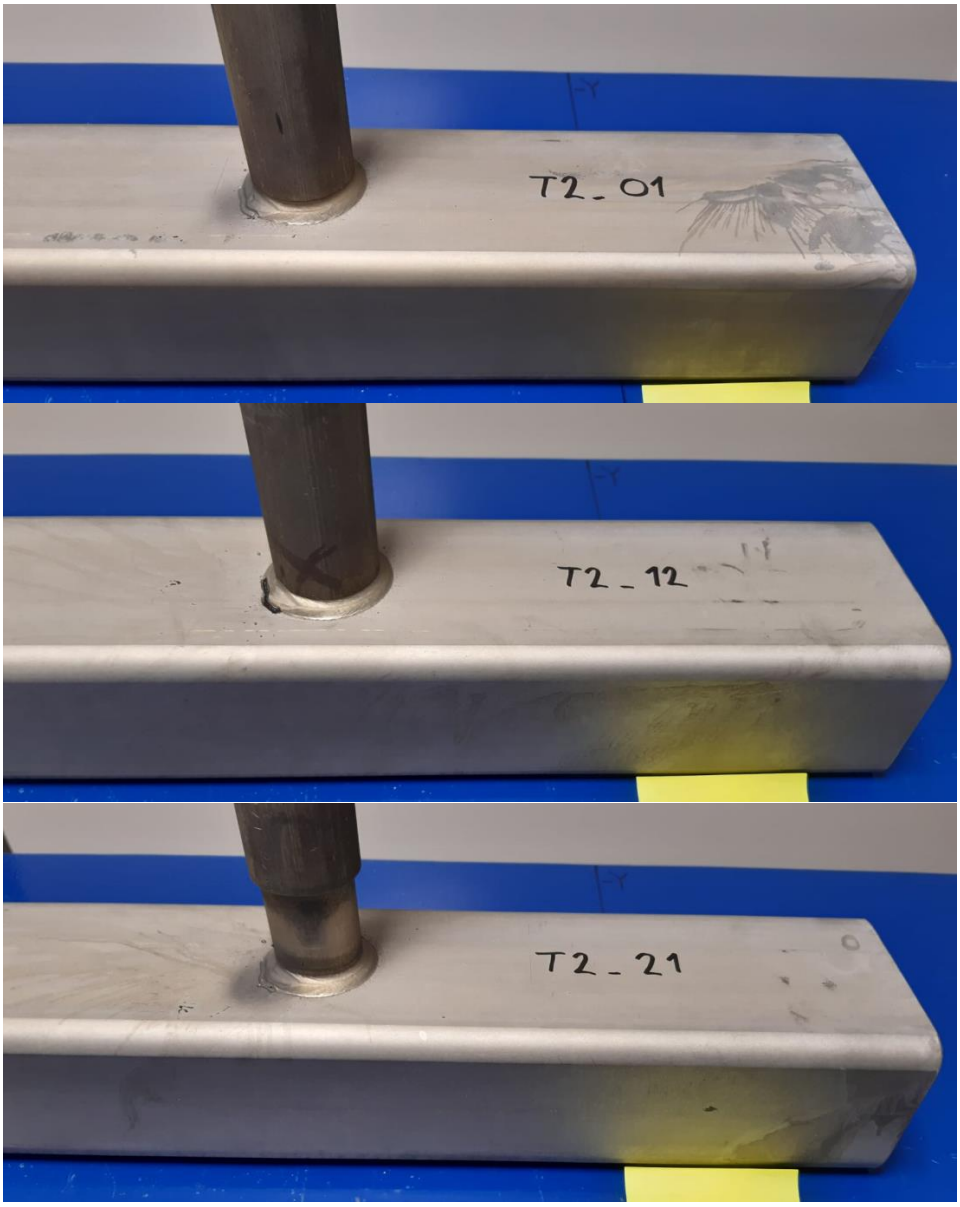

Figure B.2: Test specimens of three types: T2_01, T2_12, and T2_21.

Strain gauges were used to measure the strains at the location of interest. The instrumentation of the strain gauge is presented in Figure B.3. The typical distances of the strain gauges from the weld toe on the RHS were 3 mm and 5 mm. In cases of decreased thickness of the vertical pipe, the distances of the strain gauges from the weld toe on the pipe were 2 mm and 3 mm.

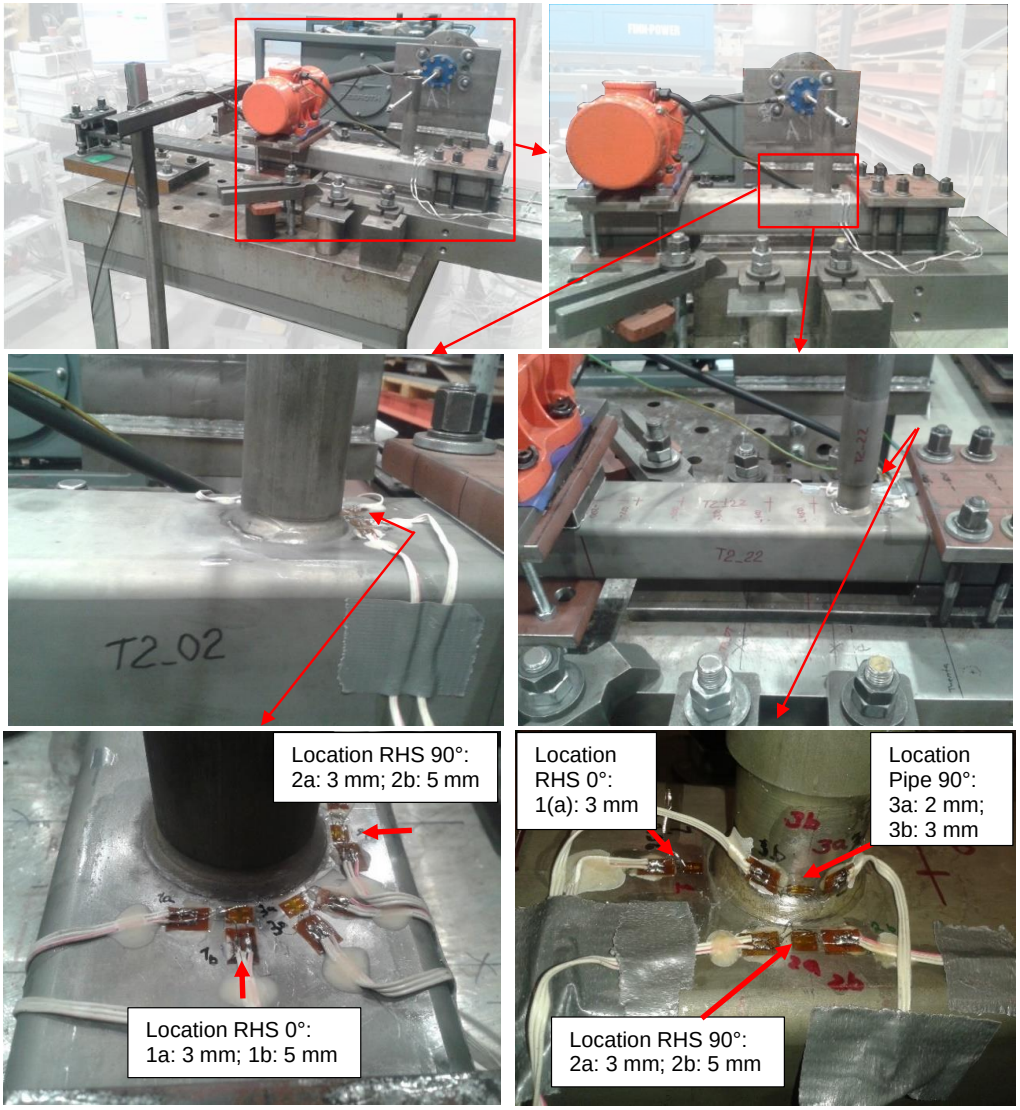

Figure B.3: Locations of the strain gauges on the test specimens T2_02 and T2_22.

Results of the measurements

Verification of the FE model was based on the measurements of the individual cyclic loading detached from another loading. The measurement results at the location of strain gauges 1a, 1b, 2a, 2b, and 3a, 3b (see Figure B.3) were used for verification.

Vertical vibration loading

Figure B.4 presents a summary of the measurements of different specimens (T2_01–T2_04, T2_11–T2_12 and T2_21–T2_22) under vertical vibration loading. Based on the results presented in Figure B.4, there is an almost linear relation between the strain range and the range of vertical displacement. The ratios of the strain range to the range of the vertical displacement at the location of strain gauges 1a (L1), 2a (L2a) are presented in Table B.1.1. The distance of these strain gauges from the weld toe is 3 mm (Figure B.3).

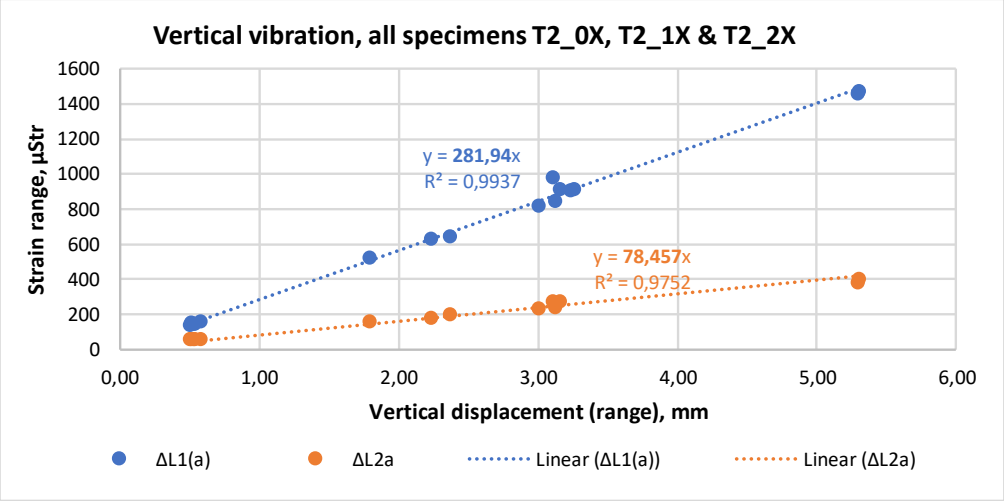

Figure B.4: Relation between the strain range and the range of the vertical displacement under vertical vibration.

Table B.1.1: Strain-displacement ratios of the ranges under vertical vibration.

Item (Figure B.3)	Location (Figure B.3)	Strain/Displacement µStr/mm (Figure B.4)
Strain gauge 1a	RHS 0° (RHS0); 3 mm from weld toe	282
Strain gauge 2a	RHS 90° (RHS90); 3 mm from weld toe	(-) 78

Transversal loading

Figures B.5.1–B5.3 present a summary of the measurements under transversal cylinder loading, grouped by different types of specimens. Table B2.1 presents ratios of strain ranges to the range of the transversal cylinder loading at the locations of strain gauges 2a (L2a) and 3b (L3b) for different types of specimens. The distance of these strain gauges from the weld toe is 3 mm (Figure B.3).

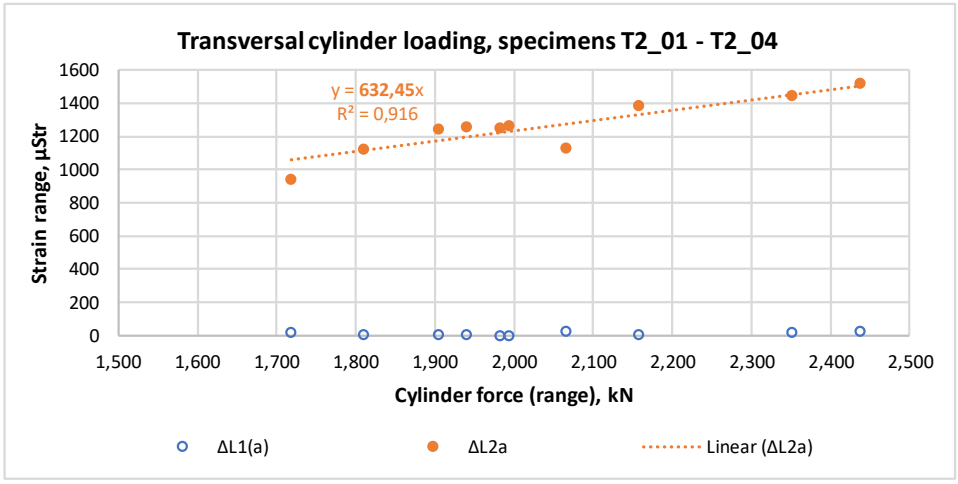

Figure B.5.1: Relation between the strain range and the range of the transversal cylinder loading for specimens T2_01–T2_04. Test specimens Ø42.4 x 6.3; weld size 6 mm (semi-V3 and fillet a3).

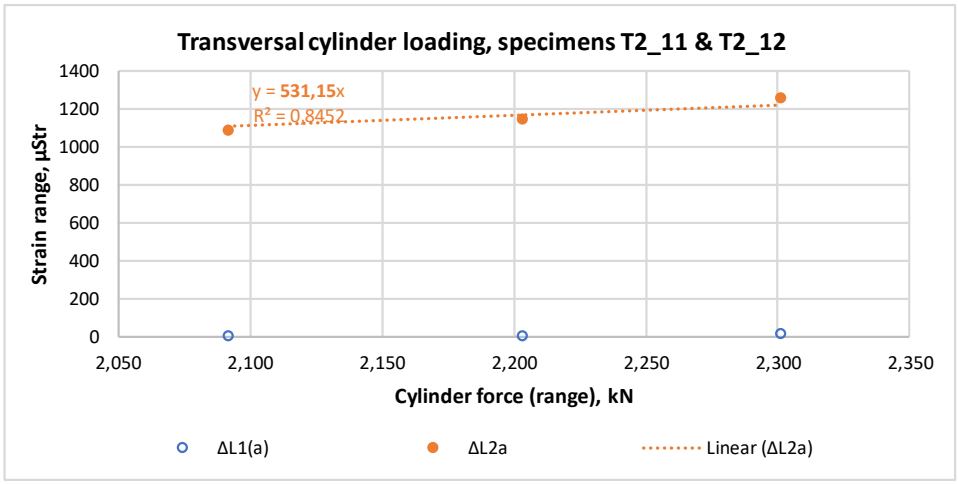

Figure B.5.2: Relation between the strain range and the range of the transversal cylinder loading for specimens T2_11–T2_12 (Ø42.4 x 6.3; weld a4).

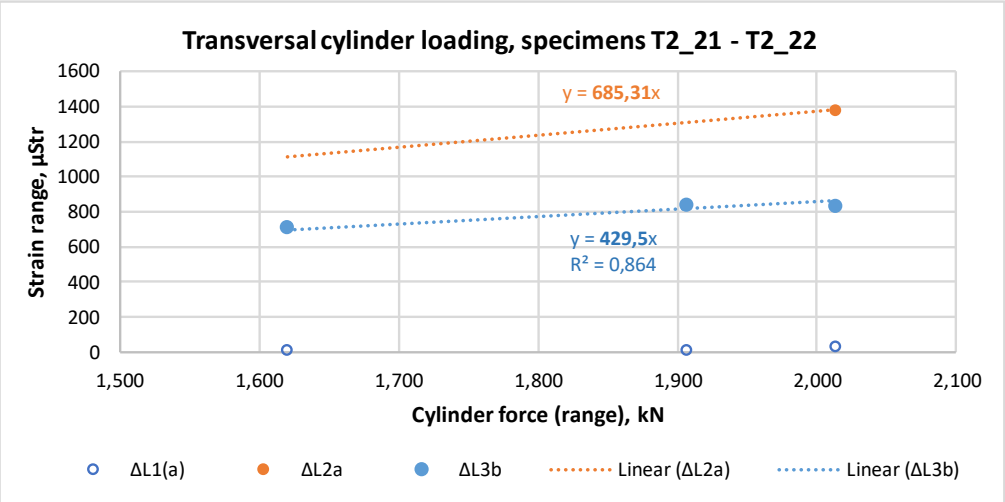

Figure B.5.3: Relation between the strain range and the range of the transversal cylinder loading for specimens T2_21–T2_22 (Ø42.4 x 3.3; weld a4.5).

Table B.2.1: Strain-force ratios of the ranges under transversal loading (Figures B.5.1–B.5.3).

Test specimen group	Description	Strain gauge and location (Figure B.3)	Strain/Force µStr/kN
T2_01 – T2_04	Ø42.4 x 6.3; weld size 6 mm (semi-V3 + fillet a3)	L2a (RHS 90°; 3 mm from weld toe)	632
T2_11 – T2_12	Ø42.4 x 6.3; weld a4	L2a (RHS 90°; 3 mm from weld toe)	531
T2_21 – T2_22	Ø42.4 x 3.3; weld a4.5	L2a (RHS 90°; 3 mm from weld toe)	685
T2_21 – T2_22	Ø42.4 x 3.3; weld a4.5	L3b (Pipe 90°; 3 mm from weld toe)	430

Verification of the FEM results by measurements

The results of the two FE models presented in this chapter are a more accurate linear solid model with an element size of 1 mm near the welded joint, and an approximative parabolic plate model with an element size of 5 mm. The flexibility of the support was taken into account in the FE model by using linear springs. The spring factor was the same for all models. The bending stiffness of the welds in the plate model was adjusted to an appropriate value based on the bending moment and membrane force in the solid model.

Tables B.3.1 and B.3.2 compare the measured normal strains to corresponding strains obtained using FE models. The tables also compare structural stresses, extrapolated from results of the FE models with a relatively fine linear solid element mesh (mesh size 1 mm) to approximate the structural stresses, based on the unaveraged corner stress of parabolic plates with an element size of 5 mm. Figure B.6 presents FE results for specimen type T2_0X (Ø42.4 x 6.3; weld size 6 mm) under vertical vibration loading and Figure B.7 presents corresponding FE results under transversal loading.

Table B.3.1: Results of measurements and FE analysis under a vertical vibration range of 1 mm.

Strain gauge / Location (Distance from weld toe)	Normal strain at the measured location, µStr		Structural stress (FEM), MPa	
	Measured by strain gauge, µStr (See table B.1.1)	Results of FE model (linear solid, mesh size 1 mm)	Defined* by results of FE model with linear solid (mesh size 1 mm)	Approximated** by results of FE model with parabolic plate (mesh size 5 mm)
Specimens T2_01 - T2_04				
L1a / RHS0 (3 mm)	282	306	74 / 69	66
L2a / RHS90 (3 mm)	- 78	-69	-8 / -7	-4
Specimens T2_11 - T2_12				
L1a / RHS0 (3 mm)	282	302	72 / -	65
L2a / RHS90 (3 mm)	- 78	-65	-7 / -	-3
Specimens T2_21 - T2_22				
L1a / RHS90 (3 mm)	282	292	70 / 65	63
L2a / RHS90 (3 mm)	- 78	-62	-5 / -4	-2

*) Structural stress by linear extrapolation on the surface / stress linearization through thickness
**) Structural stress approximation by unaveraged nodal stress

Table B.3.2: Results of measurements and FE analysis under transversal cylinder loading 1 kN.

Strain gauge / Location (Distance from weld toe)	Normal strain at the measured location, µStr		Structural stress (FEM), MPa	
	Measured by strain gauge, µStr (See table B.2.1)	Results of FE model (linear solid, mesh size 1 mm)	Defined* by results of FE model with linear solid (mesh size 1 mm)	Approximated** by results of FE model with parabolic plate (mesh size 5 mm)
Specimens T2_01 - T2_04				
L2a / RHS90 (3 mm)	632	614	210 / 193	224
Specimens T2_11 - T2_12				
L2a / RHS90 (3 mm)	531	595	204 / 189	213
Specimens T2_21 - T2_22				
L2a / RHS90 (3 mm)	685	668	227 / 210	241
L3b / Pipe90 (3 mm)	430	487	239 / 204	240

*) Structural stress by linear extrapolation on the surface / stress linearization through thickness
**) Structural stress approximation by unaveraged nodal stress

According to Tables B.3.1 and B.3.2, the correlation between the measured strains and the results of the FE analysis using linear solid elements is quite good. For the primary strain components, the maximum difference is 13%. Based on the results presented in Tables B.3.1 and B.3.2, the unaveraged corner stresses of the parabolic plate model give an acceptable approximation of the structural stresses, especially for the purpose of the relative screening of critical locations. For primary components, the difference from the solid model does not exceed 11%.

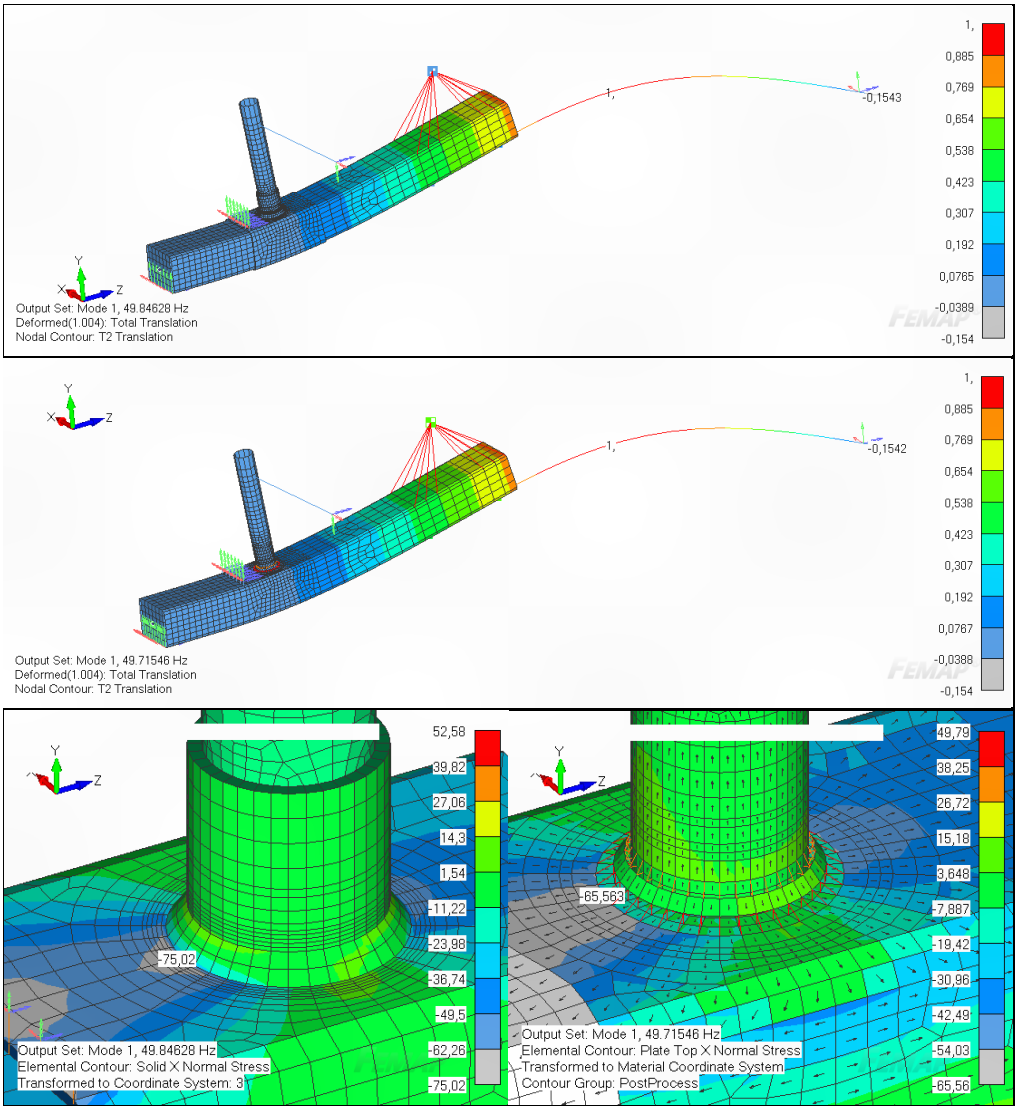

Figure B.6: FE model of test specimen T2_0X (Ø42.4 x 6.3; weld size 6 mm). Deformations and normal surface stresses (MPa) perpendicular to the weld toe under vertical vibration loading with unit vertical displacement. The upper and left-hand figures present the results of the FE model with linear solid elements (mesh size 1 mm). The middle and right-hand figures present the results of the FE model with parabolic plate elements (mesh size 5 mm).

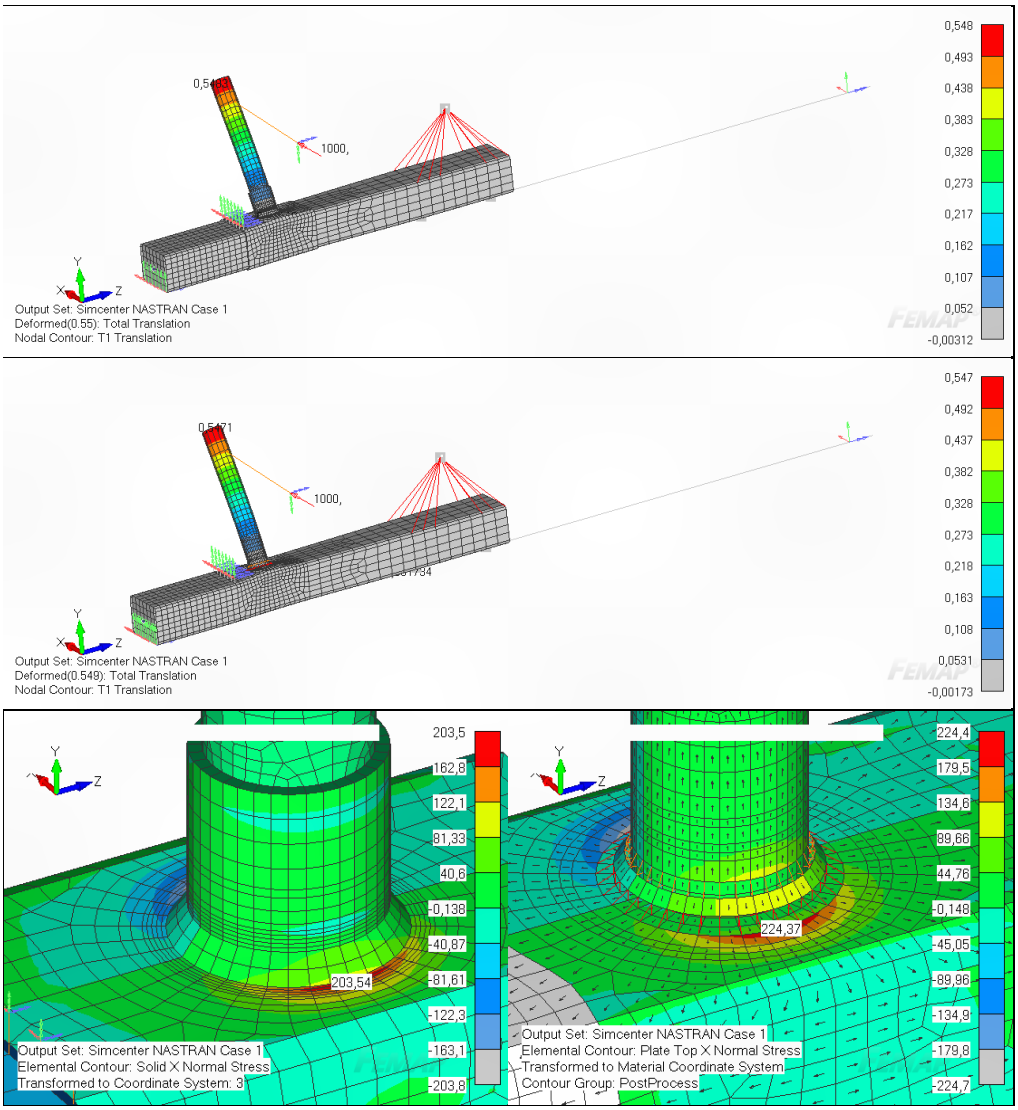

Figure B.7: FE model of test specimen T2_0X (Ø42.4 x 6.3; weld size 6 mm). Deformations and normal surface stresses (MPa) perpendicular to the weld toe under transversal cylinder loading 1000 N. The upper and left-hand figures present the results of the FE model with linear solid elements (mesh size 1 mm). The middle and right-hand figures present the results of the FE model with parabolic plate elements (mesh size 5 mm).

Based on the results presented in this appendix, the used plate model gives appropriate accuracy of the structural stress for purposes of screening analysis and even for the determination of fatigue life.

Appendix C: Effect of the mean stress in the SWT and SED-based methods

Ellyin's strain energy density (SED)-based method estimates a significantly higher influence of the mean stress than the Smith-Watson-Topper (SWT) damage parameter in the case of uniaxial fatigue loading with positive minimum stress. This appendix presents an investigation of the difference between the two methods, including a numerical example. The numerical example compares decreasing the allowable stress range related to increasing the stress ratio from R = 0 to R = 0.5, when a constant fatigue damage is required.

Comparison of the SWT parameter and SED-based method

The SWT damage parameter is based on the product of the maximum stress and amplitude of the strain and considers the influence of the mean stress. The constant value of the damage parameter is assumed for different combinations of the maximum stress and strain amplitude, according to the following equation:

$$\sigma_{\max} \cdot \varepsilon_{\mathrm{a}} = \mathrm{const} \tag{C.1}$$

where

$\sigma_{\max}$ is the maximum stress of the cycle
ε_{a} is the strain amplitude

Equation C.1 can be rewritten using the stress range, minimum stress, and strain range:

$$(\Delta\sigma + \sigma_{\min}) \cdot \frac{\Delta\varepsilon}{2} = \frac{\Delta\sigma\Delta\varepsilon}{2} + \frac{1}{2}\sigma_{\min}\Delta\varepsilon = \mathrm{const} \tag{C.2}$$

where

$\Delta\sigma$ is the stress range of the cycle
$\Delta\varepsilon$ is the strain range
$\sigma_{\min}$ is the minimum stress of the cycle

The SED used in Ellyin's method is shown in Figure C.1 and can be obtained in a uniaxial case using the following equation:

$$W^{\mathrm{e}+} = \frac{\Delta\sigma\Delta\varepsilon}{2} + \sigma_{\min}\Delta\varepsilon \tag{C.3}$$

where the symbols are explained in Equation C.2, above

The first term is same in both Equation C.2 and C.3. In the case of positive minimum stress, this term can be interpreted as a SED related to the stress range. Correspondingly, the second term of Equation C.3 relates to the SED related to the positive minimum stress

below the stress range (see Figure C.1). Thus, Ellyin's energy-based method considers the whole of this SED, while, according to Equation C.2, the SWT-parameter only considers half of it.

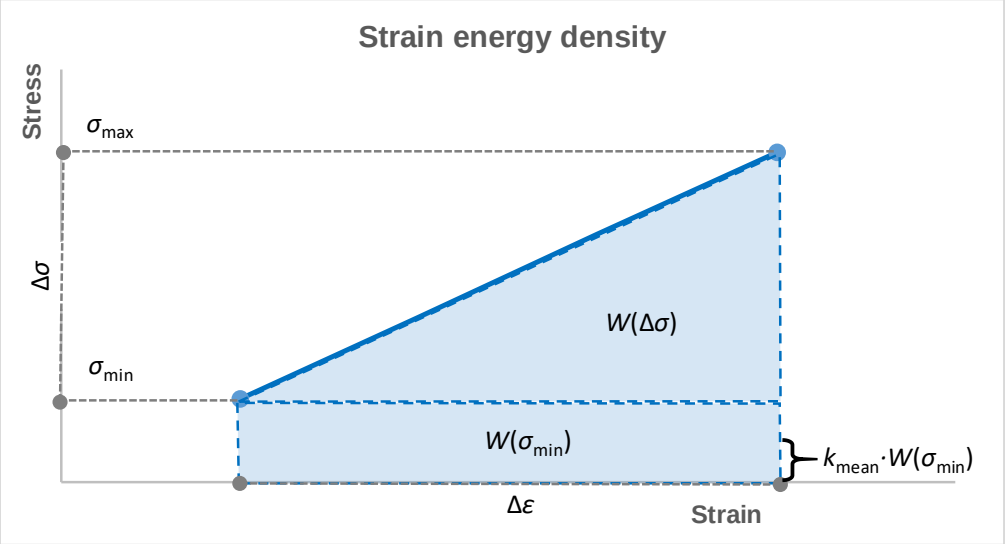

Figure C.1: Strain energy density of uniaxial loading with positive minimum stress

Numerical example

The numerical example demonstrates the difference between the SWT parameter and Ellyin's SED-based model in regard to the effect of the mean stress, presented above. Uniaxial fatigue loading with elastic constant amplitude is assumed in this example, and constant fatigue damage is required for different loadings. The example investigates decreasing the allowable stress range, influenced by increasing the stress ratio from R = 0 to R = 0.5. The reference value is the fatigue damage related to some known fatigue life under uniaxial pulsating loading with stress ratio R = 0. Minimum stress in this case is $\sigma_{min}(R{=}0) = 0$ and maximum stress is $\sigma_{max}(R{=}0) = \Delta\sigma(R{=}0)$. The numeric value to use in this example is $\Delta\sigma(R{=}0)$ = 229.1 MPa. Increasing the stress ratio to R = 0.5 leads to minimum stress $\sigma_{min}(R{=}0.5) = \Delta\sigma(R{=}0.5)$.

SWT parameter

The SWT parameter assumes a constant value of the fatigue damage for different allowed combinations of the maximum stress and the strain amplitude, according to Equations C.1 and C.2. The reference value related to the stress ratio R = 0 is obtained by inserting the numerical values into Equation C.2:

$$\frac{\Delta\sigma^2}{2E} + \frac{\sigma_{\min}\Delta\sigma}{2E} = \frac{229.1^2}{2 \cdot 210000} + 0 = 0.125$$

where

$\Delta\sigma$ = 229.1 MPa	is the stress range of the cycle with R = 0
$\sigma_{\min}$ = 0	is the minimum stress of the cycle
$\sigma_{\max}$ = 229.1 MPa	is the maximum stress of the cycle
$\Delta\sigma/E = \Delta\varepsilon$	is the strain range
$\varepsilon_a = \Delta\varepsilon/2$	is the strain amplitude
E = 2.1e5 MPa	is Young's modulus

Increasing the stress ratio to R = 0.5 changes the minimum stress to value $\sigma_{\min}(R{=}0.5) = \Delta\sigma(R{=}0.5)$. According to the SWT parameter and Equation C.2, the allowable stress range for stress ratio 0.5 and constant value of the fatigue damage 0.125 is:

$$\frac{\Delta\sigma^2}{2E} + \frac{\sigma_{\min}\Delta\sigma}{2E} = \frac{\Delta\sigma^2}{2E} + \frac{\Delta\sigma\Delta\sigma}{2E} = 0.125$$

$$\Delta\sigma(R = 0.5) = \sqrt{0.125 \cdot 210000} = 162 \text{ MPa}$$

According to the SWT parameter, increasing the stress ratio from R = 0 to R = 0.5 decreases the allowable stress range from 229.1 to 162 MPa. The decrease in the allowable stress is 67.1 MPa or 29.3 %.

Ellyin's SED-based method

Next, the same elastic uniaxial case can be investigated using Ellyin's SED-based approach with an assumption of zero threshold SED. The multiaxial constraint factor (MCF) in a uniaxial case is 1.0, and fatigue damage relates directly to positive elastic SED, according to Equation C.3. Using the same numeric values as in the SWT parameter, the result is the same for stress ratio R = 0:

$$\Delta W^{e+} = \int \sigma d\varepsilon = \frac{\Delta\sigma^2}{2E} + \frac{\sigma_{\min}\Delta\sigma}{E} = \frac{229.1^2}{2 \cdot 210000} + 0 = 0.125$$

where

$\Delta\sigma$ = 229.1 MPa	is the stress range of the cycle
$\sigma_{\min}$ = 0	is the minimum stress of the cycle
E = 2.1e5 MPa	is Young's modulus

Correspondingly, based on Ellyin's SED-based method and Equation C.3, the allowable stress range for the stress ratio 0.5 and constant value of the fatigue damage 0.125 is:

$$\frac{\Delta\sigma^2}{2E} + \frac{\sigma_{\min}\Delta\sigma}{E} = \frac{\Delta\sigma^2}{2E} + \frac{\Delta\sigma\Delta\sigma}{E} = 0.125$$

$$\Delta\sigma(R = 0.5) = \sqrt{0.125 \cdot 2 \cdot 210000/3} = 132.3\ MPa$$

where the symbols are explained above.

According to Ellyin's SED-based approach, increasing the stress ratio from R = 0 to R = 0.5 decreases the allowable stress range from 229.1 to 132.3 MPa. The decrease is 96.8 MPa or 42.3 %.

Comparison of results

Based on the case investigated above, Ellyin's method estimates a higher influence of the mean stress than the SWT parameter. When the stress ratio is increased from R = 0 to R = 0.5, the allowable stress range decreases to 58% according to Ellyin's SED-based method and, correspondingly, to 71% according to the SWT method. When using the S-N curve with slope exponent m = 3, the fatigue life estimated for stress ratio R = 0.5 by Ellyin's method is nearly twice as short as that estimated by SWT. The difference between the methods increases when there are smaller stress ranges and higher stress ratios.

Correcting the effect of the mean stress

The difference between the effect of the mean stress calculated by the SWT parameter and Ellyin's SED-based method is observed. The reliability of the SWT damage parameter is well verified by its widespread use for uniaxial loading (Stephens et al., 2001). Additionally, the SWT parameter is a special case of another commonly-used Walker equation, applied with material constant γ = 0.5 (Dowling, 2013). The results of the preliminary test series T2_0X also support the assumption that the SED-based damage parameter overestimates the influence of the SED below positive minimum stress in uniaxial or nearly uniaxial loading.

The partial effectiveness of that portion of the SED located below the positive minimum stress can be considered by correction factor k_{mean}, as presented in Figure C.1. Using correction factor k_{mean}, Equations C.2 and C.3 can be presented in a general form for an individual component:

$$\mathrm{W}^{e+} = \frac{\Delta\sigma\Delta\varepsilon}{2} + k_{\text{mean}} \cdot \sigma_{\min}\Delta\varepsilon \qquad \text{(C.4)}$$

where

$\Delta\sigma$	is the stress range of the cycle
$\Delta\varepsilon$	is the strain range
σ_{min}	is the positive minimum stress of the cycle

k_{mean} is the factor for correcting the effectiveness of the portion of SED located below positive minimum stress
k_{mean} = 1 corresponds to Ellyin's SED-based method without reduction
k_{mean} = 0.5 corresponds to the SWT parameter in a uniaxial case
k_{mean} = 0 corresponds to the conventional fatigue standards and rules for welded structures, which assume high residual stresses and a fully effective stress range, but ignore the influence of the different positive mean stresses

In multiaxial cases, Equation C.4 enables an independent correction of the mean stress effect of the individual components, transformed to a principal coordinate system. The alternative to independently correcting the individual components is the mean stress correction based on hydrostatic stress, as implemented in Sines parameter. However, using hydrostatic stress can lead to an unreasonable compensation of the positive and negative components of the mean stress in some cases. Additionally, the hydrostatic stress assumes that any individual component of the mean stress has the same influence, independently of the direction of the actual stress range. The test results published by McDiarmid (1989) show that the influence of transversal mean stress in combination with longitudinal stress range is insignificant, while that of the longitudinal mean stress is known to be significant. These results support the independent correction of individual components instead of using hydrostatic stress. The following equation presents an independent componential correction of the mean stress effect in general form for a principal coordinate system:

$$W_i^{e+} = \frac{\Delta\sigma_i \Delta\varepsilon_i}{2} + k_{mean} \cdot \sigma_{i,min} \Delta\varepsilon_i \tag{C.5}$$

where

$\Delta\sigma_i$ is the range of the principal stress component
$\Delta\varepsilon_i$ is the range of the principal strain component
σ_i^{min} is the positive minimum value of the principal stress component
i index, related to the principal components (i = 1,2 for plane stress condition)
k_{mean} is the correction factor explained above (Equation C.4)

Appendix D: Determining the yielding point inside a semi-plastic step

The yielding point of the semi-plastic step is determined using relative time with $T = 0$ at the start of the step and $T = 1$ at the end. The corresponding values of the von Mises stress at these points are $\sigma_{VM}(0)$ and $\sigma_{VM}(1)$; the first is less than the yield stress of material, and the second is greater. The linear change of the stress components during the individual step is assumed, but changes of the corresponding von Mises stress are nonlinear. The yielding point in the semi-plastic step is estimated using two interpolation points with additional correction. The first interpolation point is defined using the following equations:

$$T_{\text{int1}} = \frac{f_y - \sigma_{\text{VM}}(0)}{\sigma_{\text{VM}}(1) - \sigma_{\text{VM}}(0)} \tag{D.1}$$

$$\sigma_i(T_{\text{int1}}) = \sigma_i(0) + T_{\text{int1}} \cdot [\sigma_i(1) - \sigma_i(0)] \tag{D.2}$$

where

T_{int1}	is the first interpolation point
f_y	is the yield stress of the material
$\sigma_i(T_{\text{int1}})$	is the values of the stress components at the point T_{int1}
$\sigma_i(0)$, $\sigma_i(1)$	are the values of the stress components at the start and end of the current step, correspondingly
$\sigma_{\text{VM}}(0)$, $\sigma_{\text{VM}}(1)$	are the values of the von Mises stress at the start and end of the current step, correspondingly

The second interpolation point T_{int2} is defined using the following conditional equations:

$$T_{\text{int2}} = \begin{cases} \dfrac{(T_{\text{int1}} + 1)}{2}, & \text{if } \sigma_{\text{VM}}(T_{\text{int1}}) < \sigma_{\text{VM}}(0) \\ \dfrac{2f_y - \sigma_{\text{VM}}(T_{\text{int1}}) - \sigma_{\text{VM}}(0)}{\sigma_{\text{VM}}(1) - \sigma_{\text{VM}}(0)}, & \text{if } 2f_y - \sigma_{\text{VM}}(T_{\text{int1}}) < \sigma_{\text{VM}}(1) \\ 1, & \text{if } 2f_y - \sigma_{\text{VM}}(T_{\text{int1}}) > \sigma_{\text{VM}}(1) \end{cases} \tag{D.3}$$

$$\sigma_i(T_{\text{int2}}) = \sigma_i(0) + T_{\text{int2}} \cdot [\sigma_i(1) - \sigma_i(0)] \tag{D.4}$$

where

T_{int1}	is the first interpolation point, defined using Equation D.1
$\sigma_{\text{VM}}(T_{\text{int1}})$	is the von Mises stress at the point T_{int1}, calculated using the stress components defined by Equation D.2
$\sigma_i(T_{\text{int2}})$	is the values of the stress components at the point T_{int2} and the other symbols are explained in Equation D.2, above

The preliminary approximation of the yielding point is obtained using defined interpolation points:

$$T_y = \begin{cases} T_{\text{int1}}, & \text{if } T_{\text{int1}} = T_{\text{int2}} \\ T_{\text{int1}} + (T_{\text{int2}} - T_{\text{int1}}) * \dfrac{f_{\text{y}} - \sigma_{\text{VM}}(T_{\text{int1}})}{\sigma_{\text{VM}}(T_{\text{int2}}) - \sigma_{\text{VM}}(T_{\text{int1}})} \end{cases} \quad \text{(D.5)}$$

$$\sigma_i(T_{\text{y}}) = \sigma_i(0) + T_{\text{y}} \cdot [\sigma_i(1) - \sigma_i(0)] \quad \text{(D.6)}$$

where

T_{y} is the first estimation of the relative time related to reaching the yielding point

$\sigma_{\text{VM}}(T_{\text{int2}})$ is the von Mises stress at interpolation point T_{int2}, calculated using the stress components defined by Equation D.4

$\sigma_i(T_{\text{y}})$ is the values of the stress components at estimated point T_{y} and the other symbols are explained in Equation D.2, above

The value of the von Mises stress calculated using stress components, defined by Equation D.6, is generally very close to the yield stress f_{y}. If necessary, the additional correction of the components defined above by scale factor $f_{\text{y}}/\sigma_{\text{VM}}(T_{\text{y}})$ can be used to increase accuracy:

$$\sigma_i^y = \sigma_i(T_{\text{y}}) \cdot \frac{f_{\text{y}}}{\sigma_{\text{VM}}(T_{\text{y}})} \quad \text{(D.7)}$$

where

σ_i^{y} is the estimated value of the stress component at the yielding point

$\sigma_i(T_{\text{y}})$ is the values of the stress components at estimated point T_{y}

T_{y} is the estimated relative time related to the yielding point

$\sigma_{\text{VM}}(T_{\text{y}})$ is the von Mises stress at estimated point T_{y}, calculated using the stress components defined by Equation D.6

Since the yielding point of the semi-plastic step is defined, the step can be divided into two sub-steps: elastic before the yielding point and plastic thereafter.

Appendix E: Considering the elastic unloading on the plastic area

One special case is the temporal unloading related to a decrease of the pseudoelastic von Mises stress on the plastic area of the reversal. A special procedure must be used to process this case. In terms of pseudoelastic stresses, the unloading can seem to be located in the plastic area. However, considering the E-PP material model, the unloading starts from the yielding point and the decrease of the equivalent von Mises stress is elastic. After this elastic unloading, the next step starts from the decreased elastic value and returns to the plastic area only after the yielding point is once again reached. The plastic step which follows the unloading changes to semi-plastic or elastic, and the decrease in the stress level during elastic unloading affects all later steps. This unloading can be considered by an appropriate shifting of the stress history of the reversal starting from the unloading step. The required offset value to shift the stress history is equivalent to the difference between the yielding point and the last pseudoelastic point before unloading. The procedure for considering the temporal unloading is presented next. Using the presented procedure assumes that the stress history of the plastic reversal is forced to start from the yielding point and pass through the elastic region towards the yielding point at the other end of the reversal, as presented in Section 4.4 of the thesis.

The special case of temporal unloading on a plastic area can be identified by decreasing the pseudoelastic von Mises stress with a start value exceeding the yield stress of the material:

$$\sigma_{\mathrm{VM}}(T) > f_{\mathrm{y}} \tag{E.1}$$

$$\sigma_{\mathrm{VM}}(T) - \sigma_{\mathrm{VM}}(T+1) > 0 \tag{E.2}$$

where

$\sigma_{\mathrm{VM}}(T)$ is the pseudoelastic von Mises stress of the start of load step T under consideration

$\sigma_{\mathrm{VM}}(T+1)$ is the pseudoelastic von Mises stress of the end of load step T under consideration

f_{y} is the yield stress of the material

The fulfilment of conditions E.1 and E.2 indicates a step with temporal unloading. The stress history of the reversal can be processed using the original procedure after the appropriate replacement of the stress history for considering the temporal unloading. The required offset value can be calculated as the difference between the start point of the unloading step and the corresponding yielding point. Equations 4.14, 4.15 and 4.16, presented in Section 4.4 of the thesis, can be adopted for this purpose:

$$q = \frac{f_y}{\sigma_{VM}(T)} \tag{E.3}$$

$$\sigma_{ij}^{offset} = (q - 1) \cdot \sigma_{ij}(T) \tag{E.4}$$

where

$\sigma_{VM}(T)$	is the pseudoelastic von Mises stress of the start of the unloading step T under consideration
f_y	is the yield stress of the material
q	is the scale factor defined above by Equation E.3
$\sigma_{ij}(T)$	are the stress components at the start of the unloading step
σ_{ij}^{offset}	is the required offset for the rest of the stress history starting from the unloading step

The rest of the stress history is replaced by adding the component offsets to appropriate components of the stress history, beginning from the start of the step related to the temporal unloading:

$$\sigma_{ij}^{new}(T) = \sigma_{ij}^{old}(T) + \sigma_{ij}^{offset} \tag{E.5}$$

where

$\sigma_{ij}^{new}(T)$	are the stress components of the stress history after replacement
$\sigma_{ij}^{old}(T)$	are the stress components of the stress history before replacement
σ_{ij}^{offset}	are offset components, defined above by Equation E.4

After the stress history is replaced, processing can be continued using the original procedure. After this replacement, the step related to the temporal unloading changes to elastic, the next plastic step changes to semi-plastic or elastic, depending on the magnitude of the load, and so on.

ACTA UNIVERSITATIS LAPPEENRANTAENSIS

928. KRAINOV, IGOR. Properties of exchange interactions in magnetic semiconductors. 2020. Diss.

929. KARPPANEN, JANNE. Assessing the applicability of low voltage direct current in electricity distribution - Key factors and design aspects. 2020. Diss.

930. NIEMINEN, HARRI. Power-to-methanol via membrane contactor-based CO2 capture and low-temperature chemical synthesis. 2020. Diss.

931. CALDERA, UPEKSHA. The role of renewable energy based seawater reverse osmosis (SWRO) in meeting the global water challenges in the decades to come. 2020. Diss.

932. KIVISTÖ, TIMO. Processes and tools to promote community benefits in public procurement. 2020. Diss.

933. NAQVI, BILAL. Towards aligning security and usability during the system development lifecycle. 2020. Diss.

934. XIN, YAN. Knowledge sharing and reuse in product-service systems with a product lifecycle perspective. 2020. Diss.

935. PALACIN SILVA, VICTORIA. Participation in digital citizen science. 2020. Diss.

936. PUOLAKKA, TIINA. Managing operations in professional organisations – interplay between professionals and managers in court workflow control. 2020. Diss.

937. AHOLA, ANTTI. Stress components and local effects in the fatigue strength assessment of fillet weld joints made of ultra-high-strength steels. 2020. Diss.

938. METSOLA, JAAKKO. Good for wealth or bad for health? Socioemotional wealth in the internationalisation process of family SMEs from a network perspective. 2020. Diss.

939. VELT, HANNES. Entrepreneurial ecosystems and born global start-ups. 2020. Diss.

940. JI, HAIBIAO. Study of key techniques in the vacuum vessel assembly for the future fusion reactor. 2020. Diss.

941. KAZARNIKOV, ALEXEY. Statistical parameter identification of reaction-diffusion systems by Turing patterns. 2020. Diss.

942. SORMUNEN, PETRI. Ecodesign of construction and demolition waste-derived thermoplastic composites. 2020. Diss.

943. MANKONEN, ALEKSI. Fluidized bed combustion and humidified gas turbines as thermal energy conversion processes of the future. 2020. Diss.

944. KIANI OSHTORJANI, MEHRAN. Real-time efficient computational approaches for hydraulic components and particulate energy systems. 2020. Diss.

945. PEKKANEN, TIIA-LOTTA. What constrains the sustainability of our day-to-day consumption? A multi-epistemological inquiry into culture and institutions. 2021. Diss.

946. NASIRI, MINA. Performance management in digital transformation: a sustainability performance approach. 2021. Diss.

947. BRESOLIN, BIANCA MARIA. Synthesis and performance of metal halide perovskites as new visible light photocatalysts. 2021. Diss.

948. PÖYHÖNEN, SANTERI. Variable-speed-drive-based monitoring and diagnostic methods for pump, compressor, and fan systems. 2021. Diss.

949. ZENG, HUABIN. Continuous electrochemical activation of peroxydisulfate mediated by single-electron shuttle. 2021. Diss.

950. SPRINGER, SEBASTIAN. Bayesian inference by informative Gaussian features of the data. 2021. Diss.

951. SOBOLEVA, EKATERINA. Microscopy investigation of the surface of some modern magnetic materials. 2021. Diss.

952. MOHAMMADI ASL, REZA. Improved state observers and robust controllers for non-linear systems with special emphasis on robotic manipulators and electro-hydraulic servo systems. 2021. Diss.

953. VIANNA NETO, MÁRCIO RIBEIRO. Synthesis and optimization of Kraft process evaporator plants. 2021. Diss.

954. MUJKIC, ZLATAN. Sustainable development and optimization of supply chains. 2021. Diss.

955. LYYTIKÄINEN, JOHANNA. Interaction and barrier properties of nanocellulose and hydrophobically modified ethyl(hydroxyethyl)cellulose films and coatings. 2021. Diss.

956. NGUYEN, HOANG SI HUY. Model based design of reactor-separator processes for the production of oligosaccharides with a controlled degree of polymerization. 2021. Diss.

957. IMMONEN, HEIKKI. Application of object-process methodology in the study of entrepreneurship programs in higher education. 2021. Diss.

958. KÄRKKÄINEN, HANNU. Analysis of theory and methodology used in determination of electric motor drive system losses and efficiency. 2021. Diss.

959. KIM, HEESOO. Effects of unbalanced magnetic pull on rotordynamics of electric machines. 2021. Diss.

960. MALYSHEVA, JULIA. Faster than real-time simulation of fluid power-driven mechatronic machines. 2021. Diss.

961. SIEVINEN, HANNA. Role of the board of directors in the strategic renewal of later-generation family firms. 2021. Diss.

962. MENDOZA MARTINEZ, CLARA. Assessment of agro-forest and industrial residues potential as an alternative energy source. 2021. Diss.

963. OYEWO, AYOBAMI SOLOMON. Transition towards decarbonised power systems for sub-Saharan Africa by 2050. 2021. Diss.

964. LAHIKAINEN, KATJA. The emergence of a university-based entrepreneurship ecosystem. 2021. Diss.

965. ZHANG, TAO. Intelligent algorithms of a redundant robot system in a future fusion reactor. 2021. Diss.

LUT University

ISBN 978-952-335-666-5
ISBN 978-952-335-667-2 (PDF)
ISSN-L 1456-4491
ISSN 1456-4491
Lappeenranta 2021